MULTICAPILLARY MEMBRANE BIOREACTOR DESIGN

BY

SETENO KARABO OBED NTWAMPE

Thesis submitted in fulfilment of the requirements for the degree

MTECH: ENGINEERING: CHEMICAL

in the

FACULTY OF ENGINEERING

at the

CAPE PENINSULA UNIVERSITY OF TECHNOLOGY

SUPERVISOR: MARSHALL SHEERENE SHELDON

CAPE TOWN
2005

DECLARATION

I, **Seteno Karabo Obed Ntwampe**, hereby declare that the contents of this thesis represent my own unaided work and that the thesis has not previously been submitted for academic examination toward any qualification. Furthermore, it represents my own opinions and not necessarily that of the National Research Foundation or the Cape Peninsula University of Technology.

Date: 10/March/2006   Signature:

ABSTRACT

The white rot fungus, *Phanerochaete chrysosporium,* produces enzymes, which are capable of degrading chemical pollutants. It was determined that this fungus has multiple growth phases. The study provided information that can be used to classify growth kinetic parameters, substrate mass transfer and liquid medium momentum transfer effects in continuous secondary metabolite production studies. *P. chrysosporium* strain BKMF 1767 (ATCC 24725) was grown at 37 °C in single fibre capillary membrane bioreactors (SFCMBR) made of glass. The SFCMBR systems with working volumes of 20.4 ml and active membrane length of 160 mm were positioned vertically.

Dry biofilm density was determined by using a helium pycnometer. Biofilm differentiation was determined by taking samples for image analysis, using a Scanning Electron Microscope at various phases of the biofilm growth. Substrate consumption was determined by using relevant test kits to quantify the amount, which was consumed at different times, using a varying amount of spore concentrations. Growth kinetic constants were determined by using the substrate consumption and the dry biofilm density model. Oxygen mass transfer parameters were determined by using the Clark type oxygen microsensors. Pressure transducers were used to measure the pressure, which was needed to model the liquid medium momentum transfer in the lumen of the polysulphone membranes. An attempt was made to measure the glucose mass transfer across the biofilm, which was made by using a hydrogen peroxide microsensor, but without success.

Dry biofilm density was modelled by using a growth rate constant of 0.035 hr^{-1} which was classified as being equivalent to the specific growth rate. Glucose consumption increased with the different biofilm growth phases, with an average of 94.7 g/m^3.hr consumed over a period of 264 hrs. After 48 hrs, 90% of the ammonia fed to the SFCMBR systems, was consumed compared to 15% of the glucose. An average glucose-based growth yield, coefficient of approximately 0.202 g biofilm/g glucose, was determined compared to 14.3 g biofilm/g ammonia of ammonia tartrate. The consumption of substrates increased when a higher concentration of spores were immobilised in the bioreactors.

The biofilm structure, during the exponential phase, showed a vegetative state near the substratum, which supported the aerial mycelia. During the structural steady state, the compact aerial mycelia produced reproductive propagules, thus reducing oxygen flux during this stage. In younger mycelia, oxygen consumption was generally lower, with higher consumption rates of greater than 800 g/m^3.hr occurring during the exponential phase of the primary growth phase.

Pressure transducers were used to measure pressure at the inlet and outlet of the substratum in a bioreactor without any immobilised biofilm. Mathematical models that were modified to suit the operating conditions were used to predict the outlet pressure using the inlet pressure. Mass transfer coefficient values were determined in the range of 0.131 to 0.602 m/hr with an average oxygen penetration depth of 390µm. Oxygen based Monod's saturation constant in the range of 0.567 to 2.07 g/m^3 with average biofilm diffusion coefficients of 1.03E-05 to 1.27E-5 m^2/hr, were also obtained.

Manganese Peroxidase (MnP) and *Lignin Peroxidase (LiP)* are two of the extracellular enzymes produced by *Phanerochaete chrysosporium* biofilms. These enzymes, have demonstrated to be major components of the lignin degradation system. They are able to metabolise a variety of organic chemicals, many of which are pollutants in liquid effluents. The commissioning of vertical MCMBR systems was done by monitoring the substrate consumption, enzyme production and oxygen distribution within the biofilm, which was formed. In a period of 0 to 5 days, more *LiP* (above 5 U/L) was produced compared to *MnP*. During this operational period, *MnP* production was lower than 5 U/L. The conditions under which the MCMBR systems were operated favoured higher *LiP* production. Permeate collected from one of the MCMBR systems were used to evaluate the phenol degradation, in which 66.7% of phenol content was reduced in olive wastewaters.

DEDICATION

To my parents, **Rudolph Selelepoo** and **Peggy Ramatsobane**, with love

ACKNOWLEGDEMENTS

TABLE OF CONTENTS

ix

LIST OF FIGURES

LIST OF TABLES

CHAPTER 1 : BACKGROUND

1.1   INTRODUCTION

There are an increasing number of areas where bioreactors are alternatives to conventional chemical reactors, e.g., in the pharmaceutical industry, where microorganisms and enzymes can be used to produce specific stereoisomers selectively. In such applications, the limitations of bioreactors are clearly outweighed by the advantage in their use. Growing interest was focused on fungi, which have potentialities to solve environmental problems. This was the case of the white rot fungus (WRF), *Phanerochaete chrysosporium,* which can degrade aromatics and remove coloured compounds from effluents. Research has also focused on the applied potential of this fungus. Significantly, many of these compounds are degraded to the level of carbon dioxide by enzyme produced by this fungus (Tien & Kirk, 1988).

The commercial exploitation of enzymes, taken from fungal biomass, was restricted to conditions in which the biomass can function. Most fungi live in moderate temperatures and do not tolerate extreme pH. The vast majority of microorganisms prefer mild conditions and commercial operations depend on having the correct organisms, which would prevent inactivation or the entry of foreign organisms that could harm the process. Many bioprocesses are closed and have elaborate precautions to prevent contamination. Fungi contain no chlorophyll and, therefore, require sources of complex organic molecules for growth, which are made of carbon, oxygen, nitrogen, sulphur, phosphorus, water, trace elements and vitamins (Perry & Green, 1997).

1.1.1   Membrane bioreactors

A membrane bioreactor is a flow reactor within which membranes are used to separate fungal cells from the feed or the product streams and a common characteristic is that the feed is delivered continuously, while the products are also removed continuously. Polymeric micro-filtration or ultra-filtration membranes are most commonly used for the construction of membrane reactors, although other types of membranes have been used, including ceramic (Sheldon & Small, 2005), silicone rubber (Venkatadri & Irvine, 1993) and ion exchange membranes. The permeability of membranes was dependent not only on the pore size and

structure, but also on characteristics such as hydrophobicity (Asenjo & Merchuk, 1994). The most commonly used geometry for membrane bioreactors is the hollow fibre. A bundle of hollow fibres are potted into a cylindrical shell with epoxy or polyurethane resin. Commercial bioreactor units may contain thousands of hollow fibres, which provide large surface areas for mass transfer, fungal biomass and adhesion. In most membrane bioreactors, fungal biomass is entrapped without chemical immobilisation, wherein tissues are maintained by nutrients, which are delivered through the lumen of the hollow fibres (Asenjo & Merchuk, 1994).

1.1.2   Challenges

Bioreactor design for any culture is generally determined by the transport rates of the oxygen and nutrient medium. The most significant and widely studied challenge, which faces the application of membrane bioreactors, is the influence of mass transfer effects on the bioreactor operation. A requirement in immobilised cell systems was to enhance the activity of immobilised cell particles for application in industrial units (Garcin 2002; Asenjo & Merchuk, 1995). Several problems have been encountered whilst attempting to achieve efficient production of the ligninolytic enzymes from these white rot fungi. The application of the commercial production of ligninase has been hampered by the lack of bioreactor systems, yielding consistent levels of production under long terms of steady state conditions and controlled growth fungus (Garcin, 2002; Solomon, 2001; Leukes, 1999; Venkatadri & Irvine, 1993).

1.2   RESEARCH QUESTIONS

Many of the factors (listed as 1.2.1 to 1.2.4) which have been described in Asenjo and Merchuk (1995) which influence the choice of bioreactor design and modelling, are interrelated. These factors are separated into a checklist of questions that may be useful to consider before undertaking the development of a membrane bioreactor. Acquiring information to answer these questions, should give the necessary data to select and design the most appropriate type of reactor.

1.2.1 Microorganism species

- What special properties are involved?
- Does cell structure change under certain conditions?
- Are the substrates soluble?

1.2.2 Growth and oxygen requirements

- Oxygen requirements, aerobic, anaerobic or aerophilic?
- What is the oxygen consumption/uptake rate in the presence of air?
- What is the maximum cell density?

1.2.3 Cleaning and sterility

- Are there any sensitive conditions (E.g. extremes of pH, temperature or heavy metal concentration)?
- Is there wall growth in the bioreactor?
- Cleaning problems?

1.2.4 Measurement system

- Essential measurements: What measurements are essential to take? (E.g. pH, temperature, dissolved oxygen, ammonia and glucose concentration).
- Desirable measurements: What measurements might be desirable to take? (E.g. exit gas analysis or enzyme activity).

1.3   OBJECTIVES OF THE STUDY

Although there is information available about the growth patterns and biochemical literature of *P. chrysosporium* and its enzymes, *LiP* and *MnP,* in batch culture, there was no available data for designing a continuously engineered membrane bioreactor. The selection and specific design of

the bioreactor will include a series of decisions on matters, which range from basic microbiology to process engineering. All these disciplines should contribute to the design of the bioreactor and its dimensions to provide an optimal environment for the system and to maximise the productivity and benefits of the process. Growth kinetics, oxygen mass transfer, nutrient mass transfer and nutrient flow behaviour through the substratum (polysulphone membrane), were modelled in single fibre capillary membrane bioreactors so that the information can be used for larger bioreactors. A multi-capillary membrane bioreactor was designed and operated for continuous enzyme production.

1.3.1 The objectives of the study, therefore, encompass the following:

- Quantify the growth kinetics of the fungus;
- Mathematically model the substrate mass transfer across the biofilm;
- Mathematically model the momentum fluid flow behaviour through the polysulphone membrane; and
- Design, construct and commission a multi capillary membrane bioreactor (MCMBR) system.

1.4 SIGNIFICANCE OF THE STUDY

Much of the research work conducted thus far has been carried out in batch cultures and few studies have reported the use of *P. chrysosporium* in continuous membrane bioreactors. The lack of systems, which yield a consistent production of high levels of *LiP* and *MnP* at reasonable levels over extended periods of time, have impeded progress in the use of *P. chrysosporium* in large-scale enzyme production applications. The study will provide information, which can be used to classify growth kinetic parameters, substrate mass transfer and liquid medium momentum transfer effects in continuous membrane bioreactor systems. A demonstration on how to develop mathematical models from basic principles was also provided.

1.5   SCOPE OF THE THESIS

The research questions (listed as 1.2.1 to 1.2.4) of the study are address in subsequent chapters. Chapter 2 covers the literature review, which is used in the development of mathematical models and the bioreactor design. Mathematical models describing momentum transfer in the lumen and nutrient mass transfer across the biofilm are developed in Chapter 3. Linearization techniques are explained in this chapter and are used in the evaluation of kinetic parameters in Chapter 6. The parameters used in the bioreactor design and the detailed design are covered in Chapter 4. Materials and methods used in the study to meet the objectives are discussed in Chapter 5. Chapters 6 and 7 reviews results obtained in the study and discuss their implications. Chapter 8 discusses the multicapillary membrane system commissioning, where enzyme production is measured. The enzymes produced are used to reduce phenol content in olive wastewater.

1.6   DELINEATION OF THE STUDY

The research performed was limited to bioreactor systems in which polysulphone membranes were used. The use of a reusable membrane such as ceramic membranes was not considered. The following areas will not be covered during this study;

- Purification of enzymes;
- Optimisation of the multicapillary bioreactor system and nutrient medium;
- Building a commercial-sized unit; and
- Accommodation of different membrane sizes and types.

CHAPTER 2 : LITERATURE REVIEW

2.1 INTRODUCTION

Industrial bioprocesses are the integration of many, sometimes complex, operations. Capillary fibre membrane bioreactor devices are at the core of these processes and have many applications. For all these applications, mass transfer and flow phenomena, as well as pressure drop data, are of major importance. In membrane bioreactor configurations, diffusion and convection are the only mechanism of oxygen and nutrient medium transport.

A detailed analysis of *P. chrysosporium* (as a microorganism), enzymes produced by *P. chrysosporium* (which are used in biotransformation, biodegradations and wastewater treatment), will be covered in this chapter. This includes the metabolic products produced by these microorganisms, growth conditions, and nutrient medium used. Different characteristics of biofilms, including types, have been summarised from previous investigations by other researchers. Fundamental concepts of mass transfer (convection, diffusion and molecular fluid dynamics laws) in biofilms and information on instrumentation used to evaluate these concepts are included. Different capillary fibre membrane bioreactors are discussed, along with the different membrane types used to build these bioreactors. Different modes of bioreactor operations are highlighted with industrial applications summarised from previous research.

2.2 THE WHITE ROT FUNGI (WRF)

White rot fungi (WRF) are members of the *Enmycota*, subdivision *Basiodiomycotina*, the class of fungi that are well known for their fruiting bodies commonly recognised as mushrooms and puffballs (Bumpus & Aust, 1987). These fungi are unique in that they are the only known organisms capable of completely degrading lignin (Gold & Alic, 1993). The mechanism of lignin degradation by the WRF is complex and it was described as it pertains to the biodegradation of aromatic pollutants. The ligninolytic system of the WRF was a non-specific, extracellular oxidative process initiated by nitrogen, carbohydrate or sulphur starvation. (Bumpus & Aust, 1987). Extracellular enzymes were discovered, which were capable of the degradation of

lignin model compounds (Tien & Kirk, 1984). Lignin degradation is dependent on the presence of a readily metabolisable co-substrate such as glucose and increasing the levels of glucose in culture, has a strong activating effect on the rate of lignin degradation, which is strongly dependent on the presence of manganese (Perie & Gold, 1991).

2.2.1 Lignin biodegradation

WRF, classified as *Basidiomycetes,* are the only known organisms that are capable of degrading lignin to carbon dioxide and hydrogen peroxide in pure cultures. Researchers have screened a large number of WRF for their ability to degrade lignin. *P. chrysosporium,* which was found to exhibit high rates of lignin degradation, rapid growth in liquid cultures and rapid sporulation (Buswell & Odier, 1987; Kirk *et al.,* 1978). Martin (2000) showed that this fungus could be used to assist the process of extraction of gold from wooden supports used underground within the mining industry. *P. chrysosporium* can degrade a portion of the wood matrix and allow the gold that was locked up, to come into contact with cyanide solution during beneficiation, thereby improving recoveries.

2.2.2 Bioremediation

Bioremediation, the use of biological treatment systems to destroy or reduce the concentration of hazardous waste from contaminated sites, has found wide spread appeal. A growing interest was focused on fungi, which have potentialities to solve environment problems. This was the case of *P. chrysosporium,* which can degrade aromatic compounds and remove the coloured compounds from effluents of the pulp and paper industry (Walsh, 1998; Bumpus & Aust, 1987).

2.2.3 Biochemistry of *Phanerochaete chrysosporium*

Manganese Peroxidase (MnP) and *Lignin Peroxidase (LiP),* first discovered in *P. chrysosporium* has been identified in the cultures of numerous WRF (Kuwahara *et al.,* 1985). These enzymes have demonstrated to be major components of the lignin degradation system of this organism. They are able to metabolise a variety of organic chemicals, many of which are pollutants both in

liquid effluents and soils. When oxygen was available and nitrogen was limited in glucose based feed, *P. chrysosporium* produces *LiP* and *MnP* as enzymes (Tien & Kirk, 1988).

2.2.3.1 *Lignin Peroxidase (LiP)*

LiP catalyses the oxidation of nonphenolic lignin model compounds, such as veratryl alcohol to veratraldehyde. The unique feature of this enzyme was that it was able to oxidise aromatic compounds with redox potentials beyond the reach of horseradish peroxidase and other peroxidases. The enzyme has a low pH optimum (pH 2.5) for a peroxidase and its pH was controlled by the pH dependence of the reaction steps in the catalytic cycle (Khodui & Tien, 1994).

2.2.3.2 *Manganese Peroxidase (MnP)*

The oxidation of lignin and other phenols by *MnP* is dependent on the availability of free manganese ions. The primary reducing substrate in the *MnP* catalytic cycle is *Mn (II)*, which efficiently reduces *MnPI* and *MnPII*, generating *Mn (III)*, which oxidises the organic substrate. Organic acids, such as oxalate and malonate, which are secreted by *P. chrysosporium* (Wariishi *et al.*, 1992), stimulates the *MnP* reaction by stabilising the *Mn (III)* so that it can diffuse from the surface of the enzyme and oxidase the insoluble terminal substrate, lignin (Zapanta & Tien, 1997; Poulos & Kraut, 1980).

2.2.4 Growth conditions of *P. chrysosporium* in bioreactors

Since the discovery of ligninase, much effort has been made to develop efficient methods of producing *LiP* and *MnP*. *LiP* and *MnP* production has been studied by using complicated synthetic media based on the composition originally designed by Kirk *et al.* (1978) for lignin degradation studies by the WRF, *P. chrysosporium* (Linko, 1992). The most important external factors, which affect the activity of the organism, are temperature, pH, dissolved oxygen concentration and a fixed nitrogen concentration (Leisola *et al.*, 1984; Jeffries *et al.*, 1981; Fenn *et al.*, 1981; Fenn and Kirk, 1981; Kirk *et al.*, 1978). The optimum temperature for the growth of

the fungus has been established to be 39 °C and the optimum pH ranges from 4.0 to 4.5. Since the organism is an aerobe, its activity is influenced by the dissolved oxygen concentration. Its rate of lignin degradation was reported to be 2 to 3 times greater by using pure oxygen rather than air (Garcin, 2002; Solomon, 2001; Govender, 2000; Leukes, 1999; Leisola *et al.*, 1984; Kirk *et al.*, 1978). During its growth phase, the organism also requires a source of fixed nitrogen, but is relatively inactive in terms of ligninase production. However, if the organism then undergoes nitrogen starvation, the production of appropriate oxidation enzymes was induced (Fenn *et al.*, 1981; Fenn and Kirk, 1981; Jeffries *et al.*, 1981).

2.2.4.1 Growth cycle

The basic growth cycle of microorganisms is shown below.
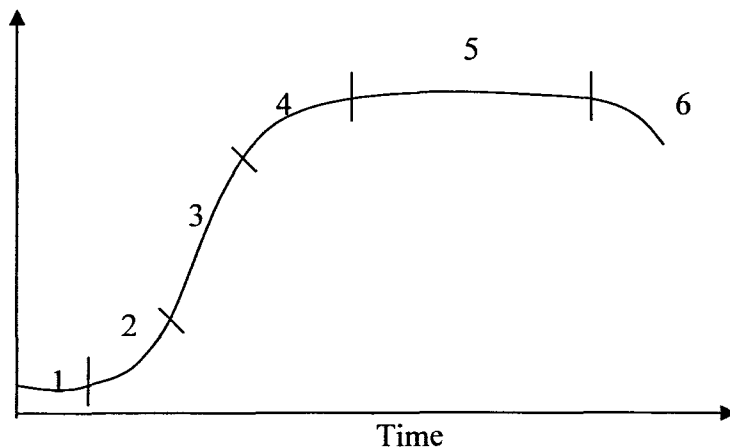
Figure 2.1: The basic growth cycle of a microorganism (Shuler & Kargi, 1992).

The basic growth cycle of microorganisms follow the following phases, as depicted in Figure 2.1. The different phases are: 1) Lag phase (period where new culture becomes used to its environment); 2) Accelerated growth (makes use of the environment); 3) Exponential growth (maturation of culture); 4) Decelerated growth (environmental limitation sets in); 5) Stationary phase (tries to stabilise); and 6) Decline, death of culture (Shuler & Kargi, 1992). By using a continuous reactor system, it was easier to keep the culture in the secondary metabolic stage (end of phase 4 to the beginning of stage 5). It is during this stage that the required enzymes are produced (Garcin, 2002; Solomon, 2001; Leukes, 1999; Venkatadri & Irvine, 1993). In theory, a continuous system should enable the culture to remain in phase 5 (stationary phase).

2.2.4.2 Growth patterns of *P. chrysosporium*

P. chrysosporium growth consists of multiple growth phases when grown in flasks using a growth medium, which consists of 10 g/L glucose. Ceribasi and Yetis (2001) observed that when *P. chrysosporium* was incubated at 35 °C, two exponential growth phases occurred: phase 1: 10 to 65 hrs and phase 2: 100 to 150 hrs. The increase observed was attributed to the diauxic growth of fungal mycelia.

2.2.4.3 The gradostat concept

The term 'gradostat' is used to describe a biofilm reactor, which shows good potential for industrial application, which uses a synthetic capillary ultrafiltration membrane (Jacobs & Sanderson, 1997; Jacobs & Leukes, 1996) as a support matrix for the biofilm. The term gradostat applies since the gas and liquid nutrient gradients flow is unidirectional, bi-directional and contact occurs between the primary and secondary growth phases of the biomass (Leukes, 1999; Leukes *et al.*, 1996). The essence of this system is depicted schematically in Figure 2.2.
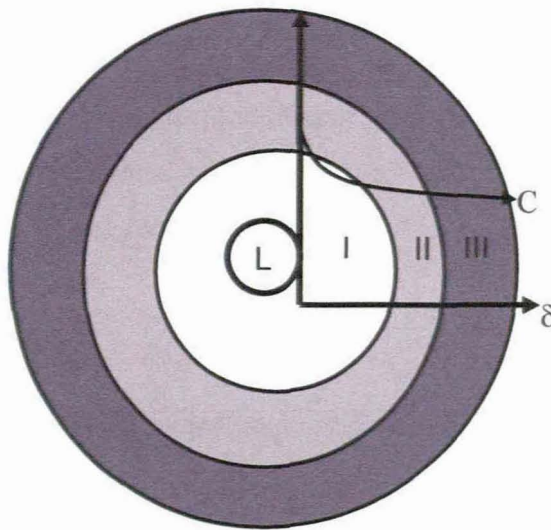
Figure 2.2: Schematic representation of the gradostat concept with a superimposed substrate concentration curve. I is the primary growth phase; II is the stationary growth phase; III is the decline phase; L- Lumen of the capillary membrane from which the nutrient is supplied; δ- Radial distance from the lumen in the direction of the nutrient flow; and C- Concentration of growth limiting substrate (Leukes, 1999).

When nutrients are supplied (by diffusion or convection) to a biofilm, which is immobilised on the wall of a capillary membrane, radial nutrient gradients are established. The biomass closest to the membrane has first access to the nutrients, while the biomass away from the membrane surface is starved. Continuous enzyme production, which utilises nutrient limiting gradients in order to achieve differentiation of biomass into different growth phases, was achieved by Leukes (1999), Solomon (2001) and Garcin (2002), using the gradostat concept.

2.2.5 Other factors influencing secondary metabolite production

2.2.5.1 Growth and production medium

Enzyme production experiments have been carried out with completely synthetic media, which are various modifications of the original nitrogen limited medium developed by Kirk *et al.* (1978) for studies on lignin degradation by *P. chrysosporium*. The medium contained mineral salts and vitamins with 10 g/L glucose as the carbon source and 2.2mM of ammonia tartrate as the nitrogen source (Tien & Kirk, 1988). The results which were obtained showed a high enzyme production. The effect of nitrogen limitation on enzyme production was not considered, which was surprising, given the low levels of nitrogen found in wood (Buswell & Odier, 1987). Various studies have focussed on the improvement of enzyme production by supplementation of the basic growth medium with various additives (veratryl alcohol, Tween 20/80 and trace elements) or adaptation of the physical environments (Govender, 2000; Linko, 1992; Bonnarme & Jefferies, 1990; Asther *et al.*, 1988).

2.2.5.2 Trace elements in production media

A number of minerals (e.g. Cu, Zn, Fe, Co, Mn and Mg) are usually neglected in laboratory-scale work, whilst these minerals are necessary (usually in trace amounts) for biomass growth. Some of these minerals are inhibitory when they are present in high concentrations within the growth media. Numerous microorganisms displayed a growth optimum, which was dependent on mineral concentration (Asenjo & Merchuk, 1994).

2.2.5.3 Oxygen requirements

The ligninolytic system of the WRF has been shown to be particularly active in cultures, which are grown in high oxygen tension (Dosoretz *et al.*, 1990). Lignin degradation was shown to be about 3-fold higher under 100% oxygen than under air (Kirk *et al.*, 1978). Faison and Kirk (1985) reported that both ligninolysis and ligninase of *P. chrysosporium* were increased in cultures, which were initially supplied with air during their growth phase, before shifting to an oxygen atmosphere. This was also established by Garcin (2002), Solomon (2001) and Govender (2000).

2.2.6 Biofilm: Fundamentals and characteristics

The conventional view of a biofilm is that it is a flat layer of cells, which cover a surface. Adjacent to the solid surface, is a boundary layer in which the transport is gradually changed from convective to diffusion at the solid interface. This view is completed with the assumption that mass transfer inside the biofilm is diffusional. These assumptions are commonly the basis for biofilm modelling (DeBeer & Schramn, 1999). Microscopic observations indicated that biofilms are not necessarily flat; instead, biofilms may form highly complex structures, which contain cell layers and clusters, as well as voids or pores. Micro-injection of a fluorescent dye, and following the plane with confocal microscopy, showed that flow was possible in voids, depending on the flow velocity of the bulk liquid, while in the cell cluster, no flow occurred (De Beer *et al.*, 1994).

Consequently, convection is possible through the voids, while cell clusters diffusion is the only transport mechanism. These observations unequivocally showed that the flow rate inside the biofilm is proportional to the flow velocity of the bulk liquid. However, it could not be ruled out that convection is insignificant and that diffusion is the dominant transport mechanism in biofilms. Proof for voids, which act as transport channels for substrates, is that the substrate concentrations in voids are higher than in adjacent biomass (De Beer & Schramn, 1999). Under growth conditions, oxygen penetrated through voids to the substratum. Due to the concentration difference between voids and cell clusters, a significant part of the oxygen supply to the cell clusters occurred from the voids. At very low oxygen velocities, diffusion determines internal mass transfer, while at higher velocities convection, through the voids, is the dominant transport mechanism (DeBeer & Schramn, 1999).

2.2.6.1 Density, porosity and pore structure of biofilms

Biofilms are multiphase systems, which consist of solids and of a liquid phase in the void space between the solids. Most biofilms are spatially heterogeneous, characterised by complex assemblages of biomass types and gradients of physical and chemical parameters. As a result of these spatial gradients, the microbial species and density, the volume fraction of the water phase (porosity) and the tortuosity of biofilms have to change as the depth of the biofilm increases. These spatial distributions, in turn, affect the mass transfer mechanics and diffusivities in the biofilms (Zhang & Bishop, 1994).

2.2.6.2 Heterogeneous and Homogeneous biofilms

Micro-scale structural heterogeneity of biofilms is emerging as a potentially important aspect of biofilm function. The term structural heterogeneity includes features such as the nonuniform distribution of cells and variable biofilm thickness (Murga *et al.*, 1995) while homogenous represents a uniform layer of microorganisms, which are attached to a surface (Lewandowski & Beyenal, 2002). Numerous studies (Costerton, 1994; DeBeer *et al.*, 1994) have shown that biofilms can no longer be considered to be homogeneous structures.

The first confocal images of biofilms precipitated the idea that the conceptual model of homogeneous biofilms was inadequate. As a result, the model of homogenous biofilms has been appended by the model of heterogeneous biofilms, which display microorganisms aggregated in microcolonies instead of being uniformly distributed throughout the matrix (Lewandowski & Beyenal, 2002). The reasons for structural heterogeneity are largely unknown, but they involve both physical and biological factors such as substrate loading, shear stress and growth rate, which influence the biofilm structure. It may be that biological mechanisms create a structure, which maximises mass transport to deep layers within the biofilm (Lewandowski *et al.*, 1999)

2.2.6.3 Differentiation within *P. chrysosporium* biofilm

A phenomenon commonly seen in a maturing biofilm of a fungus is the stratification of the biofilm in which the primary layer exposed to oxygen protects the inner layer. This is normally

referred to as biofilm differentiation. Competition between cells in a maturing biofilm, in response to environmental conditions, can lead to related stress (Leukes, 1999).

Figure 2.3: Morphological differentiation within *P. chrysosporium* biofilm taken from Solomon (2001).

Solomon (2001) showed morphological differentiation within *P. chrysosporium* biofilm attached to a polysulphone support matrix after 14 days of a single fibre capillary membrane bioreactor (SFCMBR) operation, shown in Figure 2.3. The biofilm layer (A) closer to the membrane (an area in which nutrient rich conditions prevail) appeared to be less compact compared with the biofilm layer (B) associated with the bioreactor shell side where air was supplied. This proved that the gradostat concept was feasible.

2.2.7 Quantifying biofilm density and growth kinetics

The quantification of biofilm density in a culture media is essential for the determination of the kinetics and stoichiometry of microbial growth. The rate of biofilm growth is directly related to biomass density and cellular reproduction is the normal outcome of this reaction. The rate of microbial growth is characterised by the specific growth rate, which is defined by equation 2.1 (Shuler & Kargi, 1992).

$$\bar{\mu} = \frac{1}{X} \frac{dX}{dt}$$

2.1

2.2.7.1 Substrate limited growth

The relationship of specific growth rate to substrate concentration often assumes the form of saturation kinetics. A single chemical species is assumed to be limiting (that is, an increase in the chemical species influences the growth rate), while changes in other nutrient concentrations have no effect. When applied to cellular systems, kinetics can be described by the Monod equation (Shuler & Kargi, 1992),

$$\bar{\mu} = \frac{\bar{\mu}_m C_s}{K_m + C_s}$$

2.2

2.2.7.2 The logistic equation

The shape of the biomass density curve can be predicted by combining the Monod equation 2.2 with the growth equation 2.1 and an equation for the yield of cell mass based on substrate consumption will be (Shuler & Kargi, 1992):

$$\frac{dX}{dt} = \frac{\bar{\mu}_m C_s}{K_m + C_s} X$$

2.3

Logistic equations are a set of equations, which characterise growth in terms of carrying capacity. The usual approach is based on a formulation, in which the specific growth rate is related to the amount of unused capacity (Shuler & Kargi, 1992):

$$\frac{dX}{dt} = k_f X \left(1 - \frac{X}{X_m} \right)$$

2.4

referred to as biofilm differentiation. Competition between cells in a maturing biofilm, in response to environmental conditions, can lead to related stress (Leukes, 1999).

Figure 2.3: Morphological differentiation within *P. chrysosporium* biofilm taken from Solomon (2001).

Solomon (2001) showed morphological differentiation within *P. chrysosporium* biofilm attached to a polysulphone support matrix after 14 days of a single fibre capillary membrane bioreactor (SFCMBR) operation, shown in Figure 2.3. The biofilm layer (A) closer to the membrane (an area in which nutrient rich conditions prevail) appeared to be less compact compared with the biofilm layer (B) associated with the bioreactor shell side where air was supplied. This proved that the gradostat concept was feasible.

2.2.7 Quantifying biofilm density and growth kinetics

The quantification of biofilm density in a culture media is essential for the determination of the kinetics and stoichiometry of microbial growth. The rate of biofilm growth is directly related to biomass density and cellular reproduction is the normal outcome of this reaction. The rate of microbial growth is characterised by the specific growth rate, which is defined by equation 2.1 (Shuler & Kargi, 1992).

Figure 2.4: Logistic biomass density curve (Shuler & Kargi, 1992).

2.3 MASS TRANSFER EFFECTS IN PROCESSES

Mass transfer refers to any process in which diffusion and convection plays a role. Diffusion and convection are the spontaneous mixing of molecules by random motion. In the absence of other gradients (such as temperature), molecules of a given species within a single phase will always diffuse from regions of higher concentration to regions of lower concentration. This gradient results in a molar flux of the species N_s in the direction of the concentration gradient. The flux of N_s is relative to a fixed coordinate and is a vector quantity (Fogler, 1999):

$$N_s = N_{sx} + N_{sy} + N_{sz} \qquad\qquad 2.5$$

The molar flux, N_s, is the result of two contributions: J_s, the molecular diffusion flux relative to the convective bulk motion of the fluid, which is produced by a concentration gradient, and B_s, the flux that results from the convective bulk motion of the fluid (Fogler, 1999):

$$N_s = J_s + B_s \qquad\qquad 2.6$$

The convective bulk flow term B_s can be expressed in terms of the concentration of A and the molar average velocity $\bar{v}_s$:

$$B_s = C_s \bar{v}_s \qquad\qquad 2.7$$

16

Where the molar average velocity is:

$$\bar{v}_s = \sum \xi_s v_s \qquad 2.8$$

In systems where the flux results primarily from forced convection, it may be assumed that the diffusion in the direction of the flow is assumed to be small in comparison with the convective bulk flow contribution in that direction, therefore the flux J_A is approximately equal to zero:

$$N_s \approx B_s = C_s \sum \xi_s v_s \qquad 2.9$$

2.3.1 Fick's first law

The mass transfer flux law is analogous to the laws for heat and momentum transport. The constitutive equation for J_s, the diffusion flux, which results from a concentration difference, is related to the concentration gradient by Fick's law (Fogler, 1999):

$$J_s = -C_s D \nabla \xi_s = D \frac{dC_s}{d\delta} \qquad 2.10$$

In rectangular coordinates, the gradient is in the form:

$$\nabla = \frac{\partial}{\partial x} + \frac{\partial}{\partial y} + \frac{\partial}{\partial z} \qquad 2.11$$

By combining equations 2.10 and 2.11, the following equation is formulated,

$$N_s = -C_s D \nabla \xi_s + C_s \sum \xi_s v_s \qquad 2.12$$

2.3.2 Diffusion kinetics in porous surfaces

The overall rate of reaction on a porous material is the integral sum of the rates for the differential parts of the surface, which are characterised by different accessibilities with respect to diffusion. The overall rate depends both on the shape, diameter, thickness and geometrical shape of the pores at different depths of the layer of material (Frank-Kamenetskii, 1969).

The thickness of the layer of material may be large so that it can be regarded as being infinite. To analyse the problem, regardless of the shape and diameter of the pores themselves, diffusion, within the mass of porous material, can be described with an effective diffusion coefficient defined in such a way that the diffusion equation in the mass of material has the form as (Frank-Kamenetskii, 1969):

$$\frac{dC_s}{dt} = D\frac{d^2C_s}{d\delta^2} - r_B(C_s) \qquad\qquad 2.13$$

The surface of the porous material is considered to be planar, thus diffusion is considered in one direction, namely, the direction perpendicular to the surface; there will be no characteristic lengths introduced by finite boundaries. After the lapse of a certain time, a steady state concentration is established in the mass material so that, $dC_s/dt = 0$. Provided that $r_B(C_s)$ is only a function of C_s, the diffusion for stationary conditions may be written as in equation 2.14 (Frank-Kamenetskii, 1969):

$$D\frac{d^2C_s}{d\delta^2} - r_B(C_s) = 0 \qquad\qquad 2.14$$

Equation 2.14 can be integrated as a quadrate by using substitutions obtaining:

$$\frac{dC_s}{d\delta} = \sqrt{\frac{2}{D}\int r_B(C_s)dC_s} \qquad\qquad 2.15$$

2.3.3 Mass transfer in biofilms

The transport and utilisation of nutrients in any biofilm is governed by the convective transport of the solvent, as well as diffusion of the solutes within the nutrient medium. Convective transport can be used to overcome the limitations imposed by diffusive mass transport (Kelsey *et al.*, 1990). Nutrients from the bulk medium can be rapidly brought into contact with cells (shown in Figure 2.5) within the biofilm, allowing for saturation kinetics and high metabolic efficiencies. A differential equation or mass balance for the rate limiting substrate within biofilms at a steady state is (Shuler & Kargi, 1992):

$$D\frac{d^2 C_s}{d\delta^2} = \frac{1}{Y_{x/s}} \frac{\bar{\mu}_m X C_s}{K_m + C_s} \qquad\qquad 2.16$$
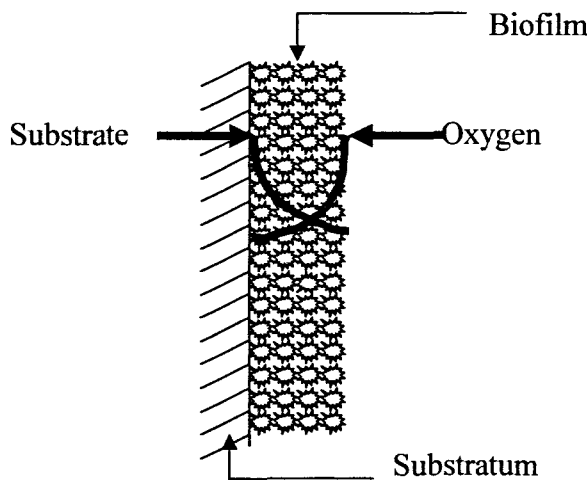
Figure 2.5: Substrate concentration profiles for biofilms immobilised on a vertically orientated membrane (Shuler & Kargi, 1992).

The following boundary conditions apply, 1) at the membrane surface $C_s = C_{s0}$ 2) across the biofilm thickness $dC_s/d\delta = 0$. The maximum rate of flux in the absence of diffusion limitations is provided by the following equation (Shuler & Kargi, 1992):

$$J_s = \beta\left(C_{bulk} - C_{surface}\right) = D\frac{dC_s}{d\delta} = \frac{1}{Y_{X/S}}\frac{\bar{\mu}_m X C_s}{\left(K_m + C_s\right)}\delta \qquad 2.17$$

Yield coefficient (i.e. $Y_{X/S}$) is defined based on the amount of consumption of the limiting substrate such as glucose. At the end of the growth period, an apparent growth yield may be observed. Because conditions can alter patterns of substrate utilisation, the apparent growth yield is provided by:

$$Y_{X/s} = \frac{\Delta X}{\Delta C_s} = \frac{X - X_0}{C_{s0} - C_s} \qquad 2.18$$

A maintenance coefficient is used to describe the specific rate of substrate uptake for cellular maintenance when biomass production is negligible. The coefficient may be calculated by using equation 2.19.

$$m_s = \frac{\left(dC_s/dt\right)}{X} \qquad 2.19$$

2.3.4 Molecular transport of fluids in biofilms

Considering the volume element in Figure 2.6, where a fluid flows through the element, a material balance is needed for a component of the fluid applicable to a differential fluid volume of this type (Treybal, 1980):
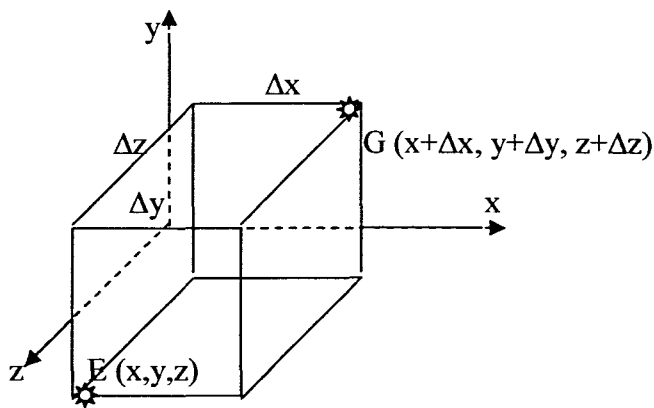
Figure 2.6: An elemental fluid volume (Treybal, 1980).

The mass rate of flow of a substrate into the three faces with a common corner at E is (Treybal, 1980):

$$M_s \left[(N_s)_x \Delta y \Delta z + (N_s)_y \Delta x \Delta z + (N_s)_z \Delta x \Delta y \right] \qquad 2.20$$

Similarly, the mass rate of flow out of the three faces with common corner G:

$$M_s \left[(N_s)_{x+\Delta x} \Delta y \Delta z + (N_s)_{y+\Delta y} \Delta x \Delta z + (N_s)_{z+\Delta z} \Delta x \Delta y \right] \qquad 2.21$$

The total component A in the element is $\Delta x \Delta y \Delta z \rho_s$, and its rate of accumulation is therefore,

$\Delta x \Delta y \Delta z \dfrac{\partial \rho_s}{\partial \theta}$. If, in addition, a substrate is generated by a chemical reaction at the rate

r_s (mol/volume. time), its production rate is $M_s r_s \Delta x \Delta y \Delta z$ (mass/time). In general, (Treybal, 1980):

Rate out – Rate in + Rate of accumulation = Rate of generation   2.22

Dividing by $\Delta x \Delta y \Delta z$ and taking the limit at the three distances, ($x; y; z$) gives:

$$M_s \left[\frac{\partial (N_s)_x}{\partial x} + \frac{\partial (N_s)_y}{\partial y} + \frac{\partial (N_s)_z}{\partial z} \right] + \frac{\partial \rho_s}{\partial \theta} = M_s r_s \qquad 2.23$$

From the balance for the substrate in one dimension (x-direction), it can be deduced that (Treybal, 1980):

$$M_s \frac{\partial (N_s)_x}{\partial x} = u_x \frac{\partial \rho_s}{\partial x} + \rho_s \frac{\partial u_x}{\partial x} + M_s \frac{\partial (J_s)_s}{\partial x} = u_x \frac{\partial \rho_s}{\partial x} + \rho_s \frac{\partial u_x}{\partial x} \\ - M_s D \frac{\partial^2 C_s}{\partial x^2} \qquad 2.24$$

Then the solution of equation 2.23 in 3 dimensions (x, y, z), assuming that the solution's density is constant, is given in equation 2.25 (Treybal, 1980):

$$u_x \frac{\partial C_s}{\partial x} + u_y \frac{\partial C_s}{\partial y} + u_z \frac{\partial C_s}{\partial z} = D \left(\frac{\partial^2 C_s}{\partial x^2} + \frac{\partial^2 C_s}{\partial y^2} + \frac{\partial^2 C_s}{\partial z^2} \right) + r_s \qquad 2.25$$

2.3.5 Diffusion coefficient and diffusivity

For diffusion of a solute through a solvent, the diffusion coefficient depends on the temperature, the type of solvent and its viscosity as well as the concentration of solute in solution. Diffusivities in liquid and gasses generally increase with temperature. Oxygen diffusion coefficients in water, at different temperatures, are shown in the Table 2.1 (Perry & Green, 1997).

Table 2.1: Oxygen diffusion coefficient in water at different temperatures (Perry & Green, 1997).

Temperature (°C)	Diffusion coefficient (m²/hr)
20	7.09E-06
40	1.17E-05
50	1.44E-05
60	1.74E-05

2.3.6 Microsensor studies in biofilm systems

2.3.6.1 Microelectrodes to quantify mass transport rate

Since most biofilm reactions are mass transport limited, it was important to quantify mass transport rates in biofilm reactors. This task was difficult because mass transport rates vary from location to location. To visualise the distribution of mass transport rates throughout a biofilm, microelectrodes are required. Depending on the experimental arrangements used, the mass transport microelectrodes can measure: 1) local mass transport coefficient; 2) local effective diffusivity; and 3) local flow velocity (Lewandowski & Beyenal, 2001).

2.3.6.2 Computing kinetic parameters from substrate concentration profiles in biofilms using microelectrodes

The available computational procedure for determining the kinetic parameters of microbial metabolic reactions from the substrate concentration profiles require the assumption that biofilms are homogeneous (uniform), and not heterogeneous. For current conceptual models of biofilms and the mathematical models available to interpret microelectrode measurements, the researcher can minimize the effect of biofilm heterogeneity by selecting locations of microelectrode measurements (Lewandowski & Beyenal, 2001).

Measuring concentration profiles at the centre of large microcolonies minimizes the effect of biofilm heterogeneity on the lateral mass transport to the location of the measurement. Measuring substrate concentration profiles near the centres of large microcolonies minimises the effect of non-uniform distribution of biomass at the location of the measurement. Such biased selection of the location for measuring substrate concentration is entirely acceptable when the purpose of the electrode measurement is to estimate biokinetic parameters of the biofilm. Assuming that the biofilms are uniform, and that mass transport in biofilms is one dimensional, normal to the substratum, the continuity equation below can be used to model mass transport and reaction in biofilms (Lewandowski & Beyenal, 2001):

$$\left(\frac{dC_s}{dt}\right)_f = D\left(\frac{d^2C_s}{d\delta^2}\right)_f - \frac{r_m C_s}{K_m + C_s} \qquad 2.26$$

The first term on the right side corresponds to the mass transport resistance within the biofilm, which is assumed to be diffusive and to follow Fick's law of mass transport. The second term corresponds to the substrate utilisation (reaction), which is assumed to follow Monod Kinetics (Lewandowski & Beyenal, 2001).

2.4   NUTRIENT CONVECTIVE FLOW PROFILES

2.4.1   Differential analysis of fluid flow

The equations of motion can be derived, either by application of Newton's second law to an element of fluid, or by the application of the impulse-momentum principle for control volumes. The derived equations are known (e.g. Hagen Poiseuilles flow) to accurately represent the flow physics for Newtonian fluids, including three-dimensional unsteady flows with variable density (Street *et al.*, 1996). These equations are known as Navier-Stokes equations.

2.4.1.1 Navier-Stokes equations for three dimensional flow

The equations of motion, when combined with conservation of mass equations, provide a complete mathematical description of the flow of incompressible, Newtonian fluids. Unfortunately, because of the general complexity of the equations (they are nonlinear, second order, partial differential equations), they are not amenable to exact mathematical solutions, except in a few instances. However, in those few instances in which solutions have been obtained and compared with experimental results, the results have been in close agreement, thus the Navier-Stokes equations are considered to be the governing equations of motion for incompressible, Newtonian fluids (Young *et al.*, 1997).

In terms of cylindrical polar coordinates, the equation can be written as (Young *et al.*, 1997):

r-direction:

$$\rho \left(\frac{\partial u_r}{\partial t} + u_r \frac{\partial u_r}{\partial r} + \frac{u_\theta}{r} \frac{\partial u_r}{\partial \theta} - \frac{u_\theta^2}{r} + u_z \frac{\partial u_r}{\partial z} \right) = -\frac{\partial P}{\partial r} + \rho g_r +$$
$$\mu \left[\frac{1}{r} \frac{\partial}{\partial r} \left(r \frac{\partial u_r}{\partial r} \right) - \frac{u_r}{r^2} + \frac{1}{r^2} \frac{\partial^2 u_r}{\partial \theta^2} - \frac{2}{r^2} \frac{\partial u_\theta}{\partial \theta} + \frac{\partial^2 u_r}{\partial z^2} \right]$$

2.27

θ-direction:

$$\rho\left(\frac{\partial u_\theta}{\partial t} + u_r\frac{\partial u_\theta}{\partial r} + \frac{u_\theta}{r}\frac{\partial u_\theta}{\partial \theta} + \frac{u_r u_\theta}{r} + u_z\frac{\partial u_\theta}{\partial z}\right) = -\frac{1}{r}\frac{\partial P}{\partial \theta} + \rho g_\theta +$$

$$\mu\left[\frac{1}{r}\frac{\partial}{\partial r}\left(r\frac{\partial u_\theta}{\partial r}\right) - \frac{u_\theta}{r^2} + \frac{1}{r^2}\frac{\partial^2 u_\theta}{\partial \theta^2} - \frac{2}{r^2}\frac{\partial u_r}{\partial \theta} + \frac{\partial^2 u_\theta}{\partial z^2}\right]$$

2.28

z-direction:

$$\rho\left(\frac{\partial u_z}{\partial t} + u_r\frac{\partial u_z}{\partial r} + \frac{u_\theta}{r}\frac{\partial u_z}{\partial \theta} + u_z\frac{\partial u_z}{\partial z}\right) = -\frac{\partial P}{\partial z} + \rho g_z +$$

$$\mu\left[\frac{1}{r}\frac{\partial}{\partial r}\left(r\frac{\partial u_z}{\partial r}\right) + \frac{1}{r^2}\frac{\partial^2 u_z}{\partial \theta^2} + \frac{\partial^2 u_z}{\partial z^2}\right]$$

2.29

2.4.1.2 Differential form of continuity equation

For certain problems it is more convenient to express the various differential relationships in cylindrical coordinates rather than Cartesian plane. The use of cylindrical coordinates is particularly convenient when the boundaries of the flow system are cylindrical. The differential form of the continuity equation in cylindrical coordinates is (Young *et al.*, 1997):

$$\frac{\partial \rho}{\partial t} + \frac{1}{r}\frac{\partial (r\rho u_r)}{\partial r} + \frac{1}{r}\frac{\partial (\rho u_\theta)}{\partial \theta} + \frac{\partial (\rho u_z)}{\partial z} = 0$$

2.30

And for incompressible fluids at a steady or unsteady state:

$$\frac{1}{r}\frac{\partial (r u_r)}{\partial r} + \frac{1}{r}\frac{\partial (u_\theta)}{\partial \theta} + \frac{\partial (u_z)}{\partial z} = 0$$

2.31

Steady, incompressible, two-dimensional plane flow represents one of the simplest types of flow of practical importance. Plane, two-dimensional flow means that there are only two velocity components. For this flow, the continuity equation reduces to (Young *et al.*, 1997):

$$\frac{\partial (u_r)}{\partial r} + \frac{\partial (u_z)}{\partial z} = 0 \qquad\qquad 2.32$$

2.4.1.3 Solution of Navier-Stokes in one dimensional flow

The flow of a fluid through a vertical fibre with a circular cross sectional is shown in Figure 2.7. To treat this problem, the following assumptions and conditions will be considered to be valid (Young *et al.*, 1997):

1.   The fluid is Newtonian and the flow is incompressible and at steady state.

2.   The flow has developed, i.e. considering a pipe section that is far enough from the entrance and exit sections so that the velocity profile has become unidirectional, $u_z \neq 0$, $u_r = u_\theta = 0$, with a velocity that exhibits angular symmetry.
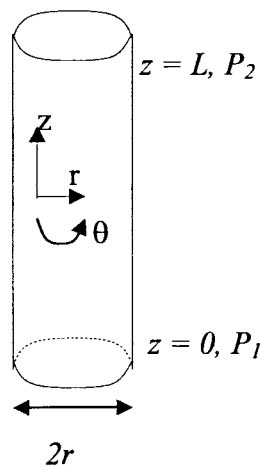
Figure 2.7: Coordinate system and geometry flow in a vertically placed membrane (Young *et al.*, 1997).

For vertical systems, the continuity and Navier-Stokes equations simplify to:

1.   Continuity equation:

$$\frac{\partial u_z}{\partial z} = 0 \qquad\qquad 2.33$$

2. Navier- stokes equations:

r – Direction: $\quad \dfrac{\partial P}{\partial r} = 0$ $\hspace{6cm}$ 2.34

θ - Direction: $\quad \dfrac{\partial P}{\partial \theta} = 0$ $\hspace{6cm}$ 2.35

z– Direction: $\quad -\dfrac{\partial P}{\partial z} + \rho g_z + \mu \dfrac{1}{r}\dfrac{\partial}{\partial r}\left(r\dfrac{\partial u_z}{\partial r} \right) = 0$ $\hspace{2cm}$ 2.36

Equation 2.36 can be rearranged to provide:

$$\dfrac{\partial P}{\partial z} - \rho g_z = \mu \dfrac{1}{r}\dfrac{\partial}{\partial r}\left(r\dfrac{\partial u_z}{\partial r} \right) \hspace{4cm} 2.37$$

The R.H.S is a function of r, while the L.H.S is the function of z and both r and z are independent variables (with partial differential equations to complete differential functions); this means that both sides are equal to a constant (Young *et al.*, 1997) i.e.,:

$$\dfrac{dP}{dz} - \rho g_z = const. \hspace{4cm} 2.38$$

$$\mu \dfrac{1}{r}\dfrac{d}{dr}\left(r\dfrac{du_z}{dr} \right) = const. \hspace{4cm} 2.39$$

Integrating equation 2.38 leads to:

$$P = \left(const. + \rho g_z \right)z + a_1 \hspace{4cm} 2.40$$

27

The constants a_1 (integration constant) and *const.*, can be found in terms of the pressures at the inlet and outlet of the membrane where, $z = 0(P = P_1)$ and $z = L(P = P_2)$. Applying the two conditions lead to:

1. $a_1 = P_1$

2. $const = -\left(\dfrac{\Delta P}{L} + \rho g\right)$

Where, $\Delta P = P_1 - P_2$

Substituting the value of *const.* into Equation 2.39 separating and integrating twice leads to (Young *et al.*, 1997):

$$u_z = -\frac{1}{4\mu}\left(\frac{\Delta P}{L} + \rho g\right)r^2 + a_2 \ln r + a_3 \qquad\qquad 2.41$$

Where a_2 and a_3 are integration constants, and can be determined by applying the following boundary conditions (Young *et al.*, 1997):

1. At $r = 0$, u_r is finite, therefore $a_2 \to 0$; and

2. At the solid surface a no-slip condition is imposed, $r = R_L$, $u_z = 0$.

Therefore, $a_3 = \dfrac{R_L^2}{4\mu}\left(\dfrac{\Delta P}{L} + \rho g\right)$

Equation 2.41 becomes:

$$u_z = \frac{1}{4\mu}\left(\frac{\Delta P}{L} + \rho g\right)(R_L^2 - r^2) \qquad\qquad 2.42$$

Equation 2.42 describes the axial velocity profile within the fibre. The volumetric flow rate can be found by integrating the velocity throughout the cross-sectional area of the fibre, which leads to equation 2.43.

$$Q = \frac{\pi R_L^4}{8\mu}\left(\frac{\Delta P}{L} + \rho g\right)$$

2.43

This equation is known as the Hagen-Poiseuille equation. It can be regarded that the flow is a result of two possible mechanisms, namely the pressure drop in the direction of the flow, as well as gravitational force.

2.4.2 Convective flow model development in hollow fibres

The continuity and momentum equations for steady-state flow developed from the Navier stokes equations in one dimensional coordinates in the fibre lumen and shell, are given in dimensionless form by Kelsey *et al.* (1990), as:

$$\frac{\partial V_z}{\partial \overline{X}} + \frac{1}{R}\frac{\partial(RV_r)}{\partial R} = 0$$

2.44

$$\frac{1}{R}\frac{\partial}{\partial R}\left(R\frac{\partial V_z}{\partial R}\right) = \frac{dP_L}{d\overline{X}}$$

2.45

Equations 2.44 and 2.45 are subject to symmetry conditions at the fibre centre, where $R = 0$. At this point, the radial velocity is negligible $(\partial V_r/\partial R = 0)$. The symmetry conditions are valid if the flows in all fibres in the multi capillary module are assumed to be identical. No slip conditions are applied at the lumen-matrix $R = 1$, where $V_z = 0$.

The pressure drop across the ultra-thin skin is given by Darcy's law as (Kelsey *et al.*, 1990):

$$V_r = \hat{K}(P_L - P_m)$$

2.46

The radial velocity is continuous across the lumen-matrix, thus:

$$V_r = \varepsilon u_m$$

2.47

Since the lumen pressure drop is only a function of dimensionless axial coordinate ($\overline{X}$), equation 2.45 can be integrated twice with respect to dimensionless radial coordinate (R), to give dimensionless axial velocity as (Kelsey et al., 1990):

$$V_z = -\frac{1}{4}(1 - R^2)\frac{dP_L}{d\overline{X}}$$

2.48

The dimensionless radial velocity is then evaluated by using equation 2.44 to give:

$$V_r = \frac{R}{16}(2 - R^2)\frac{d^2 P_L}{d\overline{X}^2}$$

2.49

The radial velocity given by equation 2.49 can be substituted into equation 2.46 to give the following second order differential equation, which describes the lumen pressure drop across the lumen radius, where $R = 1$ (Kelsey et al., 1990):

$$\frac{d^2 P_L}{d\overline{X}^2} = 16\hat{K}(P_L - P_m) = 16\varepsilon u_m$$

2.50

2.5   HOLLOW FIBRE MEMBRANE BIOREACTORS

A membrane bioreactor is a device used to conduct chemical reactions by using microorganisms or enzymes immobilised on a porous membrane. Four major membrane bioreactor formats have evolved which are currently researched or applied. They are: 1) biomass retention bioreactors; 2) bubbles oxygenation bioreactors; 3) fixed film bioreactors; and 4) extractive membrane bioreactors. The bioreactor used in this study is classified under fixed film bioreactors (Leukes, 1999).

Fixed film membrane bioreactors are operated in a mode in which the membrane acts as a support matrix for the biocatalyst. The biocatalyst can be a biofilm of living cells (bacteria, fungi or algae) resting. The membrane acts as a filtration barrier to provide the biofilm with sterile, low-molecular mass nutrients. This type of reactor is well suited for the high efficiency conversion of substrate into valuable products (e.g. enzymes). The high efficiency results from better mass transfer provided through nutrient perfusion. Further process efficiency is conferred through continuous operation over extended periods, active biomass retention and continuous product removal from the biofilm, thereby minimising product inhibition (Leukes, 1999).

The membranes which are used for the bioreactors can be capillaries, tubular membrane or hollow fibres constructed of organic polymers or ceramic materials, which are microfiltration membranes. Excellent results have been achieved in building single fibre capillary membrane bioreactors for continuous production of enzymes using ultrafiltration membranes (Leukes, 1999; Solomon, 2001; Garcin, 2002). The membrane structure was specially developed to provide a maximum surface area for the attachment of a biocatalyst. The biocatalyst can be situated on either the internal or external surface of the membrane, with the nutrient feed perfusing from the shell or lumen compartment (Leukes, 1999).

2.5.1 Membrane types

Microfiltration membranes are used to reject suspended solids, ultrafiltration membranes, which contain much smaller pores, and are able to reject macromolecular solutes in the molecular weight range of 10^{-3} to 10^{-6}. Membrane morphology may be classified into symmetric and asymmetric structures. The thickness of symmetric membranes (porous and nonporous) ranges roughly between 10 to 200 μm. Asymmetric membranes consist of a dense top layer (skin) with a thickness of 0.1 to 0.5 μm. These membranes combine the high selectivity of a dense membrane with the selectivity with a high permeation rate of a thin membrane (Howell *et al.*, 1993). According to Jacobs and Sanderson (1997), capillary membrane by definition, are narrow-bore tubular-type membranes, typically with an outside diameter, which ranges from 0.4 to 2.4 mm. Unlike the large-bore tubular membrane types, capillary membranes, because of their small diameters, are self-supporting. The capillary membranes (polysulphone) used by Garcin (2002) Solomon (2001) and Leukes (1999), fall in the category of integrally skinned asymmetric

membranes. Integrally skinned refers to the skin layer of the membrane being an integrated part of the membrane substructure. Asymmetric refers to the graded porosity of the membranes substructure, which is most dense just below the skin layer, but increasingly porous with distance away from the skin layer. The substructure is spongy-like, or it may contain finger-like microvoids (Jacobs & Leukes, 1996).

2.5.2 Polysulphone capillary membrane

The externally unskinned polysulphone membranes, which are used for projects (Garcin, 2002; Solomon, 2001; Leukes, 1999), provides a unique substructure matrix within which a fungus of a filamentous nature can be immobilised as a biocatalyst (Jacobs & Leukes, 1996). Jacobs and Leukes (1996) used the directive that the polysulphone membrane to be produced should allow the life cycle of the fungus to be manipulated in a membrane bioreactor, in order to stimulate the continuous production of enzymes, which are useful in the bioremediation of non-biodegradable organic species in water. The substructure contains closely-packed narrow-bore microvoids that extended all the way from just below the skin layer to the membrane periphery. An SEM photograph of a longitudinally section sample of the polysulphone internally skinned and externally unskinned membrane is shown in Figure 2.8.
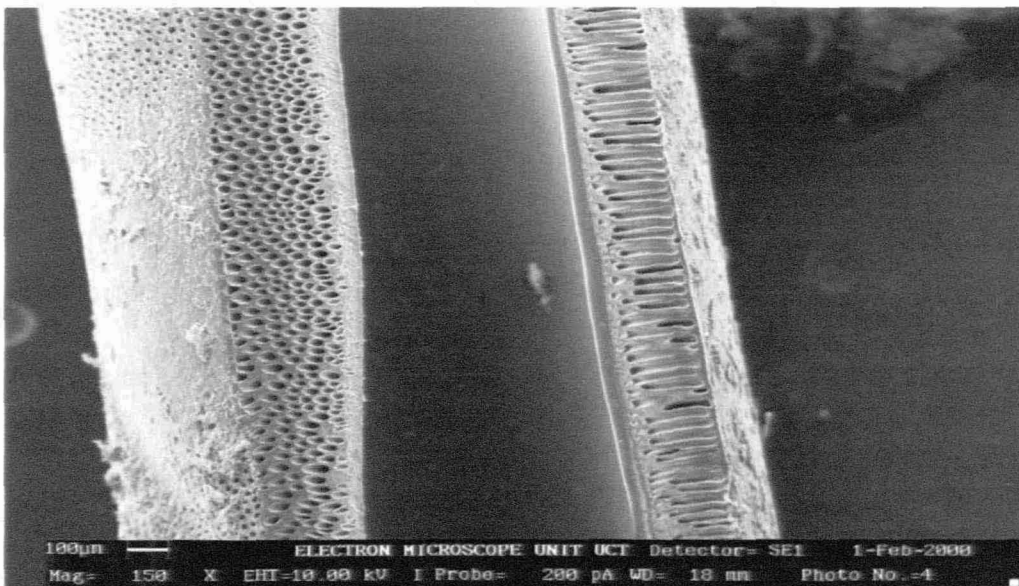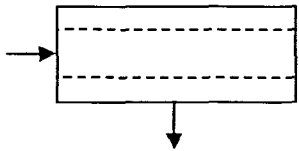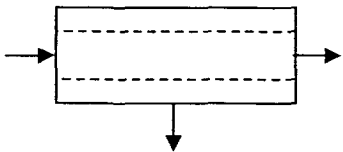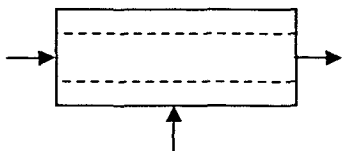
Figure 2.8: SEM of a longitudinal section of the polysulphone membrane taken from Solomon (2001).

The important feature of the polysulphone membrane was the regularity of the microvoids present in the substructure and the complete absence of the external layer, which will allow the microvoids to be inoculated with fungal spores by reverse filtration (Solomon, 2001).

2.5.3 Modes of operation for hollow fibre systems

In ultrafiltration, a feed stream is introduced to the fibre side and a permeate leaves continuously through a shell side port. The retentate flows out the down-stream end of the fibre. The following configurations were discussed by Bruining (1989).

Table 2.2: Different modes of operation for hollow fibre systems.

Permeation Process	Situation	Retentate (F_2)
Dead-end filtration		$F_2 = 0$
Continuous open-shell mode		$0 < F_2 < 1$
Closed shell mode		$F_2 = 1$
Suction of permeate		$F_2 > 1$

33

2.5.4 Applications for enzymes produced

2.5.4.1 Paper and pulp industry

Enzymes produced by *P. chrysosporium* have been investigated and, under the appropriate conditions, are capable of either degradation or polymerisation of lignin preparations (Tien and Kirk, 1984). Lignin by-products from the pulp bleaching process can be removed by enzyme enhanced biodegradation and by converting low molecular weight waste compounds into higher mass polymers, which could be more easily filtered out of the process stream for subsequent incineration or landfill. Presently, bleaching by-products are a major source of water pollution. Complicated and expensive treatment systems are currently used to eliminate as much waste as possible and can be replaced (Griselda & Eduardo, 1990; Livernoche *et al.*, 1981).

2.5.4.2 Gold industry

The enzyme produced has commercial applications in the mining industry to assist in the process of the extraction of gold from wooded supports, which are used underground by the mining industry. The large quantities of wood chips produced at mines from damaged underground timber, contain gold that cannot be completely recovered by cyanidation. *P. chrysosporium* and enzymes produced can degrade a portion of the wood matrix to allow the gold that was previously locked up, to come into contact with cyanidation solution during benefication, thereby improving recoveries (Martin, 2000).

2.6   SUMMARY

The WRF, *P. chrysosporium*, which degrades lignin with its extracellular oxidative process initiated by nitrogen and carbohydrate starvation, can be used to biodegrade aromatic pollutants both in liquid effluents and soils. Its extracellular enzymes, *LiP* and *MnP*, which are major compounds in the lignin degradation system, are produced as enzymes. Optimum growth conditions have been established at 39 °C, a pH of 4.0 - 4.5 and humid conditions. During fungal growth, the organism requires a source of fixed nitrogen and carbohydrates.

The growth cycle of microorganisms follows the following growth pattern: 1) lag phase; 2) accelerated growth; 3) exponential growth; 4) decelerated growth; 5) stationary phase; and 6) decline phase (death of the culture). By using a continuous reactor system, it is easier to keep the culture in the stationary phase and a gradostat will be established, as explained by Leukes (1999). A synthetic nutrient medium, developed by Kirk (1978) has been used to enhance growth and enzyme production. Additives such as surfactants Tween 20/80, oxygen and minerals (e.g. Cu and Zn) are used to optimise the nutrient medium (Govender, 2000).

Biofilms formed by microorganisms (fungi, algae and bacteria) are normally heterogeneous (i.e. features nonuniform distribution of cells). This was observed on a *P. chrysosporium* biofilm immobilised on a polysulphone membrane, which was classified as an externally unskinned asymmetric membrane. The rate of growth can be quantified by determining the biofilm density (which was a combination of water in cells and dry biomass), which can be described by a logistic curve. Substrate mass transfer, through the biofilm, is by convection and diffusion transport effects. The diffusion is related to the concentration gradient by Fick's law, while convection can be described by Navier-Stokes equations. Convective transport can be used to overcome the limitations imposed by diffusive mass transport, which was described by a differential equation for the limiting substrate.

Biofilm reactions are mass transport limited; therefore, it is important to quantify mass transport rates in biofilm reactors. To visualise the distribution of mass transport rates throughout biofilms, microsensors are required, which measure: 1) local mass transfer coefficient; 2) effective diffusivity; and 3) flow velocity. To determine biokinetic parameters in biofilms, the assumption that biofilms are homogeneous is considered and the researcher can minimise the effect of biofilm heterogeneity by selecting locations of microelectrode measurements. Convective nutrient flow in the fibre lumen is described by the continuity and momentum equations developed from three dimensional coordinates.

CHAPTER 3 : MATHEMATICAL MODELLING

3.1 INTRODUCTION

The MCMBR system of interest consists of a bundle of fibres, potted at both ends with epoxy resin and encased in a cylindrical cartridge. The fibres were arranged in a triangular pitch, as this arrangement provides for more membranes to be placed into the bioreactor, while providing space for biofilm growth. The models developed in this section provided a description of convective flow (through some average fibre that is representative of the overall system geometry) and mass transfer across the thickness of *P. chrysosporium* biofilms immobilised on a polysulphone membrane. Linearization techniques will be described to provide a clear description of how to evaluate various kinetic constants from standard equations.

3.2 MOMENTUM TRANSFER IN THE MEMBRANE LUMEN

In this application nutrient flow behaviour, through the lumen of the polysulphone hollow fibre membrane, was a convective process only, as nutrient supply was by a peristaltic pump at a known flow rate. The flow models were developed for vertical systems, similarly to those developed by Kelsey *et al.* (1990), as shown in section 2.4.

3.2.1 Momentum transfer models

For steady or unsteady flow, the flow is incompressible with constant density, while considering axial (z-direction) and radial (r-direction) flow only, the continuity equation is given by (Kelsey, 1990):

$$\frac{\partial u_z}{\partial z} + \frac{1}{r}\left[\frac{\partial(r u_r)}{\partial r}\right] = 0 \qquad 3.1$$

In terms of the cylindrical polar coordinates, the Navier-Stokes equation can be written as (z/axial direction):

$$\rho\left(\frac{\partial u_z}{\partial t} + u_r\frac{\partial u_z}{\partial r} + \frac{u_\theta}{r}\frac{\partial u_z}{\partial \theta} + u_z\frac{\partial u_z}{\partial z}\right) = -\frac{\partial P}{\partial z} + \rho g_z + \mu\left[\frac{1}{r}\frac{\partial}{\partial r}\left(r\frac{\partial u_z}{\partial r}\right) + \frac{1}{r^2}\frac{\partial^2 u_z}{\partial \theta^2} + \frac{\partial^2 u_z}{\partial z^2}\right]$$

3.2

Equation 3.2 was considered to be the governing differential equation of motion for incompressible, Newtonian fluids, which flowing in the axial direction between two parallel plates. The following conditions were considered to prevail in the system (vertically placed hollow fibre membranes):

1.　$\frac{\partial u_z}{\partial t} = 0$ (Steady laminar flow through fibres).

This condition was assumed to prevail as a peristaltic pump continuously supplies nutrient feed at a constant rate.

2.　$\frac{\partial u_z}{\partial \theta} = 0$; $\frac{\partial u_r}{\partial r} \approx 0$　$u_r = 0$ (Bulk flow in the z direction only).

Bulk flow is unidirectional (in the z direction), with radial flow being very small (due to low membrane permeability), compared to axial flow.

3.　$\frac{\partial u_z}{\partial z} = 0$ (Reduction of continuity equation, considering condition 2 above).

4.　$\rho g_z \approx 0$ (The hydrostatic pressure in single capillary membrane systems operated at dead-end filtration mode, which was considered negligible compared to gauge pressure).

From the above conditions the following momentum equation can be deduced:

$$\frac{\partial P}{\partial z} = \mu\left[\frac{1}{r}\frac{\partial}{\partial r}\left(r\frac{\partial u_z}{\partial r}\right)\right]$$

3.3

37

The solution of the momentum equation was obtained by separating and integrating twice (see Appendix E1). The integration constants are evaluated by physical conditions, i.e., 1) at the solid surface, no slip conditions prevail; and 2) while at the lumen centre, symmetry conditions are applied within the operating parameters. The axial velocity profile developed from the momentum equation in appendix E1, which was then given by:

$$u_z = \frac{1}{4\mu}\left(r^2 - R_L^2\right)\frac{dP}{dz}$$ 3.4

Equation 3.4 was rewritten in a differential format for axial velocity profiles as shown in equation 3.5. The profiles, which were generated, were evaluated at different axial positions on the hollow fibre membrane.

$$\frac{du_z}{dr} = \frac{r}{2\mu}\frac{dP}{dz}$$ 3.5

The solution of equation 3.1 was determined by using equation 3.4 to obtain the radial velocity profile equation (equation 3.6), which was evaluated at different axial positions on the membrane.

$$u_r = -\frac{1}{16\mu}\left(r^3 - 2rR_L^2\right)\frac{d^2P}{dz^2}$$ 3.6

The equation was rewritten in a differential format similarly to equation 3.5.

$$\frac{du_r}{dr} = \frac{1}{16\mu}\left(2R_L^2 - 3r^2\right)\frac{d^2P}{dz^2}$$ 3.7

As shown in Chapter 2 (literature review), Kelsey et al. (1990) developed the relationship between the lumen radial velocity, and the fibre matrix velocity as shown in equation 3.8:

$$u_r = \varepsilon u_m = \hat{K}_p\left(P - P_s\right) \text{ At } r = R_L$$ 3.8

Where ε is the porosity of the inner lumen skin, at the lumen-matrix inter-phase ($r = R_L$), equation 3.6 was then reduced to:

$$u_r = \frac{R_L^3}{16\mu} \frac{d^2 P}{dz^2}$$

3.9

Therefore, the radial velocity profile in the fibre matrix was described by the following differential equation:

$$u_m = \frac{R_L^3}{16\mu\varepsilon} \frac{d^2 P}{dz^2}$$

3.10

Considering the thickness of the fibre matrix (l_m), the following differential equation was developed (can be evaluated at different axial positions):

$$\frac{du_m}{dl_m} = \frac{R_L^3}{16\mu\varepsilon} \frac{d^2 P}{dz^2}$$

3.11

3.2.2 Solution to the second-order differential equation

From section 3.2.1, the axial velocity profile was given by:

$$u_z = \frac{1}{4\mu}\left(r^2 - R_L^2\right)\left(\frac{dP}{dz}\right)$$

3.12

The volumetric flow rate can be found by integrating the velocity profile throughout the cross section of the membrane (similar to the solution of the Navier-stokes equations in one-dimensional flow, (see Appendix E1) :

$$Q = \int_A u_z \, dA$$

3.13

The solution developed was (see appendix E1):

$$\frac{dP}{dz} = \left(\frac{8Q\mu}{\pi R_L^4} \right)$$

3.14

From equation 3.8 and 3.9, the following relationship between the lumen radial velocity profile and the membrane permeability (at $r = R_L$) was developed as:

$$u_r = \frac{R_L^3}{16\mu} \frac{d^2 P}{dz^2} = \hat{K}_p (P - P_s)$$

3.15

Therefore, $\quad \dfrac{d^2 P}{dz^2} = \omega (P - P_s)$

3.16

Where $\omega = \dfrac{16\mu \hat{K}_p}{R_L^3}$.

The solution of the second order differential equation, in terms of complimentary function and particular integral, was given by equation 3.17, with the following initial conditions; 1) $P(z = 0) = P_1$, 2) $dP/dz(z = 0) = 0$. The solutions of the constants are shown in Appendix E1. The solution to the second order differential equation was as shown in equation 3.17:

$$P = (P_1 - P_s)\cosh(\sqrt{\omega} z) + P_s$$

3.17

3.2.3 Evaluation

The following pressure drop equations (equations 3.18 and 3.19) were used to simulate pressure profiles by using an ordinary differential solver (e.g. Polymath 5.1) in SFCMBR, thus solving axial and radial velocity profile equations which were generated.

$$\frac{dP}{dz} = (P_1 - P_s)\sqrt{\omega}\sinh(\sqrt{\omega}z)$$
3.18

$$\frac{d^2P}{dz^2} = (P_1 - P_s)\omega\cosh(\sqrt{\omega}z)$$
3.19

3.3   OXYGEN MASS TRANSFER ACROSS THE BIOFILM

In this application, oxygen mass transfer was assumed to be a diffusion process only as the biofilm will be placed in direct contact with the gas phase. Diffusion is a phenomenon of mass transfer, i.e. diffusion operations involve the contact of either a gas or a liquid, accompanied by the transfer of material between the contacted phases.

3.3.1   Oxygen model

The oxygen distribution in the *P. chrysosporium* biofilms was simulated with the Monod equation with regard to oxygen consumption through biological reactions (for a detailed description see Appendix E2). The mass transfer equation for oxygen distribution in the biofilm was described by equation 3.20:

$$\frac{dC_{O_2}}{dt} = D_f\left(\frac{d^2C}{d\delta^2}\right)_f - \frac{k_{O_2}XC_{O_2}}{K_m + C_{O_2}}$$
3.20

At a steady supply of air to the bioreactor, it was assumed that the oxygen concentration which was available did not change $(\therefore dC/dt = 0)$. The consumption rate was computed to be equal to the diffusion rate as shown in equation 3.21:

$$D_f\left(\frac{d^2C_{O_2}}{d\delta^2}\right)_f = \frac{k_{O_2}XC_{O_2}}{K_m + C_{O_2}}$$
3.21

To solve kinetic constants in equation 3.21, the inverse of the equation was used to obtain a linear expression, as shown in equation 3.22, where the value of the Monod's saturation constant, K_m, was calculated by dividing the slope $\left(D_f K_m / k_{O_2} X\right)$ by the intercept $\left(D_f / k_{O_2} X\right)$:

$$\left(\frac{d^2 C_{O_2}}{d\delta^2}\right)_f^{-1} = \left(\frac{D_f K_m}{k_{O_2} X}\right)\frac{1}{C_{O_2}} + \frac{D_f}{k_{O_2} X} \qquad 3.22$$

3.3.2 Experimental profiles

By experimentally measuring the oxygen distribution in the biofilm at different depths by using an oxygen microsensor, the experimental profiles obtained were best fitted by an exponential equation with the format:

$$C_{O_2} = a_4 e^{-a_5 \delta} \qquad 3.23$$

Equation 3.23 was differentiated twice to obtain a second order deferential equation as shown in equation 3.24:

$$\left(\frac{d^2 C_{O_2}}{d\delta^2}\right) = a_4 a_5^2 e^{-a_5 \delta} \qquad 3.24$$

By plotting $1/\left(a_4 a_5^2 e^{-a_5 \delta}\right)$ against $1/C_{O_2}$, a trend-line was obtained. The gradients with high correlation coefficients were used to evaluate the kinetic constants.

3.3.3 Simulation

Using the calculated parameters $\left(D_f / k_{O_2} X\right)$ and K_m, the first derivative of oxygen concentration distribution across the biofilm was simulated by using Equation 3.25 (developed from Equation 2.16):

$$\frac{dC_{O_2}}{d\delta} = -\sqrt{2\frac{k_{O_2}X}{D_f}\left(C_{O_2} - K_m Ln\left(\frac{K_m + C_{O_2}}{K_m}\right)\right)}$$

3.25

3.4 NUTRIENT MASS TRANSFER ACROSS THE BIOFILM

Nutrient mass transfer in the biofilm matrix constitutes three distinct areas that are classified as constituents of mass transfer phenomena. The areas are: 1) convective nutrient transport closer to the substratum (membrane), as the nutrient medium was supplied by a peristaltic pump; 2) diffusion, which occurs further away from the substratum surface (see section 2.2.2.2); and 3) the biological reaction, which was assumed to follow Monod's equation.

Treybal (1980) has shown that the flow of a component in terms of 1) diffusion, 2) convection, 3) the rate of generation and 4) accumulation, in three dimensional coordinates is provided by equation 3.26:

$$u_x \frac{\partial C_s}{\partial x} + u_y \frac{\partial C_s}{\partial y} + u_z \frac{\partial C_s}{\partial z} + \frac{\partial C_s}{\partial \theta} = D\left(\frac{\partial^2 C_s}{\partial x^2} + \frac{\partial^2 C_s}{\partial y^2} + \frac{\partial^2 C_s}{\partial z^2}\right) + r_B \quad 3.26$$

Where r_B is the biological generation,

$\dfrac{\partial C_s}{\partial \theta}$ is the accumulation of the substrate.

Equation 3.26 was adjusted for substrate flow through a fungus matrix, which was situated in a vertical position. The following general conditions were considered:

1. Substrate consumption was in terms of the biological reaction, therefore,

$$r_B = -\frac{k_s X C_s}{K_m + C_s}$$

2. Mass transfer was one-dimensional (z direction, i.e. across the biofilm) and there was no accumulation of substrate in the biofilm, therefore $(\partial C_s / \partial \theta) = 0$.

43

The equation was then reduced to:

$$u_z \frac{\partial C_s}{\partial z} = D\left(\frac{\partial^2 C_s}{\partial z^2}\right) - \frac{k_s X C_s}{K_m + C_s} \qquad 3.27$$

Two distinctive regions were identified in the biofilm. The two regions were classified as: 1) convection dominant area; and 2) diffusion dominant area. The mass transfer in the two regions was modelled by using different mathematical models for the sake of simplicity.

3.4.1 Convection dominant area

The maximum rate of flux, in the absence of diffusion limitations, was given by equation 3.28, as developed from equation 3.27.

$$-\frac{dC_s}{dz}\Big|_{z=\delta} = u_z \frac{k_s X C_s}{K_m + C_s} \delta \qquad 3.28$$

Experimental concentration profiles were evaluated across a certain biofilm thickness and parameters, such as the Monod's saturation constant, were evaluated (similar to the oxygen profiles) and then used in the simulation model by using a first order differential solver to obtain appropriate curves.

3.4.2 Diffusion dominant area

Equation 3.28 is then reduced to:

$$D\frac{d^2 C_s}{dz^2}\Big|_{z=\delta} = \frac{k_s X C_s}{K_m + C_s} \qquad 3.29$$

The equation was evaluated similar to the oxygen concentration profile using the mass balance equation (equation 2.15) developed by Frank-Kamenetskii (1969).

3.5 LINEARIZATION TECHNIQUES

A standard equation used to express kinetic constants, under the Michaelis-Menton hypothesis, as shown in equation 3.30, can be rearranged to generate other useful equations (Shuler & Kargi, 1992):

$$r_B = \frac{r_m C_s}{K_m + C_s}$$

3.30

There are two ways in which the hyperbolic relationship between the rate of reaction and substrate concentration can be arranged to give linear plots. Plots shown in Figures 3.1 and 3.2 were taken from Shuler and Kargi (1992).

(a) Lineweaver-Burk (double reciprocal) plot of $1/r_B$ against $1/C_s$ providing intercepts at $1/r_m$ and $-1/K_m$:

$$\frac{1}{r_B} = \frac{K_m}{r_m} * \frac{1}{C_s} + \frac{1}{r_m}$$

3.31
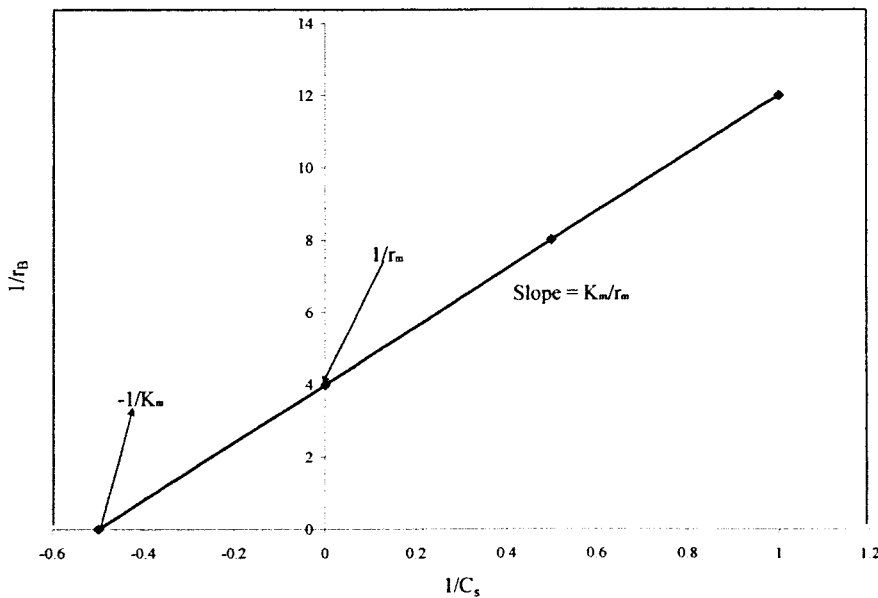
Figure 3.1: Lineweaver-Burk plot (Shuler & Kargi, 1992).

(b) Eadie-Hofstee plot of r_B against r_B / C_s providing intercepts at r_m and r_m / K_m:

$$r_B = -K_m * \frac{r_B}{C_s} + r_m$$

<div align="right">3.32</div>
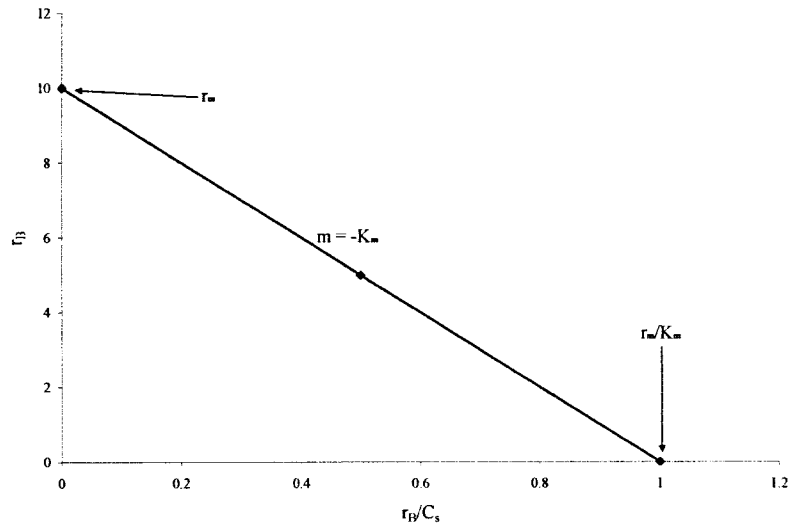
Figure 3.2: Eadie-Hofstee plot (Shuler & Kargi, 1992).

CHAPTER 4 : BIOREACTOR DESIGN

4.1   INTRODUCTION

The design of a bioreactor system includes a series of decisions on matters, which range from microbiology to process engineering. All these disciplines contribute to making possible the proper determination of the bioreactor system and its correct dimensions in order to provide an optimal environment for operation. The key issues for the bioreactor system, which was designed, were related to a series of concepts clarified for each specific case, among which optimal biomass density and specific rate of oxygen uptake, were of outmost importance. In this chapter the main concepts in the design are described and references are made to work done by other researchers.

The actual design of the multicapillary membrane bioreactor (MCMBR) was based on the kinetic expressions that were obtained in SFCMBR systems. In preliminary studies a six-membrane MCMBR was operated in the horizontal position, based on a SFCMBR design, as was done by various researchers (Leukes, 1999; Solomon, 2001; Garcin, 2002). This MCMBR was used to identify parameters and significant problems, which affected the design. The new bioreactor, which was designed, sought to optimise overall efficiency, with known biofilm growth kinetics and substrate mass transfer parameters. Controllable factors, which affected the bioreactor's performance, needed to be accurately controlled and the effect of uncontrollable variables needed to be minimised.

4.2   FEATURES OF MEMBRANE MODULES

4.2.1   Membrane characterisation

Choosing the correct membrane for a specific bioprocess is crucial to bioreactor performance. The membrane should be compatible with the organisms that will be used in the bioreactor and should have suitable properties and filtration characteristics. The most suitable membrane will lead to optimal bioreactor performance (Asenjo & Merchuk, 1995).

The type of membrane used in the SFCMBR systems was specifically developed for this purpose by Jacobs and Leukes (1996) and its suitability for the growth of fungal biofilms was tested by Ryan *et al.* (1998). It was manufactured at the Institute of Polymer Science, University of Stellenbosch and is coded as IPS 763. The membrane is an externally unskinned polysulphone capillary membranes (ID = 1.395mm, OD = 1.925). The advantage of this kind of membrane is that it has a: 1) large surface to volume ratio; 2) self-supporting structure with good mechanical strength; 3) broad chemical compatibility; 4) a wide pH range (1-14); and 5) good temperature resistance (Scott, 1996).

4.2.2   Factors affecting membrane attached biofilms

It should be noted that the conditions that are optimal for biomass accumulation are not necessarily the same as those for secondary metabolite production. Three main factors have been identified as being relevant and which fundamentally affects the growth and enzyme production of biofilms, which are cultivated on hollow fibre membranes. These factors are: 1) transmembrane nutrient flux; 2) the extracapillary gaseous phase; and 3) the extracapillary fluid regime (Garcin, 2002).

4.2.2.1 Transmembrane nutrient flux

The gradostat system is unique in that nutrients can be supplied in a convective manner through the membrane lumen and into the biofilm, and can thus be theoretically, accurately controlled. It has been assumed that there is no resistance to convective solute transport across the membrane, as the nutrients are relatively small compared to membrane pores (MWCO ~30 kDa, nutrient << 30 kDa) (Garcin, 2002).

Garcin (2002) performed dead-end flow experiments to evaluate permeate flux distribution due to pressure effects in SFCMBR. The permeate flux was measured at various points along the capillary length.   A considerable variation of flux along the fibre length, as well as between different fibres, was observed. This was ascribed to the local variation of membrane permeability, and not to axial pressure gradient.

The variation of membrane permeability (both along the membrane length and between different membranes) was a cause for concern, as this resulted in a significant flux maldistribution leading to uneven biofilm growth, which was perceived to severely affect the productivity of the SFCMBR systems and reproducibility of results. In cross flow experiments, as the biofilm grew, more pressure was required for appropriate nutrient flux, leading to a poor gradostat system. This can contribute to poor biofilm densities, which will result in biofilm sloughed off by air even at lower flow rates. Garcin (2002) observed that local nutrient concentrations varied with axial position in clean membranes. Membranes with high permeability appeared to achieve better and uniform nutrient concentrations along the axial length. It was postulated that the variation of nutrient concentration was the restriction of molecule transport through the pores due to the variation of pore size and pore distribution (Garcin, 2002).

According to various researchers (Asenjo and Merchuk, 1995; Thakaran & Chau, 1986), the growth medium can circulate by diffusing across the hollow fibre membranes in cross flow configuration, then be converted by cell suspension into an extracellular product and diffuses back into the lumen. This was clearly not suitable for the purposes of the gradostat bioreactor. The dead-end ultrafiltration mode was, therefore, decided upon for application of the gradostat system. The liquid medium needs to be sterile, quantifiable (in terms of supply rate and composition) and supplied in a manner that produces the most uniform permeate flow possible, minimises axial gradients, has a high enough permeation rate to provide a thick biofilm, but low enough so that nutrient gradients could be established and biofilm washout would not occur. The biofilm produced was required to be thick enough so that the gradostat concept can be attained (Leukes, 1999).

4.2.2.2 The extracapillary gaseous phase

The gaseous phase is generally oxygen or air and is important because it determines the diffusion of oxygen into the biofilm. Several factors can affect this, such as the volumetric flow rate, pressure, temperature, oxygen concentration and whether the flow is turbulent or laminar. The oxygen/air concentration stream is also responsible for sloughing off dead fungal matter; hence the volumetric flow rate is perceived to play an important role in the determination of steady state active thickness. It should not be high enough to cause shear damage to the biofilm. Another

aspect is whether the flow is perpendicular to the fibres. For a specific flow rate, the hydrodynamic boundary layer is thicker when the flow is parallel (Douglass *et al.*, 1986). This implies that oxygen mass transfer is better when the flow is perpendicular (as the air will be forced directly onto the biofilm at a 90° angle), although the effects (e.g. sloughing) on the biofilm will be greater (Garcin, 2002).

4.2.2.3 The extracapillary fluid regime

A uniform hydrodynamic boundary layer external to the capillary, but retained within the biofilm, is perceived to be the optimal situation for the creation of radial nutrient gradients. On a horizontal membrane this might not be the case due to uneven permeation rates across the length of the capillaries and the random droplet formation, which results in uneven growth. Vertical fibres have the added advantage that permeate will proceed down the length of the membrane and not create droplets as is the case with horizontal fibres. This is an important factor in multi-capillary modules (horizontally placed), as falling droplets from the top membranes could interfere with biofilms on the membranes below and this could reduce bioreactor performance (Garcin, 2002).

4.3   PARAMETERS (DATA) FOR BIOREACTOR DESIGN

The data required for the MCMBR bioreactor design, (listed in sections 1.2.1 to 1.2.4), was obtained and used to properly select and design an appropriate bioreactor. Accurate determination of parameters is essential in a bioreactor design, as this will determine how accurately the results (output) are reproduced. The design of the bioreactor should be within given (known parameters established by other researchers) parameters for continuous enzyme production. In this section, known data/parameters were tabled, while unknown data was obtained by performing experiments.

4.3.1 Microorganism species

The *P. chrysosporium* strain BKMF 1767 (ATCC 24725) was the fungus, which was chosen for use in the bioreactor. This strain was chosen for its fast growth and secondary metabolite production. The organism is a mesophile (growth at 10 to 47 °C, optimum 30 to 45 °C) and a pH of 4.5. Cell lyses is particular important in the case of *P. chrysosporium* since up to 40% of biomass can be lost due to cell lyses in the decline phase (Leukes, 1999).

4.3.2 Growth and oxygen requirements

P. chrysosporium is an aerobic organism. The maximal growth rate is dependent on oxygen availability, while the growth yield is dependent primarily on the substrate used. Garcin (2002), Solomon (2001) and Govender (2000) used 100% oxygen after initially supplying the fungi with air. There was a peak in enzyme concentration after which production descended rapidly to zero. According to Garcin (2002), it was possible that the oxygenation was excessive and oxidative stress killed the biofilm. Oxygen related mass transfer parameters were not determined for the systems used by Garcin (2002), Solomon (2001) and Govender (2000).

4.3.3 Bioreactor orientation

In preliminary experiments, wall growth was evident in horizontally placed bioreactors, which caused fungal growth in the permeate port compared to vertically placed bioreactors, as shown in Figure 4.1. Garcin (2002) indicated that in vertically operated systems, substrate utilisation was improved. Quantifying maximum or optimal biomass density for vertical bioreactors was not previously researched and was covered in this study.

(a)

(b)

Figure 4.1: Continuously operated SFCMBR systems after 14 days. (a) Horizontally placed bioreactor; and (b) Vertically placed bioreactor.

4.3.4   Cleaning, sterility and measurement system

Before each experiment, apparatus (tubing, beakers and water) were autoclaved. The MCMBR and SFCMBR was flushed with a 4% formaldehyde solution for at least six hours, and then rinsed with distilled, sterile water, as indicated by Garcin (2002), Solomon (2001) and Leukes (1999). Measurements of pH and redox potential, using a Hanna HI 8314 membrane pH meter, ammonia and glucose concentration, as well as enzyme production, were essential. Substrate consumption was used as an indirect method to determine different biofilm growth stages. Substrate concentration was measured for each sample; this was subtracted from the initial concentration and multiplied by the corresponding flux to provide glucose and ammonia, which were consumed by the biofilm. This information was used to better understand the function of *P. chrysosporium* in continuous systems and to monitor contamination.

4.4 BIOREACTOR REQUIREMENTS AND CONSTRAINTS

4.4.1 Bioreactor requirements

Any design process should meet certain requirements in terms of what the system should do (Garcin, 2002):

- Durability. The system should be able to operate trouble-free for extended periods of time (months);
- Consistency and reproducibility. The system should be able to operate repeatedly, giving the same results with minimal variation;
- Robustness. The system should be insensitive to small fluctuations of inputs; these should not cause large changes in outputs;
- Sterility. The system should not only be easy to sterilise, but should also be capable of long periods of operation without contamination;
- Visibility. It is desirable to be able to observe the biofilms inside the bioreactor;
- Versatility. It is desirable to be able to use the same design for many applications;
- Re-use. The system should be designed so that it can be dismantled, sterilised and used again. Components of the design should therefore, not be susceptible to fatigue;
- Ease of use. The design should not be overly complicated (so that personnel with limited technical training encounter difficulty with operations).
- Adequate control of the parameters. Flow rates, temperature and pressures should be accurately controlled and consistent; and
- Efficiency. The device should maximise productivity and yields.

4.4.2 Bioreactor constraints

Constraints list factors that should be met to keep the design possible and feasible, as indicated by (Garcin, 2002):

- Manufacturing cost. The system should be designed so that costs are kept to a minimum, i.e. it should be cheaper than stirred tank reactors;

- Operating costs. These should be kept to a minimum, particularly in terms of energy costs, which are required for operation;

- Manufacture. The design should be such that all components are readily (and preferably easily) manufactured. Care should be taken to avoid inaccessible corners and dead spaces to assist with easy sterilisation;

- Materials. Material for manufacturing should be readily available and should also be resistant to degradation (biological or chemical attack); and

- Strength. The bioreactor should be able to withstand operating temperatures and pressures without the danger of failure.

4.5 DESIGN AND CONSTRUCTION OF A LAB-SCALE MULTI-CAPILLARY MEMBRANE BIOREACTOR

The MCMBR system was designed so that nutrient flow to all membranes was even in order to sustain evenly grown biofilms for longer periods of time. This determined the orientation in which the system was operated. Other contributing factors considered in the design process for the system, were based on the literature reviewed for continuous enzyme production in single capillary membrane bioreactors, as listed in sections 4.2.2 and 4.3.

4.5.1 Design details

The bioreactor was designed so that it minimised problems, which were encountered in SFCMBR, used for continuous enzyme production by various researchers (Garcin, 2002; Solomon, 2001; Leukes, 1999). The bioreactor was operated vertically because in horizontally placed bioreactors, polysulphone membranes sagged as the biofilm density increased, while droplet formation on the biofilm caused the biofilm to detach and grow on the bioreactor wall as shown in Figure 4.1 (a). To further improve the supply of fresh nutrients along the length of the membrane consistently, the MCMBR systems were equipped with nutrient capsules (see Figure 4.4), at the bottom and top of the bioreactor, and these were supplied with fresh nutrients at all times during the operation (see assembled MCMBR system in Figures 4.6 and 4.7).

The shell casings, air entry port, permeate port and nutrient capsules were made of PVC tubing because of its durability. The shell and nutrient capsules encased the membrane cartridge. The membrane cartridge consisted of an epoxy mould, where the membranes were attached (Figure 4.5). The nutrient medium was supplied from the bottom capsule throughout the membrane to the top capsule. The air or oxygen was supplied directly into extra capillary space and exited at the permeate port at the bottom of the bioreactor. In the design, provision was made so that there was no liquid build-up in the bioreactor, which could cause growth at the bottom of the bioreactor. Table 4.1 lists relevant details about the bioreactor.

Table 4.1: Details of the MCMBR.

Detail/description	Value
Extracapillary space length	220 mm
Bioreactor inner diameter	60 mm
Bioreactor volume	1.2 L
Number of membranes	15
Active membrane length	210 mm
Membrane outer diameter	1.925 mm
Total membrane surface area	0.0013 m^2
Membrane spacing	6 mm
Pitch	Triangular pitch
Nutrient capsule length	67 mm
Nutrient capsule volume	0.38 L
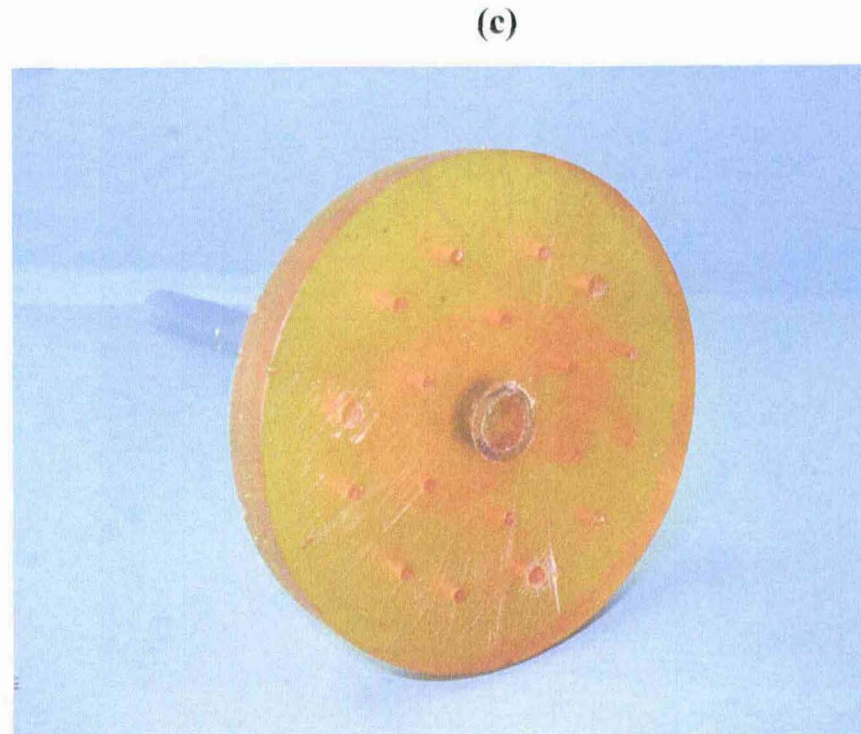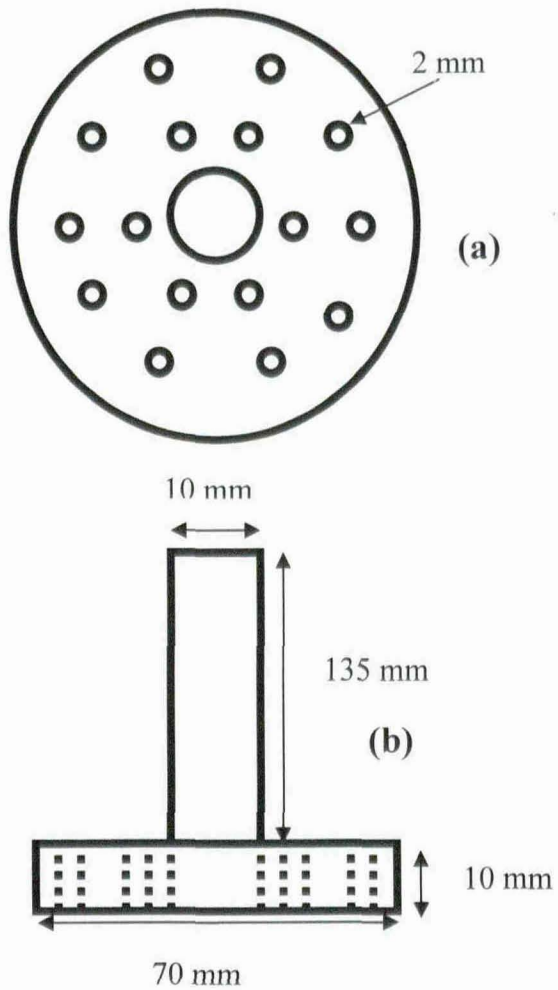
Figure 4.2: Epoxy resin mould for the top-end of the MCMBR: (a) top view of the epoxy mould; (b) side view of the epoxy mould; and (c) photograph of the epoxy mould.
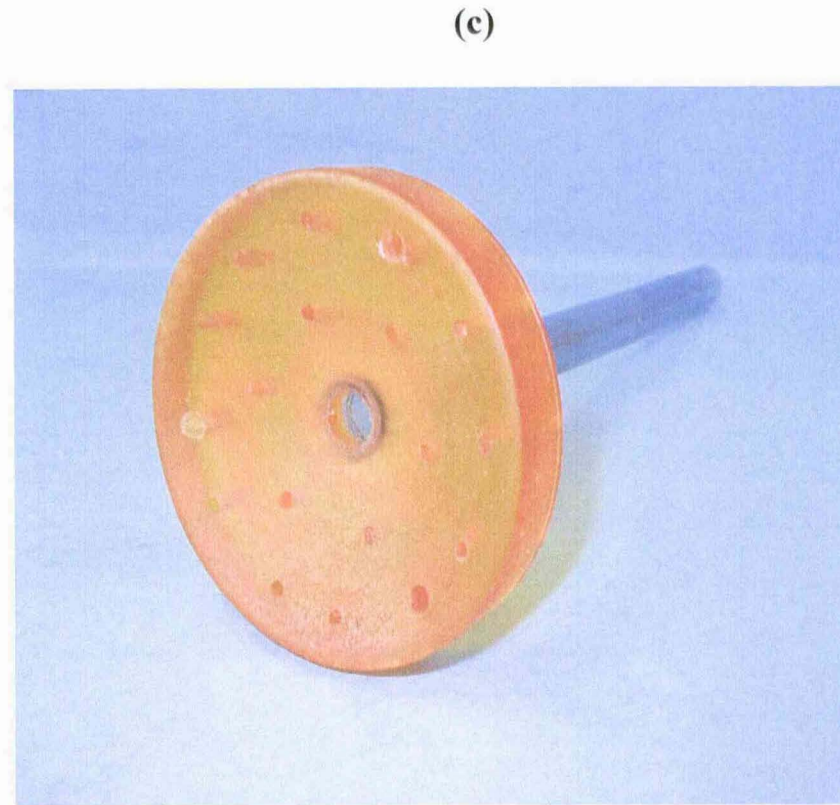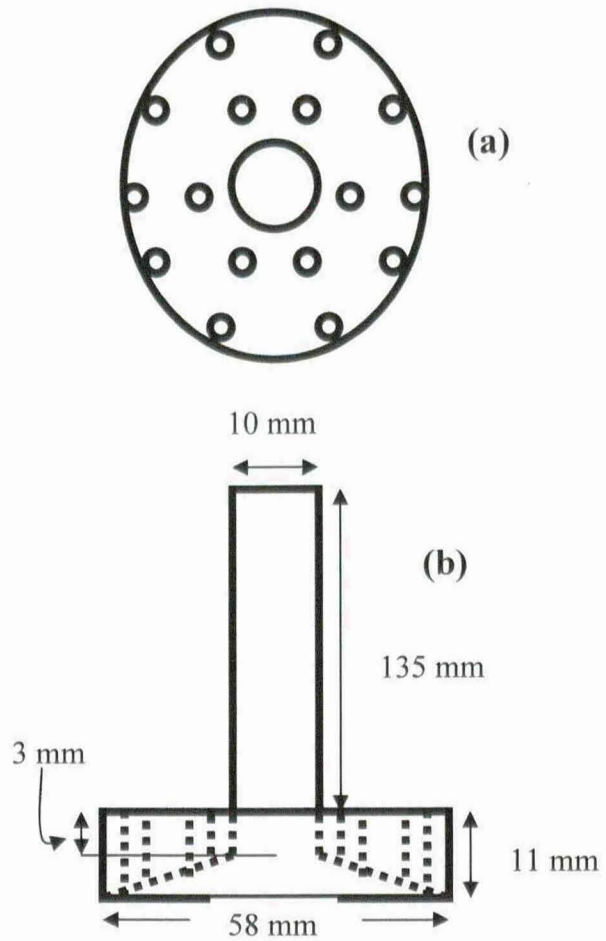
Figure 4.3: Epoxy resin mould for the bottom-end of the MCMBR: (a) top view of the epoxy mould; (b) side view of the epoxy mould; and (c) photograph of the epoxy mould.
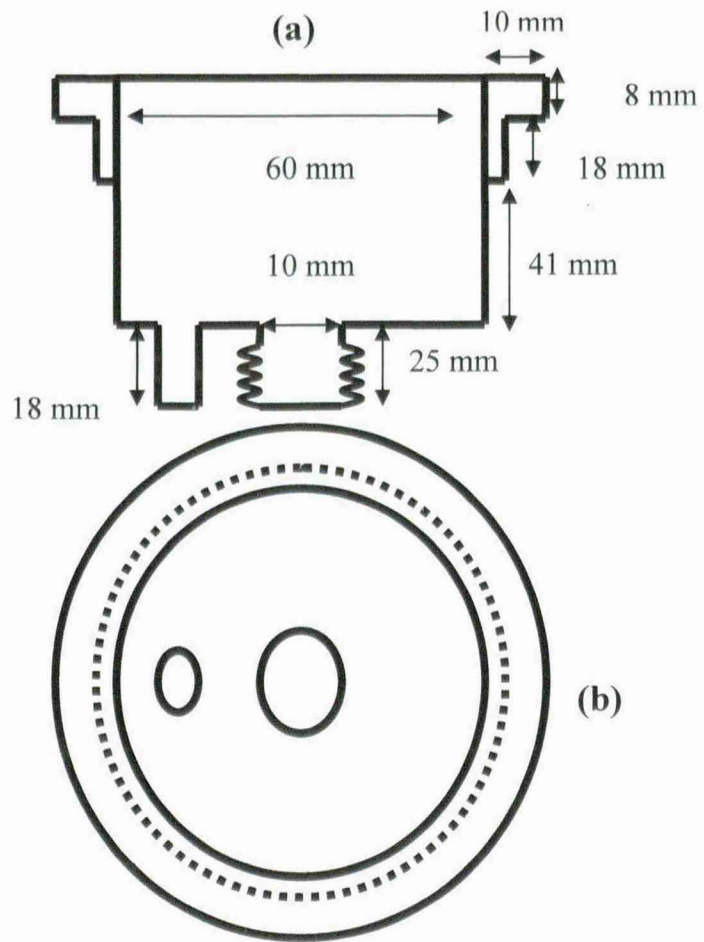
Figure 4.4: Nutrient capsule for the MCMBR: (a) side view of the nutrient capsule; (b) top view of the nutrient capsule; and (c) photograph of the nutrient capsule.

(a)

220 mm

(b)
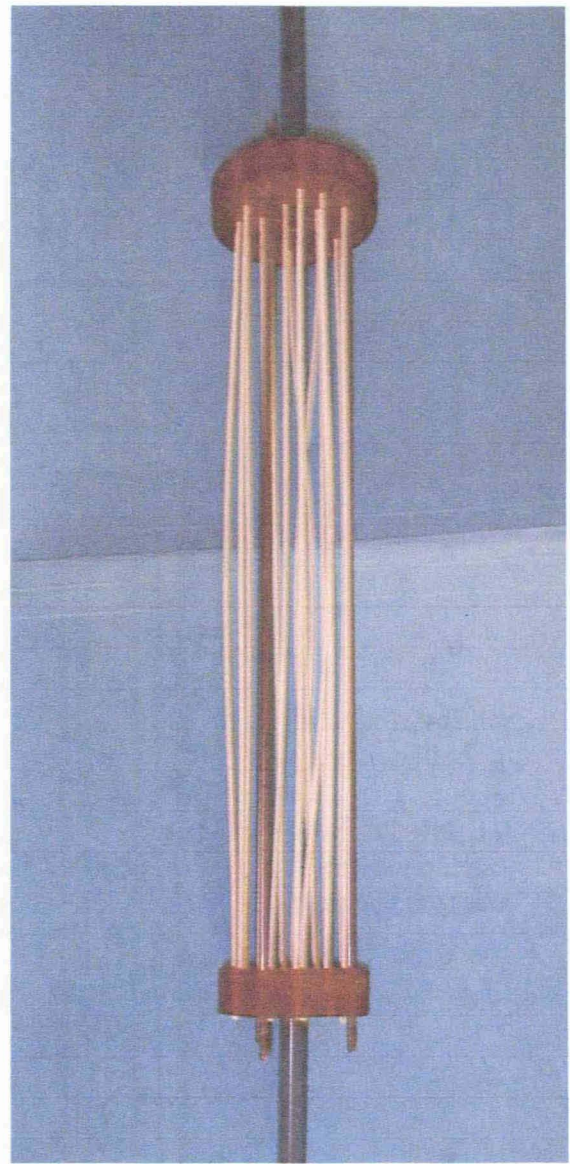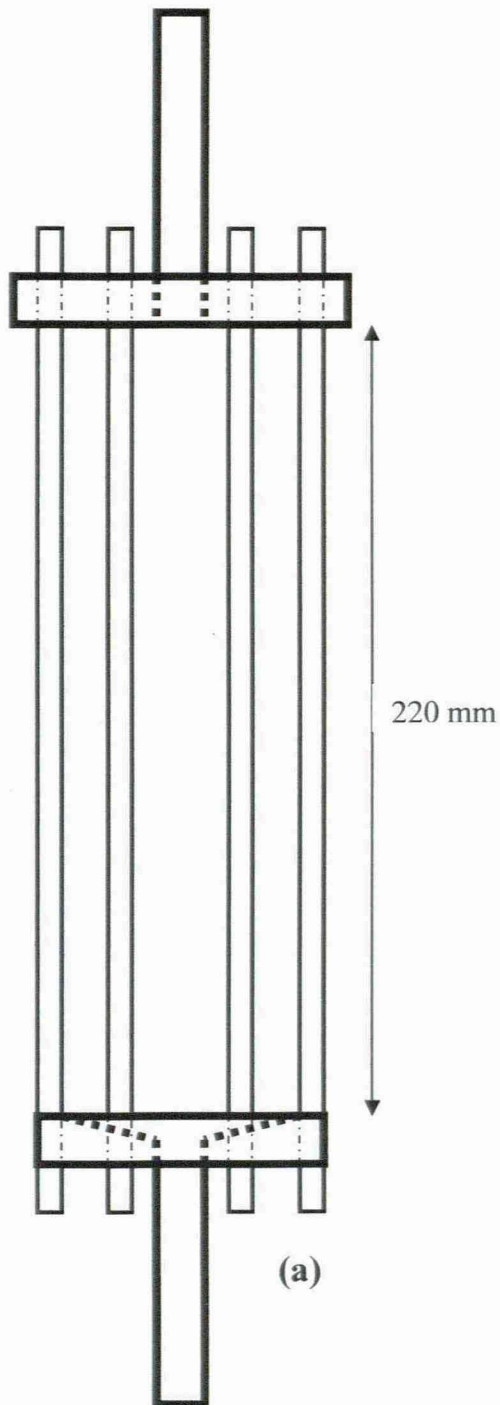
Figure 4.5: (a) Schematic diagram of the membrane cartridge for MCMBR; and (b) Photograph of the membrane cartridge.

1 - Nutrient capsules
2 - Extra capillary space
3 - Air inlet port
4 - Permeate port
5 - Nutrient medium entry port
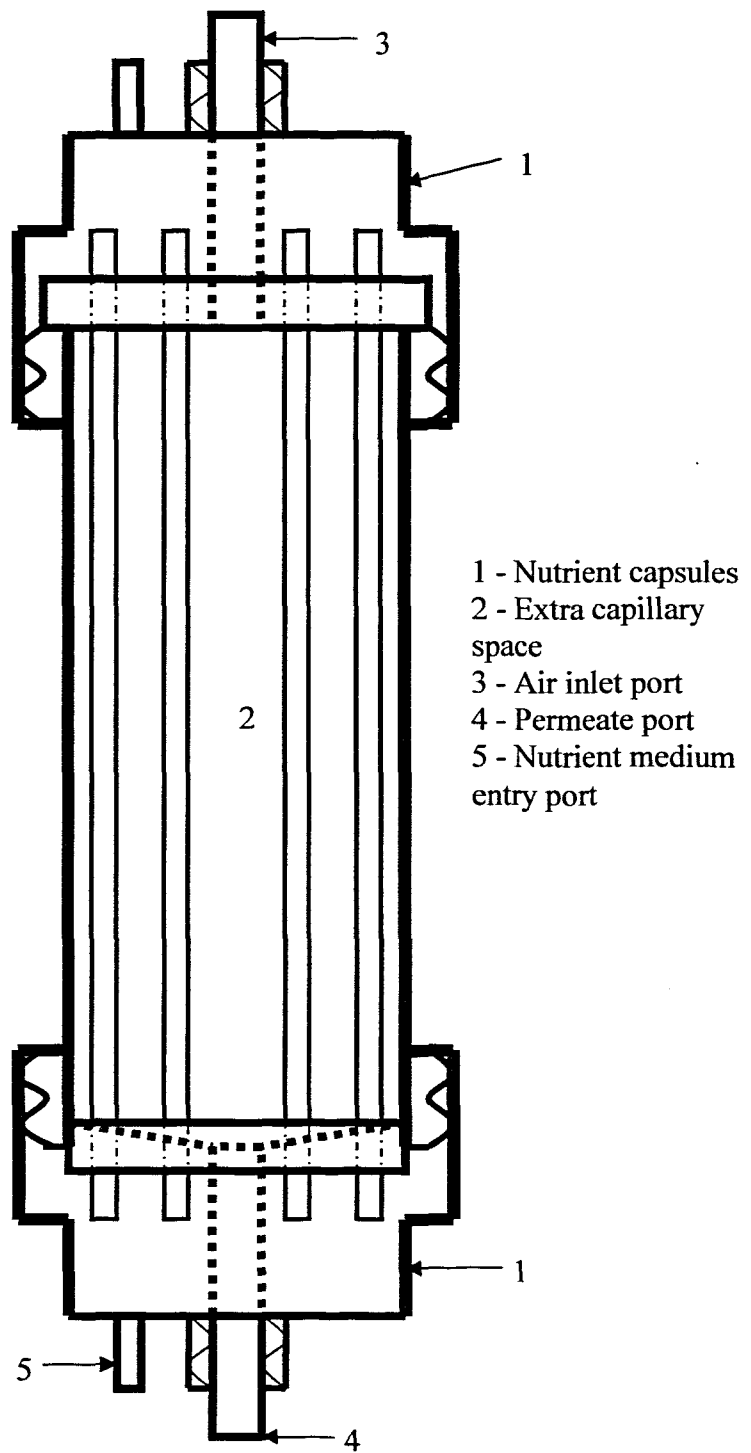
Figure 4.6: Schematic diagram of the assembled MCMBR.

Figure 4.7: A photograph of the complete MCMBR assembly operated in a vertical position.

4.5.2 Manufacturing procedure

The multicapillary membrane bioreactor was manufactured in the Chemical Engineering department workshop at the Cape Peninsula University of Technology, with the assistance of a technical officer. The polysulphone membranes, which were used for the bioreactor, were supplied and manufactured by the Institute for Polymer Science at the University of Stellenbosch (S.A). Considering the size and shape of the required epoxy resin slabs for the top and bottom end of the bioreactor, two wooden moulds were manufactured and silicon rubber was potted into the moulds to provide the required shape. The epoxy resin was potted into the silicon mould with

PVC tubing (O.D = 10mm; length = 135 mm), which was placed in the centre of the mould (see Figures 4.2 and 4.3 for completed epoxy resin mould). A template was used for drilling 18 x 2 mm holes on the resin mould (see Figures 4.2 and 4.3), three of which were used to insert stainless steel rods for support. The 3mm rods were threaded at both ends to fit into the 2 mm holes. The bioreactor shell and nutrient capsules were manufactured using PVC tubing (O.D = 64mm; I.D = 60mm). Two screw caps, a PVC rod and sheet were used for finishing.

4.6   SUMMARY

Three factors were identified as fundamentally affecting growth and enzyme production of *P. chrysosporium* biofilms cultivated on a polysulphone membrane. These factors were: 1) transmembrane flux; 2) extracapillary gaseous phase; and 3) extracapillary fluid regime. Information obtained by other researchers (Garcin, 2002; Solomon, 2001; Leukes, 1999) was used to determine the operation and orientation of the multicapillary bioreactor system. The bioreactor was designed according to listed requirements, whilst also abiding to constraints. This was done by minimising the problems, which were encountered in the single fibre capillary membrane bioreactor used for continuous enzyme production. Details of the multicapillary membrane bioreactor, of which only the membranes need replacing, are listed in Table 4.1.

CHAPTER 5 : MATERIALS AND METHODS

5.1   INTRODUCTION

The actual design of any bioreactor system is based on quantified kinetic parameters for the process; heat and mass transfer rates required. In this chapter, materials and methods, which were used to obtain data, were analysed to attain objectives and to respond to questions from the study. The criteria used to determine whether the data are valid, were included with evidence of validity from the investigation procedures of other studies.

5.2   EXPERIMENTAL SET-UP AND PROCEDURE

A membrane gradostat bioreactor was shown to compare favourably with more conventional systems of enzyme production. A gradostat bioreactor provides a porous substratum, which has a biofilm attached to it. A nutrient solution flows through the substratum at a rate that was sufficiently low for a nutrient gradient to be established across the biofilm. The nutrient concentration at a high level along the gradient should be sufficiently high in order to support primary growth of the microorganism as well as the nutrient concentration at a low level (further away from the substratum), along the gradient being sufficiently low to induce enzyme production. The substratum was in the form of a hollow fibre membrane, which has a relatively thin, porous skin on the inside and a relatively thick, finger-like externally unskinned void structure, which radiates outward from the skin (Garcin, 2002; Solomon, 2001; Govender, 2000; Leukes, 1999; Leukes et al., 1996).

5.2.1   Microorganism and nutrient medium

Phanerochaete chrysosporium BKMF 1767 (ATCC 24725) was used in this study as it has been reported to produce the highest ligninase activity (Govender et al., 2004; Govender, 2000; Leukes, 1999; Venkatadri & Irvine, 1993; Linko, 1992; Kirkpatrick & Palmer, 1987). The strain was grown at 37 °C and pH of 4.5 in fibre capillary membrane bioreactors. The nutrient medium

as stipulated in Tien and Kirk (1988), which was used for all the experiments (see Appendix B for preparation of the nutrient solution). The medium had a limited amount of nitrogen in order to trigger secondary metabolism and contained excess minerals salts, which aimed to enhance ligninolytic enzyme production.

5.2.2 Bioreactor sterilisation

All materials (tubing, bioreactor and flasks) which were used, were autoclaved (steam sterilised) for 20 minutes before they were used. Sterile deionised water was used in the humidifier and in the nutrient medium make-up. The experimental setup was then chemically sterilised with a 4% (v/v) formaldehyde solution and was rinsed with sterile distilled water before inoculation (Leukes 1999).

5.2.3 Preparation of spore solution and immobilisation

A spore solution (see Appendix A1 – A5 for preparation of spore inducing media and harvesting of spores) was prepared by measuring the concentration using a spectrophotometer at 650 nm, where an absorbency value of 1 is equivalent to a concentration of 5 million spores per ml (Tien & Kirk, 1984; see Appendix A6 for determination of spore concentration). Spore solutions of 3 million spores per 40 ml sterile distilled water was used. The spores were immobilised by pumping the spore solution through the permeate port membrane in order to immobilise the spores on the membrane by reverse filtration, as described in Govender et $al.$ (2004).

5.2.4 Nutrient flow and airflow rate

The nutrient medium was pumped at a rate of 1.67 ml/hr through the lumen of the polysulphone membrane by using a peristaltic multi channel Watson-Marlow 505S pump (Germany). Permeate samples were taken every 24 hrs. The nutrient flow rate was calculated in such a way that the dimensionless laminar flow transport modulus, representing the ratio between viscous flow resistance ($128KL^2$) inside the fibre and fibre wall permeation resistance ($d_i^3d_w$) was greater than

one (Bruining, 1989). A permeability constant of 1E-12 m^2 (Solomon, 2001) was used to calculate the ratio. In order to avoid sloughing of the biofilm, an airflow rate of 1-3 L/hr was used (using a HAILIPAI, ACO-9620 multi-port aquarium air pumps with flow control to ensure that the flow was consistent through all the bioreactor modules). Air was filter sterilised (using a 0.22μm, CAMEO filter) and humidified before passing it through the shell side of the bioreactor systems and exited at the bottom through the permeate port .

5.2.5 Bioreactor start-up and monitoring

The SFCMBR and MCMBR systems were placed inside an incubator with in an operating temperature of 37 °C. The nutrients were supplied to the bioreactors from individual reservoirs with filters to avoid contamination. The permeate pH and redox potential was monitored on a daily basis using a Hanna HI 8314 (Hanna Instruments, Portugal) membrane pH meter to determine whether the bioreactors were biochemically identical. Permeate collection was done on a daily basis. At time zero (identified when calculations were performed), the bioreactors would have operated for 24 hrs.

5.2.6 Single fibre capillary membrane bioreactor (SFCMBR)

The glass SFCMBR systems (manufactured by Glasschem, Stellenbosch, R.S.A) with working volumes of 20.4 ml and an active membrane length of 160 mm were used to cultivate *P. chrysosporium* biofilms, positioned vertically, as shown in Figure 5.1. The SFCMBR was developed with dimensions, as indicated in Table 5.1.

Table 5.1: Dimensions of vertically orientated SFCMBR systems.

Parameter	Details
Module length	230 mm
Module diameter	12 mm
Active membrane length	160 mm
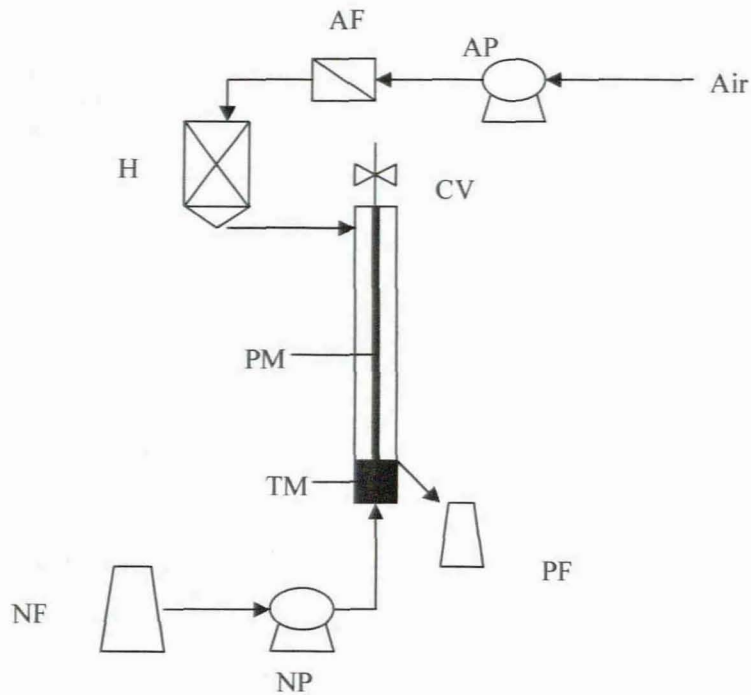
Figure 5.1: Schematic illustration of a single fibre capillary membrane bioreactor. AF: air filter; AP: air pump; CV: closed valve (dead-end filtration mode applied); H: humidifier; NF: nutrient flask; NP: nutrient pump; PF: permeate flask; PM: polysulphone membrane TM: Teflon mould.
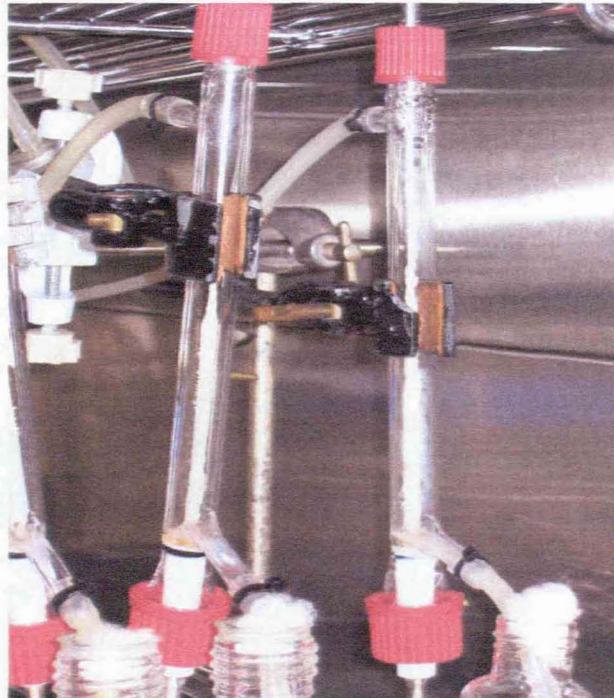
Figure 5.2: Photograph of SFCMBR systems in operation at 37 °C inside an incubator.

The internally skinned and externally unskinned capillary polysulphone membranes, which were used were manufactured by the Institute of Polymer Science (Stellenbosch University, S.A) using the wet-phase inversion process, according to the fabrication protocol of Jacobs and Leukes (1996). A Teflon mould was used at the bottom of the SFCMBR to avoid accumulation of permeate from the biofilm. The bioreactor was operated in the dead-end filtration mode.

5.3   ANALYTICAL METHODS

5.3.1   Biofilm density

The SFCMBR systems were inoculated with the same number of spores and operated in parallel under the same conditions. On days 3, 5, 7, 9 and 11, three SFCMBR systems were taken off simultaneously to measure the dry biofilm density, which developed on the polysulphone membranes after drying at 60 °C for 12 hours. The dry density of the biofilm was determined by using a helium pycnometer (Accupyc 1330, as shown in Figure 5.3).
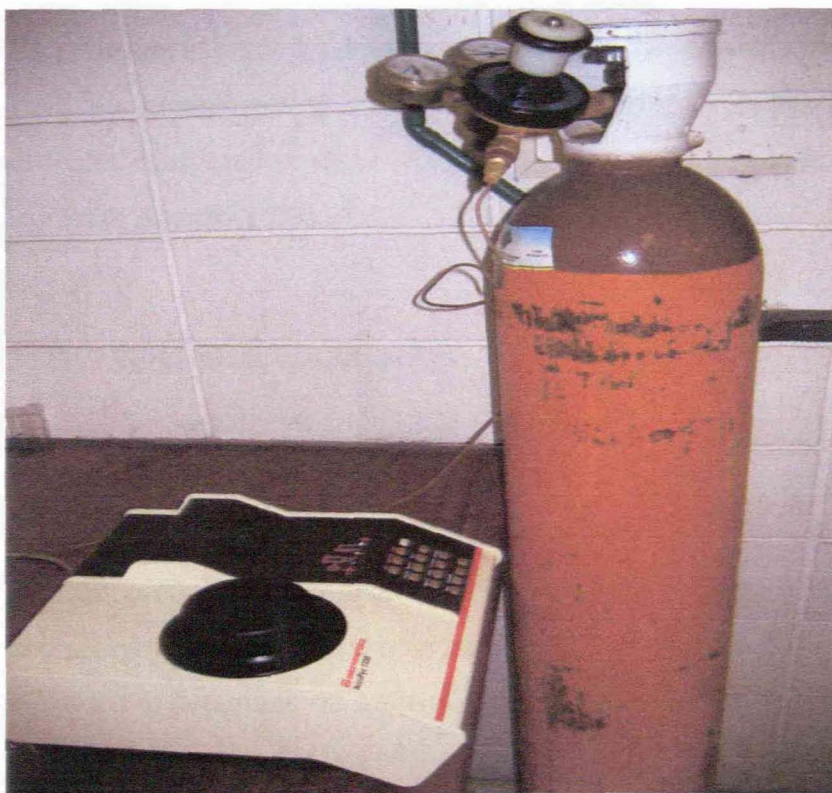
Figure 5.3: Helium pycnometer which was used to measure biofilm density.

The accuracy of the pycnometer was checked by using a steel sphere with a known volume before measurements on a series of samples. The experimental samples were accurately weighed and loaded into the sample chamber. The samples were measured by filling the sample chamber with ultra-high pure helium. Discharging the gas into a second empty chamber followed and the difference in volume was quantified. The measurements were repeated 3 times for accuracy with the average used for calculations. After calibration, the accuracy of the pycnometer was checked by using water. A density of 1.01 $g.cm^{-3}$ was obtained. When measuring density with a helium pycnometer, 0.02% accuracy can be obtained, otherwise it can fail to 0.1% or less, depending on the material and the variations in the standard volume (Viana *et al.*, 2002). The individual dry biofilm densities, from the three SFCMBR systems, were averaged for a specific day.

5.3.2   Glucose consumption

The concentration of glucose content in the permeate samples was determined by using a Roche® D-glucose test kit (AEC Amersham, R.S.A). The concentrations of glucose obtained for the permeate of each SFCMBR were subtracted from the initial concentration of feed (10 g/L), to yield the corresponding consumption. Daily glucose consumption was evaluated to monitor different consumption stages during the biofilm development. The glucose assay procedure is shown in Appendix D1.

5.3.3   Ammonium concentration

A Spectroquant Ammonium Test Kit (Merck, R.S.A) was used to measure the amount of ammonia present in permeates. Because the suite of ligninolytic enzymes from *P. chrysosporium* are only produced under conditions of nutrient limitation, in this case nitrogen limitation, it was necessary to monitor whether or not nitrogen limitation did indeed occur. The assay employed, was used to determine the ammonium tartrate present in permeate samples. The rationale behind this was to monitor the use of the ammonium tartrate, as the initial concentration of 39 mg/L of ammonium tartrate is present in the nutrient media. The assay was carried out by using the manufacturer's specifications. The ammonium assay procedure is shown in Appendix D2.

5.3.4 *Lignin Peroxidase (LiP)* activity

LiP catalyses the H_2O_2 dependent oxidation of a wide range of lignin-related aromatic compounds. A number of assays are available to measure its activity. Among the most convenient is the oxidation of 3, 4-dimethoxybenzyl (veratryl alcohol) to yield veratraldehyde. Veratraldehyde absorbs intensively at 310 nm and the alcohol does not. Although the activity shows a pH optimum to be ±2, assays were typically performed at pH 2.5 - 3.5, due to the instability of the *LiP* at pH values lower than 2.5 (Tien, 1987). Care was taken not to incubate the enzyme in H_2O_2 in the absence of veratryl alcohol or in pH 2.5 buffer since these treatments result in the inactivation of activity, which is the oxidation of veratryl alcohol to veratraldehyde, as described in Appendix C1 (Tien & Kirk, 1988). Samples were done in duplicate with the average results used to quantify the amount of enzymes available. An extinction coefficient of 9300 $M^{-1}.cm^{-1}$ was used.

5.3.5 *Manganese Peroxidase (MnP)* activity

This assay is based on the oxidative coupling of 3-methyl-2-benzothiazolinone hydrazone (MBTH) and 3-(dimethylamino) benzoic acid (DMAB). The reaction of MBTH and DMAB in the presence of H_2O_2, Mn^{2+} and *MnP*, gives a deep purple-blue colour with a broad absorption band with a peak at 590 nm. The extinction coefficient (EC) is high (53 000 $M^{-1}cm^{-1}$), so low *MnP* activities can be detected. *LiP* and laccase, usually present in cultures of WRF, gave little or no interference at the concentrations tested. The method used for *MnP* activity is described in Appendix C2. Samples were done in duplicate with the average results used to quantify the amount of enzymes available.

5.3.6 Oxygen mass transfer across the biofilm surface

Oxygen concentration profiles were measured at axial coordinates selected by the researcher to minimise the effect of biofilm heterogeneity, as indicated by Lewandowski and Beyenal (2001) in biofilms cultivated in membrane bioreactors using an oxygen microsensor.

5.3.6.1 Oxygen microsensor set-up and operation

To determine mass transfer, kinetic and diffusion parameters from oxygen concentration profiles obtained from *P. chrysosporium* (BKM-F 1767) biofilms, a Clark-type oxygen microsensor (OX 10, outer-tip diameter less than 20 μm, shown in Figure 5.4b), supplied by Unisense (Denmark), was used to take measurements across the biofilm at intervals of 50 μm. Oxygen profiles were measured in the three different bioreactors that was taken off on days 3, 5, 7, 9 and 11. The microsensor was connected to a high-sensitivity picoammeter and the cathode was polarised against the internal reference. Driven by the external partial pressure, oxygen from the environment penetrated through the sensor tip membrane and was reduced at the gold cathode surface. The picoammeter converts the resulting current to a signal. The internal guard cathode was also polarised and it scavenges oxygen in the electrolyte, thus minimising zero-current and pre-polarisation time.

By experimentally measuring the oxygen distribution in the biofilm at different depths using an oxygen microsensor, the experimental profile was used in PROFILE 1.0 software (Berg *et. al.*, 1998) to quantify the flux and consumption of oxygen. The program uses a series of least square fits to the measured oxygen profiles, followed by comparisons through statistical F-testing. The approach leads to an objective selection of the simplest flux profile that reproduces the oxygen concentration profiles, which were obtained by using the oxygen microsensor. See Appendix F for oxygen microsensor operation.

<center>(a)   (b)</center>
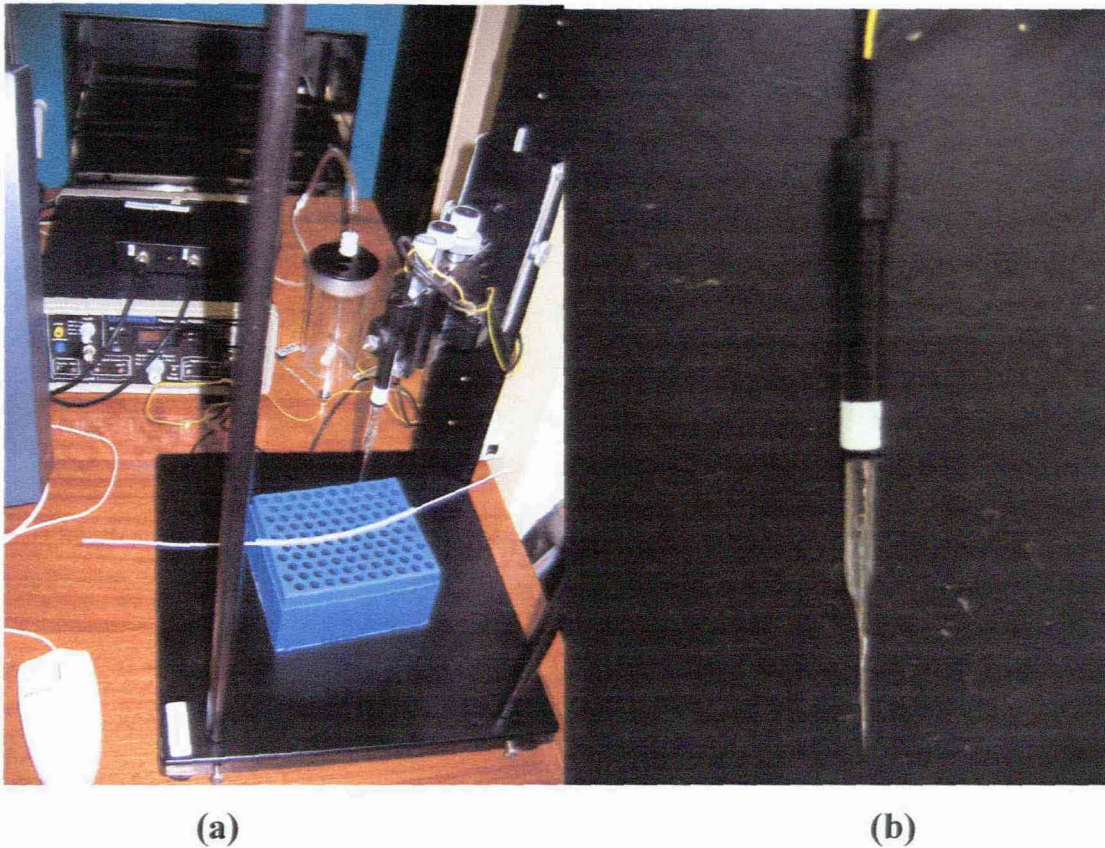
Figure 5.4: Photograph of the microsensor setup; (a) the microsensor connected to a picoammeter and fixed on a micromanipulator with a visible calibration chamber in the background, (b) the OX 10 microsensor with a glass tip of less than 20 μm.

5.3.6.2 Considerations for the input file for PROFILE 1.0 software

The input file was done by using Microsoft® Notepad. The following boundary conditions were considered for the interpretation of the input file: (a) the concentration of oxygen at the biofilm surface; and (b) the oxygen flux near the substratum (assumed to be zero). 1.161E-5 m^2/hr (nutrient medium had a salinity of 3%, measured using a hydrometer) which was used as the diffusivity of oxygen at 37 ^{0}C. The biofilm diffusivity was assumed to be proportional to the diffusivity of oxygen in the nutrient medium with the porosity being the proportionality constant. The porosity of the biofilm was assumed to be 80% throughout the biofilm thickness, while the biodiffusivity and irrigation coefficients were both considered to be negligible. An example of the input and output files from PROFILE 1.0 program are shown in Appendix G.

5.3.7 Nutrient flow behaviour in the substratum

Distilled water was pumped from the bottom of vertically placed SFCMBR systems (operated in a dead-end mode) to the top of the bioreactors, through the lumen of the polysulphone membrane(s), which acts as the substratum. Pressure transducers (connected to an online LABVIEW® system) were used to measure the pressure at the inlet and outlet nutrient ports continuously for the duration of the experiments. A mathematical differential equation solver (Polymath 5.1), which solves systems of first order ordinary differential equations, was used to predict the nutrient velocity profiles in the lumen of the membrane. This was done by determining the outlet pressure (using the measured inlet pressure, membrane permeability, membrane length and the lumen radius) by using the mathematical models developed in Chapter 3.

5.3.8 Nutrient mass transfer across the biofilm

Due to the unavailability of a suitable glucose microsensor (which can measure in a range of 0 – 12 g/L, glucose), an innovative way had to be found to model nutrient distribution across the biofilm surface. It was shown that in the elucidation of the mechanism of the WRF that hydrogen peroxide was produced under ligninolytic conditions (Forney *et al.*, 1982), thus prompting the researcher to use a hydrogen peroxide microsensor. A hydrogen peroxide microsensor (supplied by the Centre for Biofilm Engineering, University of Montana, Bozeman, USA), was used to measure hydrogen peroxide concentration profiles in *P. chrysosporium* biofilm at depth increments of 50 µm. This was done by initially growing the biofilm with the nutrient medium and then feeding the system with a 1.887g/L solution of hydrogen peroxide solution through the lumen. The concentration of hydrogen peroxide used in the study was determined by using the complete mole conversion of 10 g/L glucose to hydrogen peroxide in the presence of glucose oxidase, as explained by equation 5.1. It was assumed that the distribution of hydrogen peroxide in the biofilm was a true reflection of the distribution of glucose in the cultivated biofilms. The kinetic parameters were evaluated by using mathematical models, which were developed in sections 3.4.1 and 3.4.2.

$$Glucose + O_2 \xrightarrow{\quad Glucose \quad oxidase \quad} Gluconic \quad acid + H_2O_2 \qquad 5.1$$
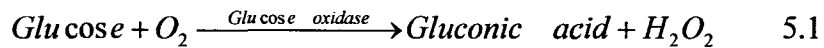
The profiles were measured in different bioreactors on days 5, 9 and 11. The microsensor was connected to a high-sensitivity picoammeter, using the following settings: 1) Polarisation: +0.80; and 2) Range: 200na. A standard calomel electrode was used as an external reference. A calibration curve was developed by using different hydrogen peroxide concentrations to link the response current with the hydrogen peroxide concentration.

5.3.9 Biofilm preparation for microscopic imaging

To better understand the substrate mass transfer phenomena at different stages during biofilm development, biofilm morphology should be properly analysed. Biofilm sections from SFCMBR systems were sectioned off and preserved in a 10% glutaraldehyde solution before analysing it by using a Scanning Electron Microscope (SEM).

5.4 MULTICAPILLARY MEMBRANE BIOREACTOR (MCMBR) SETUP AND OPERATION

The multicapillary membrane bioreactors (described in Chapter 4) were assembled and operated in an incubator at 37°C for 18 days. The bioreactors were simultaneously inoculated in a vertical position and the dead-end filtration mode was used for nutrient supply from the bottom of the bioreactor. An airflow rate of 6 L/hr was used for the MCMBR systems and was supplied from the top on the shell side and exited with permeate (taken every 24 hrs) at the bottom. The nutrient capsules were firstly filled with fresh nutrient before the experiments began. 45 million spores (3 million spores per membrane) were used for inoculation. A nutrient supply rate of 0.835 ml/hr per membrane (300 ml/day of permeate produced per MCMBR) was utilised. The MCMBR operation was related to the SFCMBR operation, as nutrient medium, spore concentration per membrane and general operating conditions were similar. The following measurements were taken daily: 1) pH; 2) redox potential; 3) ammonia concentration; 4) glucose concentration; 5) oxygen profiles; and 6) enzyme (*LiP* and *MnP*) production.

CHAPTER 6 : GROWTH KINETICS AND BIOFILM DEVELOPMENT

6.1   INTRODUCTION

Growth kinetic rates are one of the most important and critical parameters for studying biofilms as they can be used to model mass transport and reactions. However, there are few growth kinetic constants that have been specifically developed for a continuous membrane bioreactor system with immobilised *P. chrysosporium* biofilm. Dry biofilm density was determined over a period of 264 hrs using SFCMBR systems, which were operated simultaneously. Glucose and ammonia consumption was profiled to describe the use of substrates over the duration of the study. Linearization techniques were used to evaluate substrate consumption based kinetic constants. Growth yield coefficients based on glucose and ammonia were quantified at different stages of the biofilm development, with the glucose based maintenance coefficient determined during the period when the immobilised biofilm mass did not change. The effect of different spore concentrations on substrate consumption and biofilm development were also investigated.

The structure of biofilms in bioreactor systems is known to have great importance, as it affects substrate mass transfer across the surface of the biofilms. By clearly describing the morphology of the filamentous biofilm (using SEM images), growing on the surface of the substratum, growth kinetics and other parameters can be better understood. The structure of *P. chrysosporium* biofilm immobilised in vertically orientated SFCMBR was described according to different growth phases. As sufficient biofilm was not developed before 72 hrs of operation, the structural morphology was described in SFCMBR systems, which operated beyond the lag phase. In order to establish a clear or constant pattern, different SFCMBR systems were used to evaluate the morphology of the biofilms.

6.2 QUANTIFYING GROWTH KINETICS OF *P. CHRYSOSPORIUM*

6.2.1 Dry biofilm density

From the literature considered, it is apparent that the basic growth of the fungus for batch systems follows a logistic growth curve (Ceribasi & Yetis, 2001; Yetis *et al.*, 2000; Barclay *et al.*, 1993). The shape of the growth curve was predicted by using equation 2.4. The dry biofilm density curve was modelled by estimating the growth rate constant, k_f until the curve, which was obtained, fitted the experimental values in the period's 72 to 216 hrs as shown in Figure 6.1. This was done by using an ordinary differential equation solver (Polymath 5.1), with a known maximum density (at 216 hrs) from the experiment.
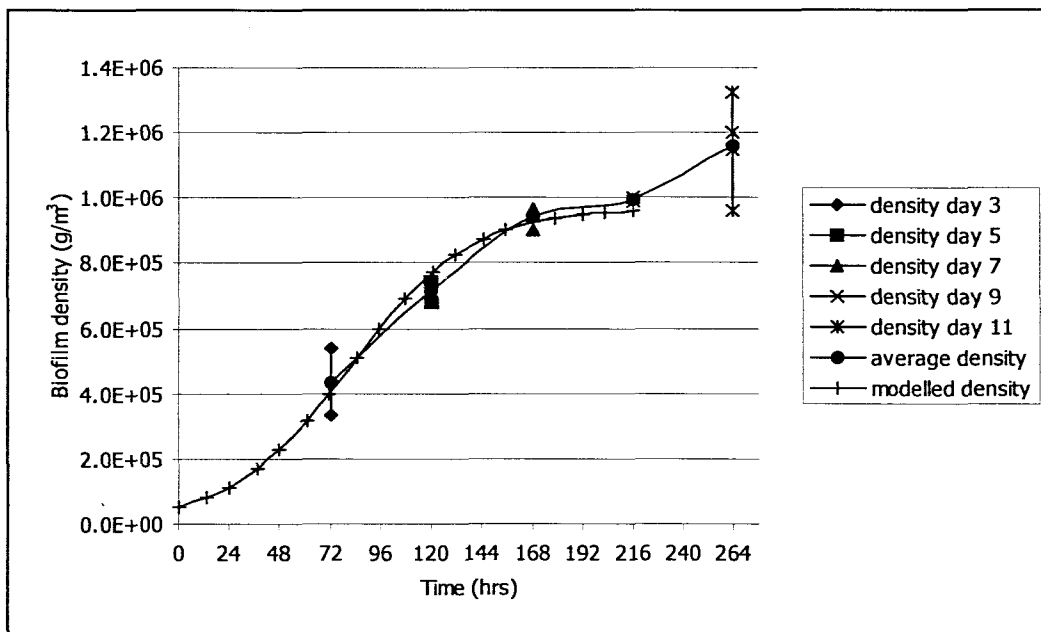
Figure 6.1: Dry biofilm density as measured using the helium pycnometer from different SFCMBR systems.

The logistic curve showed primary and secondary biofilm growth phases, which is a phenomenon in *P. chrysosporium* biofilms, as the regeneration of mycelium occurs in successive growth cycles (Ceribasi & Yetis, 2001; Yetis *et al.*, 2000; Kirk *et al.*, 1978). The dry biomass increased during the first 168 hrs (7 days), after which it stabilised until 216 hrs (day 9), with the secondary phase occurring thereafter. The secondary growth phase obtained by Kirk *et al.* (1978) occurs after 10 days (mycelia cultured at 39 °C, in a 125 ml flask with 21% O_2), which is in agreement

75

with the results obtained. The following phases were identified in Figure 6.1: 1) lag phase (0 to 48 hrs); 2) exponential growth phase (72 to 120 hrs); 3) stationary phase (144 to 216 hrs); and 4) secondary growth phase (>216 hrs)]. The stationary phase (where the biofilms mass did not change) lasted for 48 hrs at an average dry biofilm density of $9.7E05$ g/m^3. The dry density profile was modelled between 0 to 216 hrs by manipulating the growth rate constant, k_f, (carrying capacity constant), with a ± 8% error occurring between experimental and modelled values (calculated using the difference in experimental and modelled density values). The representative growth rate constant, k_f was determined as 0.035 hr^{-1}, with an initial density (X_0) after 24 hrs, of $5.33E04$ g/m^3.

6.2.2 Substrate consumption

6.2.2.1 Glucose consumption

Daily glucose consumption was quantified to monitor different stages of glucose consumption during biofilm development, as shown in Figure 6.2. The glucose consumption profile showed different rates of glucose usage as the biofilm developed on the polysulphone membranes. This was consistent with different growth phases during the growth of microorganisms [i.e. lag phase (0 to 48 hrs), exponential growth phase (72 to 120 hrs), stationary phase (144 to 216 hrs) and secondary growth phase (>216 hrs)].
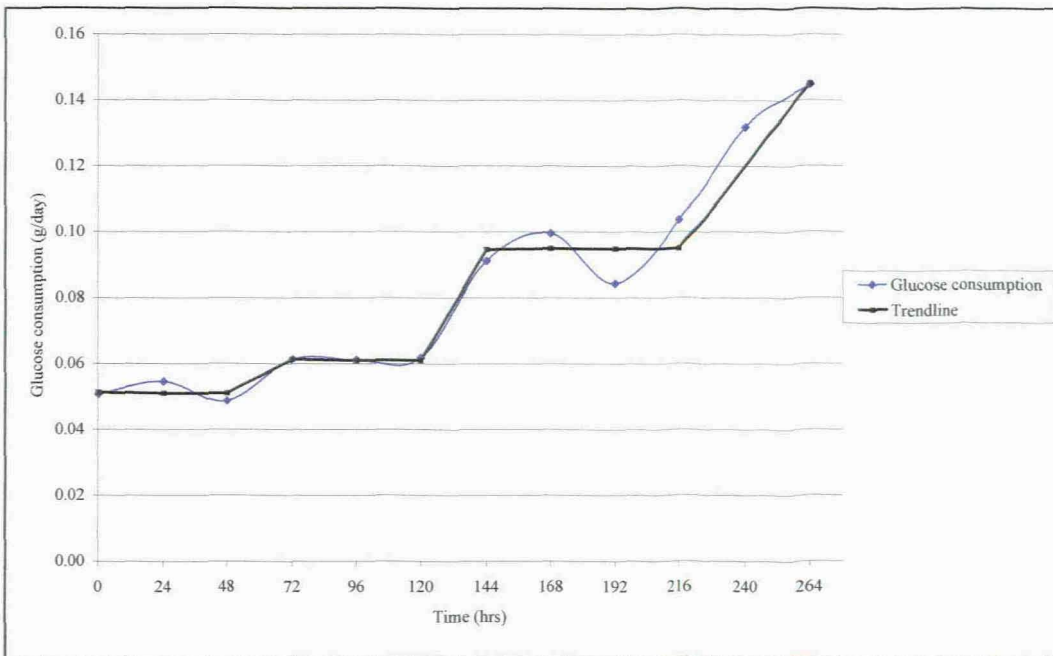
Figure 6.2: Concentration of daily glucose consumed during different times of the study.

The accumulative glucose consumption curve, as shown in Figure 6.3, was best described by a third order polynomial function. The differential format was used to evaluate glucose-based kinetic constants, as described in Appendix I, using linearization techniques. The average glucose consumption rate was 94.7 g/m^3.hr over the whole run, compared to 43 g/m^3.hr obtained in a Trickle Fixed Bed Reactor (TFBR), determined by dividing the total accumulative glucose consumed within the period in which the experiment was performed (Bosco *et al.*, 1996). The basis for comparison was that both systems were continuous enzyme production systems where the nutrient medium, as designed by Tien and Kirk (1988), was used. The maintenance coefficient, (described by equation 2.19), was determined as 0.0001 hr^{-1}. This value was unreasonable because the two volumes bases in the calculation were determined to be inconsistent. The correct maintenance coefficient value was calculated as 0.028 hr^{-1} (calculated using the amount of glucose consumed during the stationary and the biomass generated after 168 hrs. i.e. 0.188 g/ 48 hr/ 0.14 g). During this period no new mycelium was generated, it was assumed that the glucose consumed was for other biological processes, other than mycelia generation.

$$y = 0.0004x^3 + 0.0386x^2 + 51.341x + 1293.6$$
$$R^2 = 0.9996$$
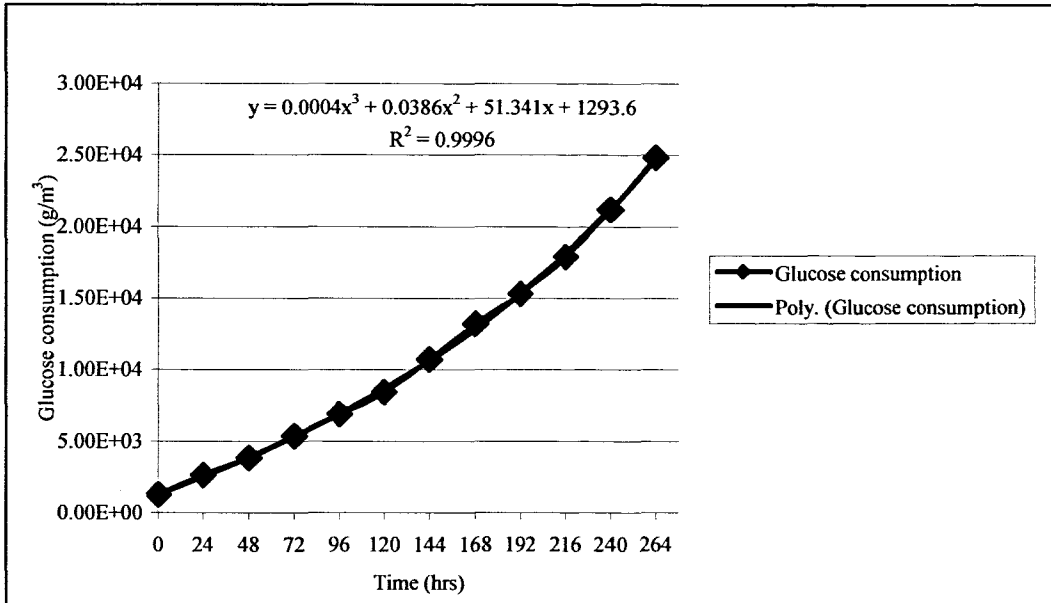
Figure 6.3: Accumulative glucose consumption curve.

The standard equation used to express kinetic constants under the Monod hypothesis can be rearranged to generate plots, which can be used to evaluate kinetic constants. The hyperbolic relationship between the initial rate of reaction and the substrate concentration can be arranged to give linear plots by using linearization techniques of: 1) Lineweaver-Burk; and 2) Eadie-Hofstee (explained in section 3.5) and shown in Figures 6.4 and 6.5. The Lineweaver-Burk plot gave the best fit with correlation coefficients (R^2) of 0.87, compared to 0.042 of the Eadie-Hofstee plot over the period of the study. However, the Eadie-Hofstee plot showed improved correlation coefficients ($R^2 = 0.71$) at low consumption rates of between 0 to 72 hrs.
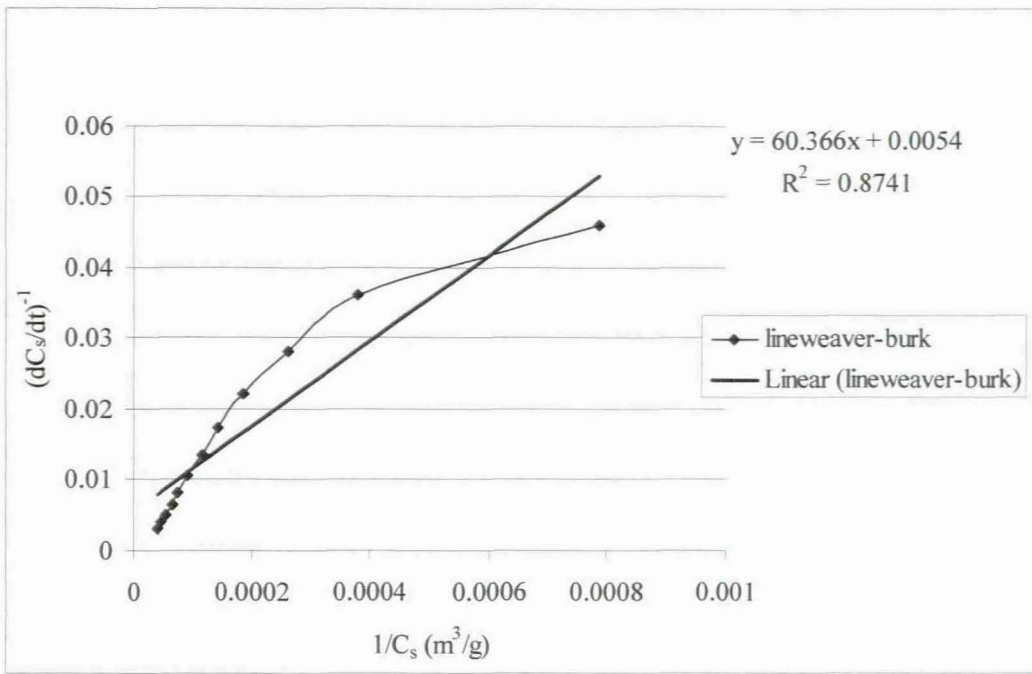
Figure 6.4: Lineweaver-Burk method used to evaluate kinetic constants between 0 to 264 hrs.
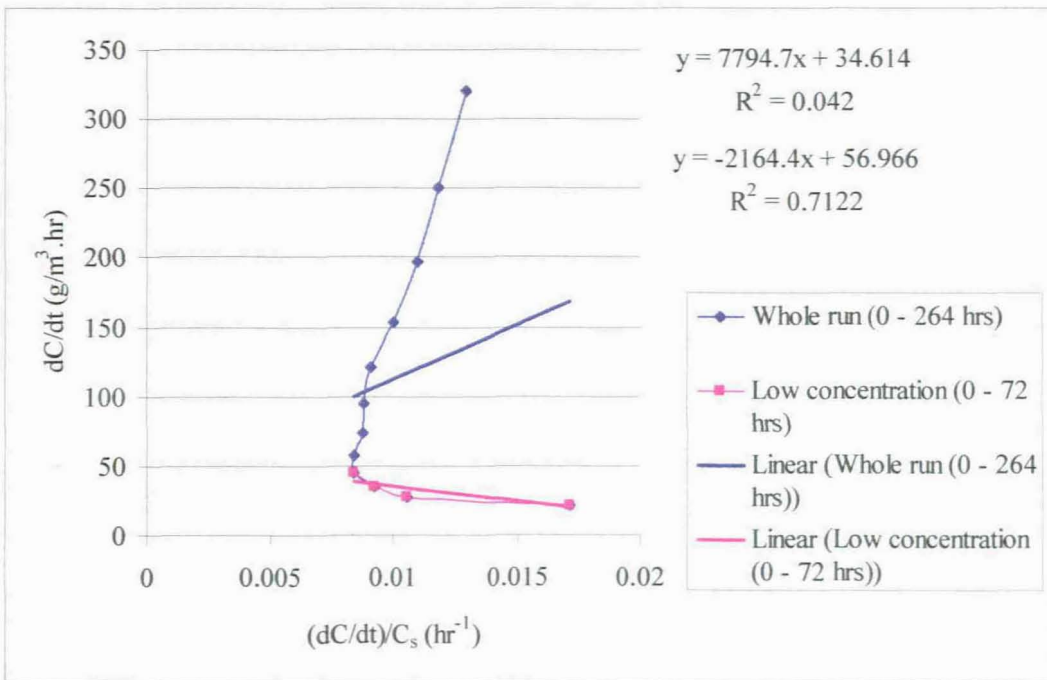
Figure 6.5: Eadie-Hofstee method used to determine kinetic constants between 0 to 264 hrs and at low glucose consumption rate (0 to 72 hrs).

As determined from the Lineweaver-Burk plot, the maximum glucose consumption rate, r_m, for the experiment (0 to 264 hrs) was determined as 185 g/m^3.hr and the Monod saturation constant,

K_m, as 1.12E04 g/m^3. As determined by using the Eadie-Hofstee plot, during the initial stages (0 to 72 hrs) of biofilm development, the maximum glucose consumption rate, r_m, was evaluated as 56.97 g/m^3.hr and the Monod saturation constant, K_m, as 2.16E03 g/m^3.

6.2.2.2 Ammonia consumption

Approximately 0.00156 g/day (calculated by multiplying the ammonium tartrate concentration with the permeate volume collected over a period of 24 hrs), ammonia was supplied to the SFCMBR systems daily. After 48 hrs (lag phase), 90% of all the ammonia supplied to the bioreactors was consumed, as shown in Figure 6.6. This was acceptable, as the biofilm requires a source of fixed nitrogen when new mycelia are generated. This also meant that the biofilms probably experienced nitrogen starvation to produce appropriate enzymes.
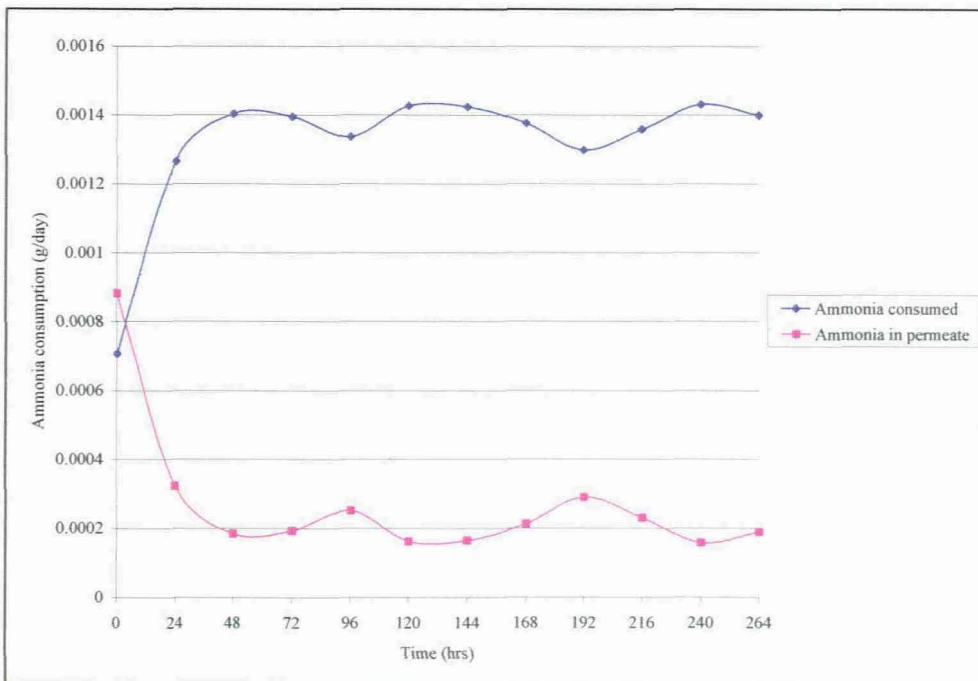
Figure 6.6: Mass of daily ammonia consumption curve over the length of the experiment.

The concept of the gradostat system was clearly implemented in terms of nitrogen gradients across the biofilm, as newly generated mycelia (near the substratum) clearly consumed most of the ammonia supplied, while the biofilm on the shell side was starved of nutrients. From Figure 6.6, it was not easy to see the various stages in which ammonia was consumed compared to

glucose (as shown in Figure 6.2). The average ammonia consumption rate over a period of 264 hrs was determined as 1.46 g/m^3.hr. The determination of ammonia kinetic data was done similarly to that of glucose by using the accumulative ammonia utilisation profile, as shown in Figure 6.7.
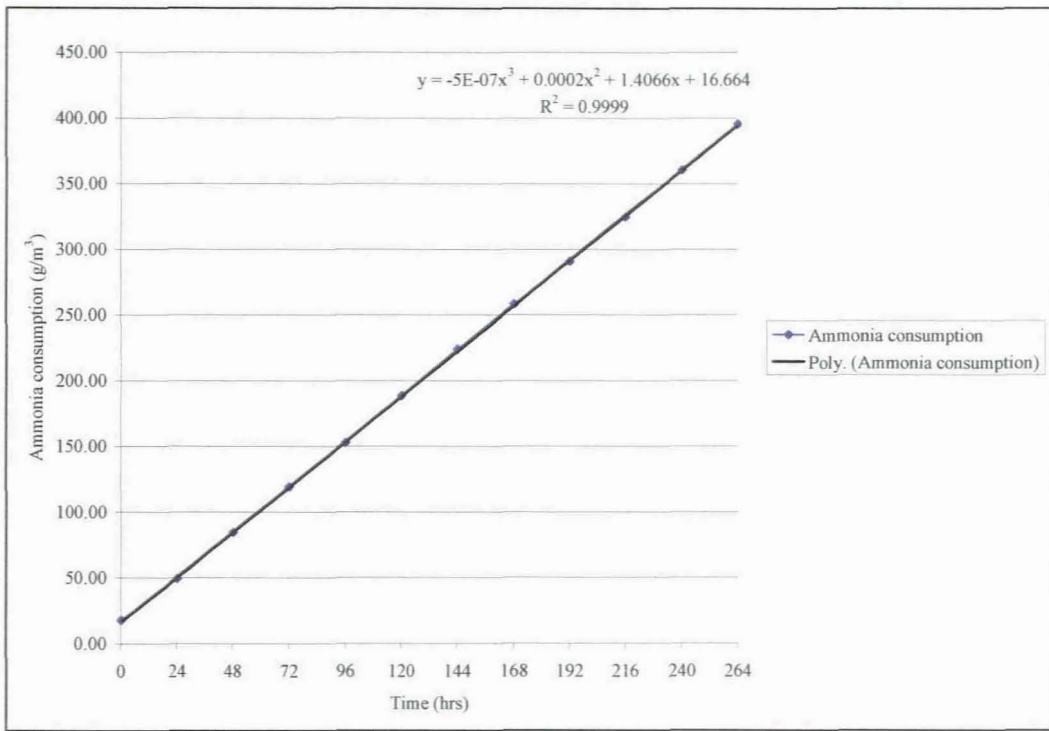
Figure 6.7: Accumulative ammonia consumption curve over time.
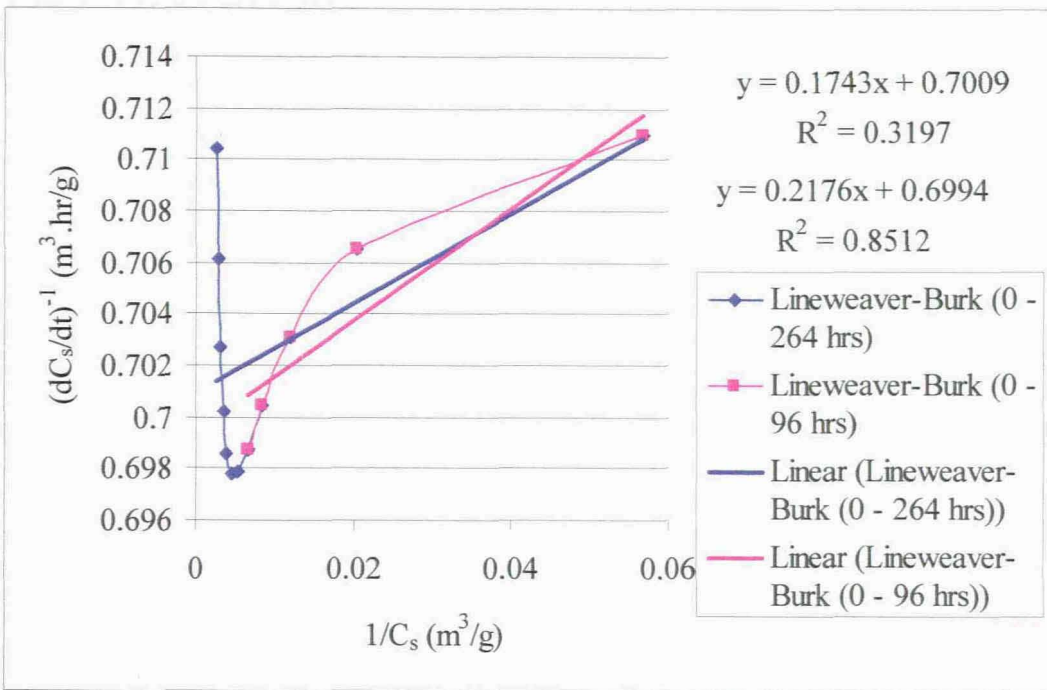
Figure 6.8: Lineweaver-Burk plot for evaluating kinetic constants.

Both the linearization techniques of Lineweaver-Burk and Eadie-Hofstee were evaluated over the whole period of the experiment with low correlation coefficients (R^2 = 0.3197 – 0.3162) achieved. However, the highest correlation coefficients were obtained in the period 0 to 96 hrs as shown in Figures 6.8 and 6.9. The kinetic constants were determined by using plots with high correlation coefficients. A maximum substrate consumption rate, r_m of 4.60 g/m^3.hr and the ammonia-based Monod saturation constant, K_m, of 1 g/m^3 were obtained by using the Lineweaver-Burk plot. The maximum substrate consumption rate, r_m, of 1.43 g/m^3.hr and the Monod saturation constant, K_m of 0.32 g/m^3 were obtained by using the Eadie-Hofstee plot.
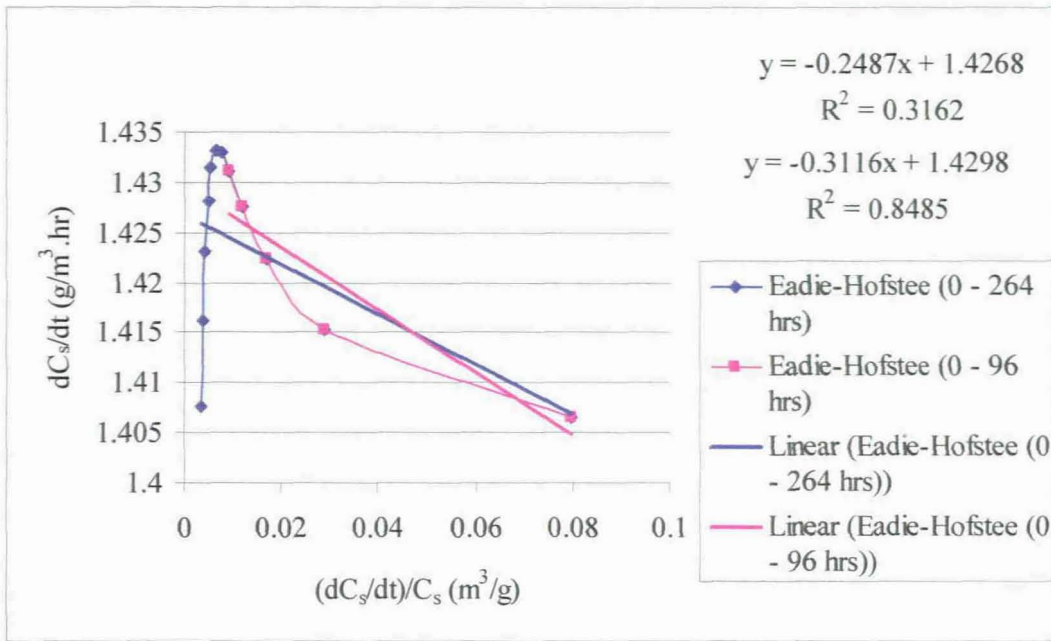
Figure 6.9: Eadie-Hofstee plot for evaluating kinetic constants.

6.2.2.3 Maximum specific growth rate

The evaluation of the maximum specific growth rate was completed by using the primary substrate (glucose). The maximum substrate consumption, r_m can be described as $r_m = (\overline{\mu}_{max} X_m)/Y_{X/S}$. From sections 6.2.2.1, the Lineweaver-Burk plot clearly provided the best fit when kinetic constants for glucose consumption were evaluated. The following constants (previously determined) were used to evaluate the maximum specific growth rate: 1) growth yield coefficient of 0.202 g biofilm/g glucose; 2) Mass of dry biofilm, 0.141 g (from the average maximum density, primary growth phase); and 3) the amount of glucose consumed to produce 0.141g of biofilm (calculated as 0.716g/216 hrs = 0.0033 g/hr) . The maximum specific growth rate was determined as 4.75E-03 hr^{-1}.

6.2.3 Growth yield coefficient(s)

In order to better described growth kinetics, stoichiometric related parameters (e.g. growth yield coefficients) should be quantified. The yield coefficients are based on the relation between the

amount of biomass generated and the amount of substrate consumed in order to produce the biomass, as described by equation 2.18. Figures 6.11 and 6.12 were used to calculate the growth yield coefficients for the SFCMBR systems over a period 264 hrs. The mass of glucose consumption over the length of the experiment was determined, as shown in Figure 6.10. The growth yield coefficients were evaluated at different growth phases, as indicated in Figures 6.11 and 6.12. During the primary growth phase, the growth yield was determined to be the highest at 0.299 g biofilm/g glucose, compared to the average growth yield coefficient, which was determined as 0.202 g biofilm/g glucose. The high value of the yield coefficient during the primary growth phase was expected as the biofilm grows exponentially, while trying to establish and stabilise in its new environment.
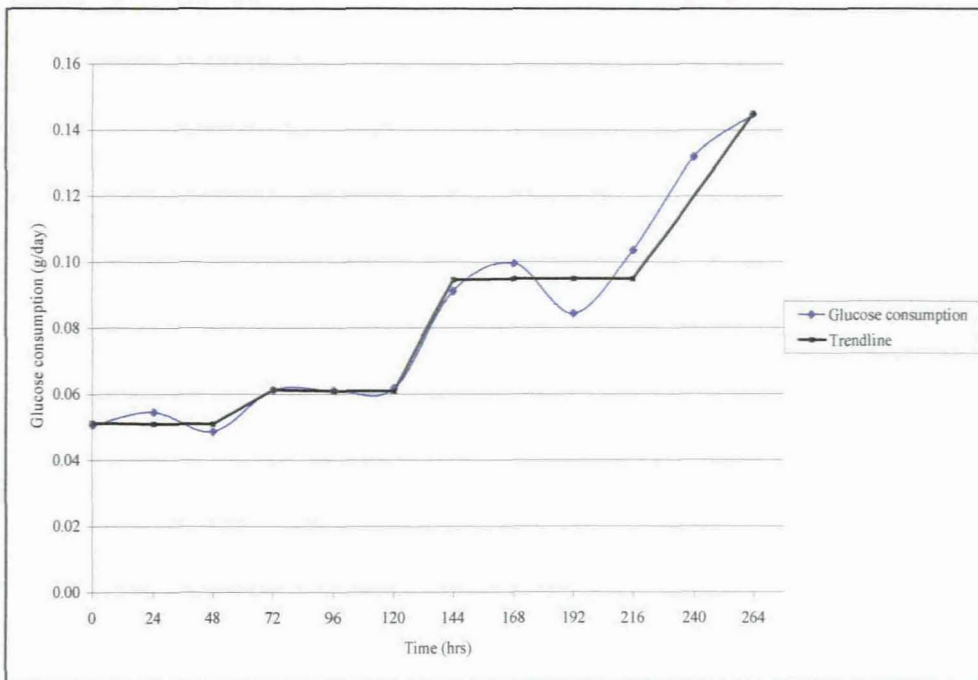
Figure 6.10: Mass of glucose consumption for the duration of the experiment.

The secondary phase growth yield coefficient was 0.230 g biofilm/g glucose, which was lower than that of the primary phase. The yield was lower as the biofilm has already established itself. The average ammonia-based growth yield coefficient was determined as 14.36 for ammonia. The vast difference between the growth yield coefficient values was dependent on the amount of substrates, which were available in the fresh nutrient medium and how much the biofilm consumed during its development. The biofilm used the glucose sparingly compared to ammonia, as 0.4 g/day of glucose was fed to the bioreactor system, of which less than 15% (0.06 g/day) was

84

consumed daily by the biofilm, compared to more than 84% of the ammonia, which was supplied (at a rate of 0.00156 g/day) to the bioreactor systems.
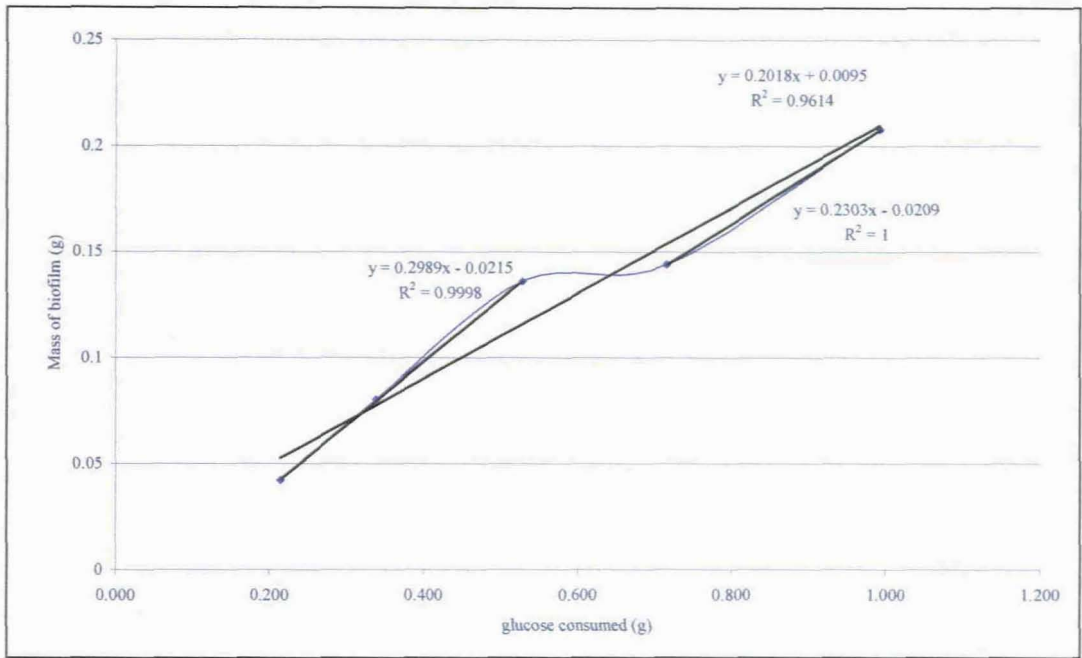
Figure 6.11: Plot of glucose consumed against biofilm generated over time. This was used to calculate the glucose based growth yield coefficient.
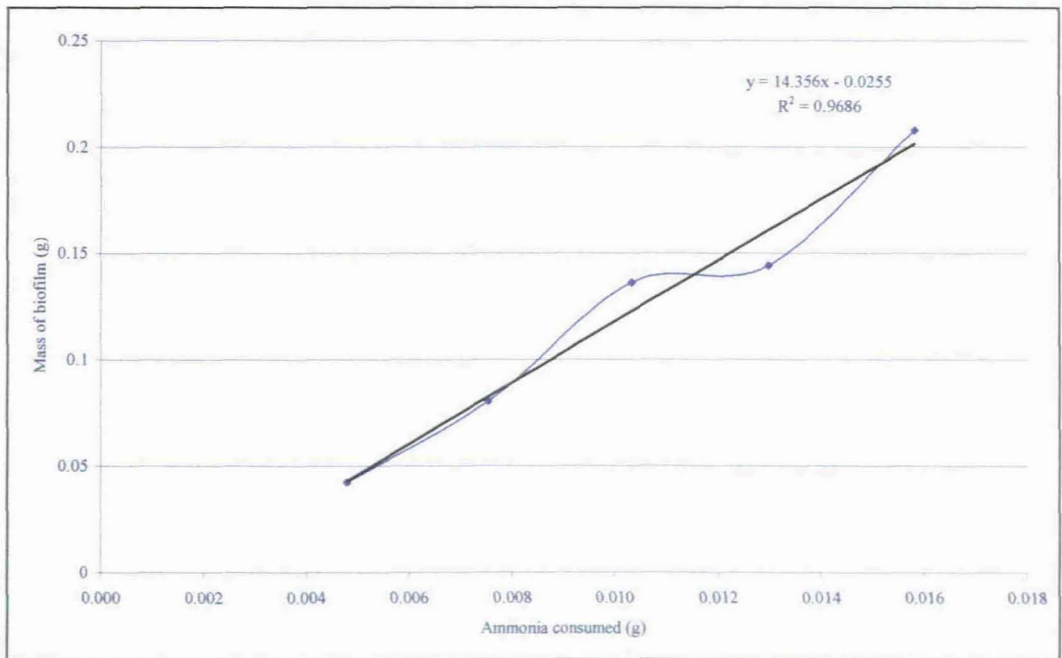
Figure 6.12 Plot of ammonia consumed against biofilm generated over time. This was used to calculate the glucose based growth yield coefficient.

6.2.4 Quantifying growth kinetics from biofilm density data: Alternative approach

In solving equation 2.1 by integrating from an initial dry density to a maximum dry density, which was obtained in the simulated model in section 6.2.1, the value of the specific growth rate obtained was 0.024 hr^{-1}, which was higher compared to the maximum specific growth rate of 4.75E-03 hr^{-1}, which was obtained from the glucose consumption results in section 6.2.2.3. The kinetic parameters were obtained by using glucose consumption (obtained using the Lineweaver-Burk and Eadie-Hofstee plots) clearly needed to be reviewed and compared with the results obtained from the kinetic parameters obtained from the dry biofilm density data. In this section the obtained results were generated from the simulated density data.

6.2.4.1 Determination of maximum specific growth rate

In the exponential growth phase, biomass doubling occurs and the maximum slope of the curve will be a representation of the specific growth rate of the biofilm in its particular environment. The biofilm density profile was described mathematically by a growth function, which was derived from equation 2.4, in which a growth rate constant, k_f, of 0.035 hr^{-1} was obtained and this was identified as the primary model.

In order to evaluate the maximum specific growth rate, the natural logarithm of equation 2.1 was used by using data obtained from the primary model. The natural logarithm of biofilm density was plotted against time, as shown in Figure 6.13. The steepest slope of the curve was found to be 0.032 hr^{-1} between 0 to 17.5 hrs. This slope represents the maximum specific growth rate and it was reasonable compared to the value of the growth rate, k_f constant of 0.035 hr^{-1} obtained. It may be concluded that the maximum specific growth rate, $\bar{\mu}_{max}$ was equivalent to the growth rate constant, k_f, even though this was not implicitly stated in any literature, which was reviewed.
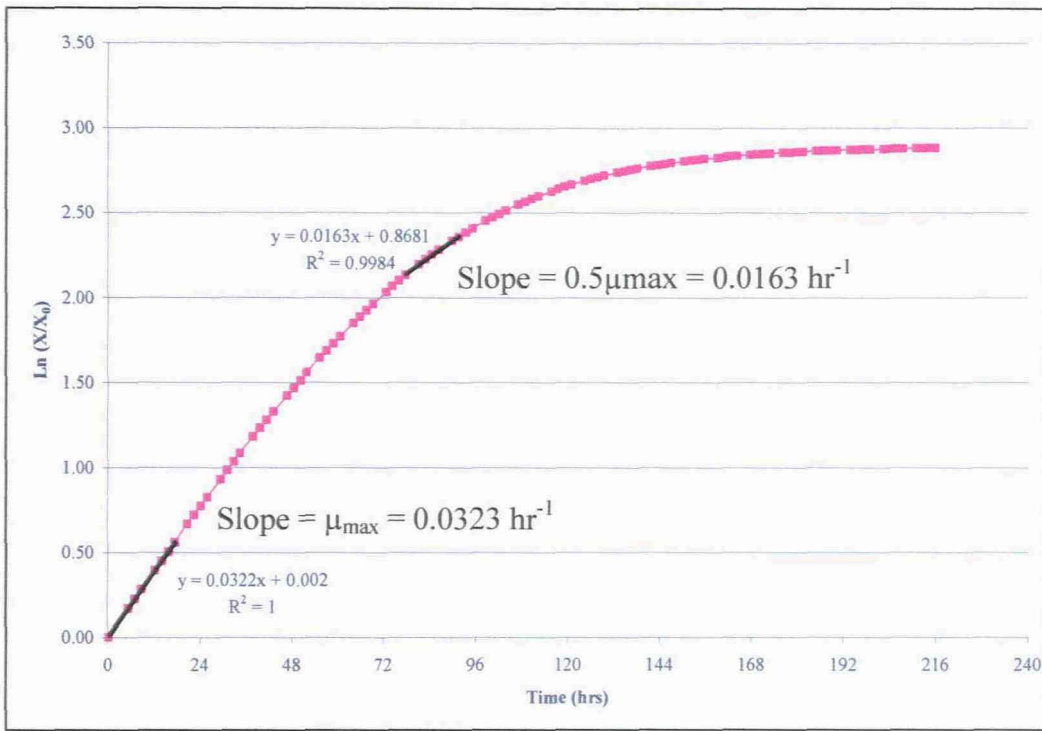
Figure 6.13: Evaluation of the maximum specific growth rate by using biofilm data obtained from simulated density data.

6.2.4.2 Determination of specific growth rate

The specific growth rate was determined by using equation 2.1 at different densities over the primary growth phase period, as shown in Figure 6.14. It was observed that the specific growth rate reduces with time as the biofilm develops in the SFCMBR systems. The highest specific growth rate was achieved in the earlier stages of the biofilm development, with values of 0.0329 to 0.0314 hr^{-1} during 0 to 17.5 hrs. This confirmed the results, which were obtained for the maximum specific growth rate which falls within the range of the highest specific growth rate.
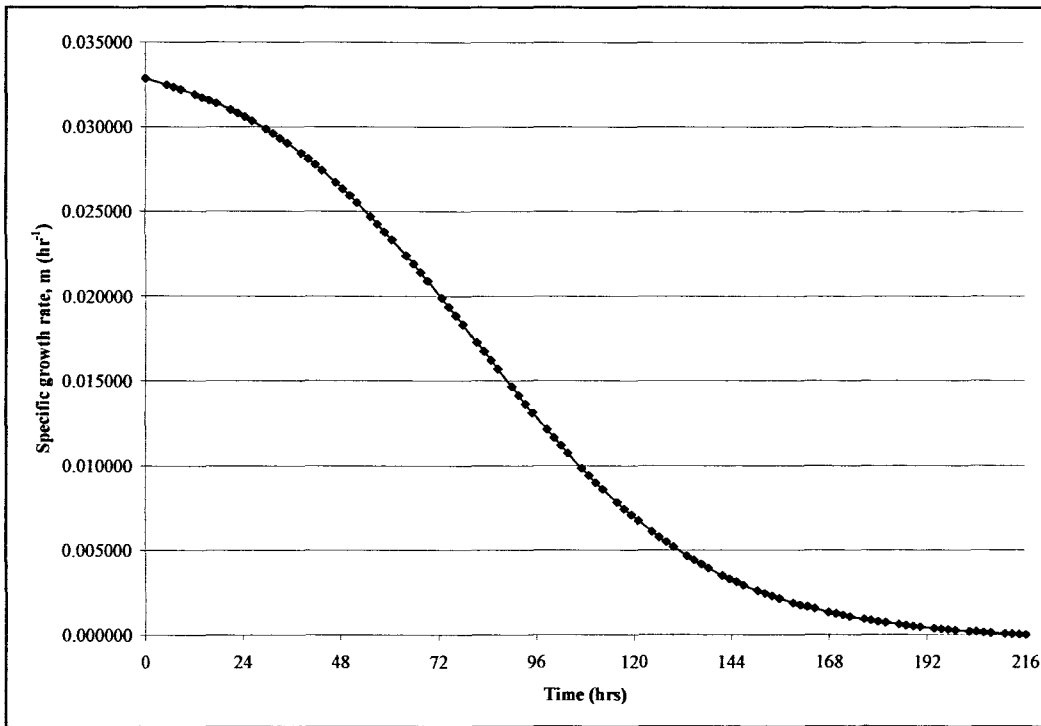
Figure 6.14: The specific growth rate determined over the primary growth phase period using simulated density data.

6.2.4.3 Monod's saturation constant

Microsoft Excel Solver® was used to determine Monod's saturation constant by using the specific growth rate curve, which was obtained in 6.2.4.2 (Figure 6.14). The program uses non-linear regression to solve equations by estimating one or more unknown parameters. The range of Monod's constant was not limited to any range and the initial values of the primary substrate (glucose) and density should be predetermined for use in the program. The initial substrate concentration (S_0) and initial density (X_0), which was used in the program, were 9.72E03 g/m^3 and 5.33E4 g/m^3, respectively.

The growth curve was predicted by combining the Monod equation (equation 2.2) and the equation for the growth yield of cell mass based on substrate consumption (equation 2.18), by using the rate of cell growth, as characterised by the specific growth rate as defined in equation 2.1, to yield the following rate expression (Shuler and Kargi, 1992):

$$\frac{dX}{dt} = \frac{\mu_{max}\left(Y_{X/S}S_0 + X_0 - X\right)X}{\left(K_m Y_{X/S} + Y_{X/S}S_0 + X_0 - X\right)} \qquad 6.1$$

The Monod's saturation constant can be evaluated where the specific growth rate equals to half the maximum specific grow rate (i.e. $\bar{\mu} = 0.5 * \bar{\mu}_{max}$). By using Figure 6.13, it was established that the slope of 0.0163 hr^{-1} was between 77.9 to 91.7 hrs, which is almost equivalent to half the slope that was used to determine the maximum specific growth rate. By using equation 6.1, with the required input parameters, the value of the Monod's saturation constant was established as 2772.3 g/m^3 which was lower than that obtained from glucose consumption data.

6.2.4.4 The effect the lag phase has on modelling growth kinetics

In this study, the lag phase was technically difficult to study, as quantitative data was lacking. By clearly not understanding the lag phase biofilm distribution, the obtained kinetic parameters can be both misleading and inaccurate. The biofilms physiological state during the lag phase will have direct impact on the primary growth phase, thus affecting values of the kinetic parameters, which were obtained. By determining the biomass, which developed during the lag phase, growth kinetic modelling can be improved.

6.2.5 The effect of different spore concentrations on substrate consumption and biofilm development

Spore concentrations of one, three and six million were used for inoculation. The spore solutions were prepared, as described in section 5.2.2 and Appendix A6. Dry biofilm mass and density was determined by using a helium pycnometer, after drying the biofilm at 60 ^0C for 12 hours in an incubator to remove excess moisture. A concentration of glucose and ammonia content in the permeate samples were determined by using test kits.

The SFCMBR systems used were similar to those described in the material and methods section. The bioreactors were positioned vertically. The daily and accumulative concentrations of glucose

and ammonia consumption obtained for each SFCMBR were subtracted from the initial concentration of feed, to yield a corresponding consumption in g/m^3 over a period of 11 days.

6.2.5.1 Consumption of glucose and ammonia

The glucose and ammonia, which were used daily was as shown in Figure 6.15 and 6.16. The nutrient medium contained 0.00156 g/day and 0.4 g/day of ammonia and glucose respectively, which were continuously fed to the SFCMBR systems daily. Bioreactors inoculated with one million spores showed a lag phase in ammonia consumption, compared to those inoculated with higher spore concentrations. After 72 hrs, 95% of the ammonia supplied to the SFCMBR systems was consumed in all the bioreactor systems inoculated with different spore concentrations compared to 15% of glucose. Glucose consumption increased with an increase in the inoculated spore concentration between 72 to 192 hrs as more biomass was generated.

Clearly for SFCMBR systems, which were inoculated with six million spores, there was a decline in the use of glucose during the period of 168 to 240 hrs. This was due to acute biomass losses in the bioreactors, attributed to the heaviness of the biofilms, which led to sloughing (see Table 6.1). The glucose consumption pattern for the bioreactors inoculated with one and six million spores was erratic because of the limited amount of samples, which were available for analysis, as compared to those inoculated with three million spores. Different consumption rates and stages were not established for the bioreactors inoculated with one and six million spores, as was done using three million spores in sections 6.2.2 and 6.2.3.
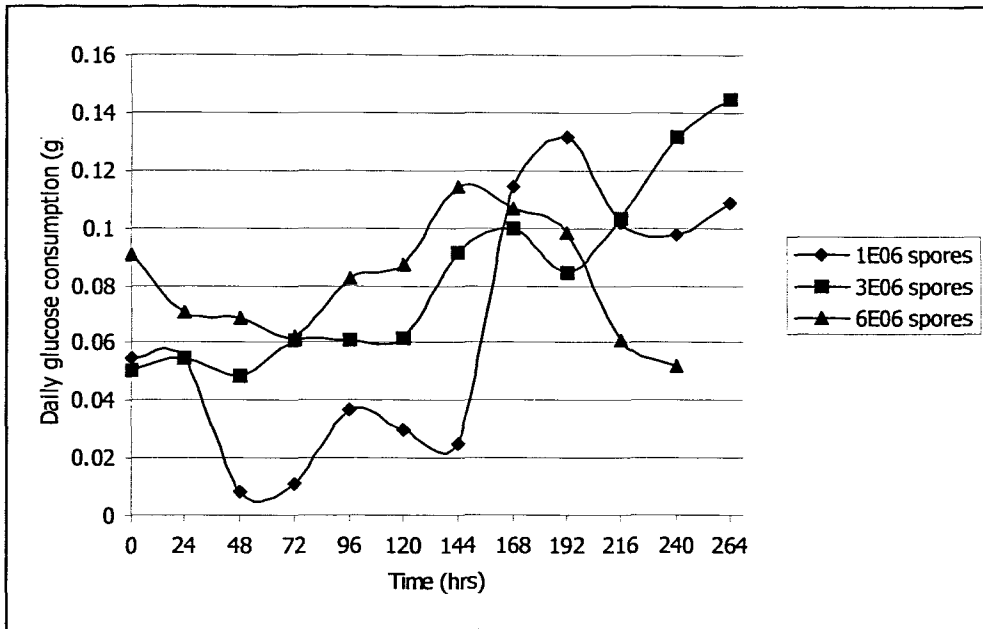
Figure 6.15: Daily glucose consumption curves for different biofilms cultivated by using different spore concentrations.
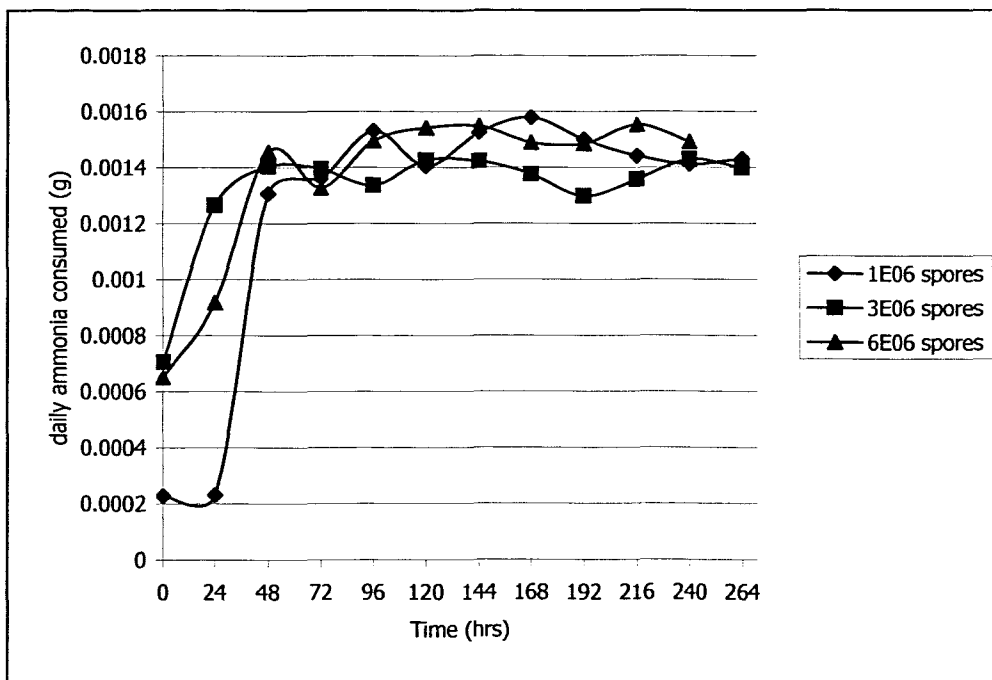
Figure 6.16: Daily ammonia consumption curves for different biofilms cultivated by using different spore concentration.

The accumulative consumption of glucose and ammonia increased with an increase in spore concentration inoculated on the membrane, as shown in Figures 6.17 and 6.18. This clearly

indicated that more biomass was generated in bioreactors that were inoculated with higher concentrations of spores (also shown in the sloughing of biofilms in the six million spore bioreactors). Accumulative ammonia consumption in bioreactors of three and six million spores was similar due to the small concentrations of the nitrogen source present in the nutrient medium.

By using the dry density curve (Figure 6.1) as a guide, glucose consumption after 144 to 168 hrs almost doubled as spore concentration was increased from one million to three million. Doubling the spore concentration from three million to six million, did not constitute the doubling of glucose consumption. During the same period, an increase in ammonia consumption was rated at approximately 17% when the spore concentration was increased from one to three and six million, as shown in Figure 6.18.
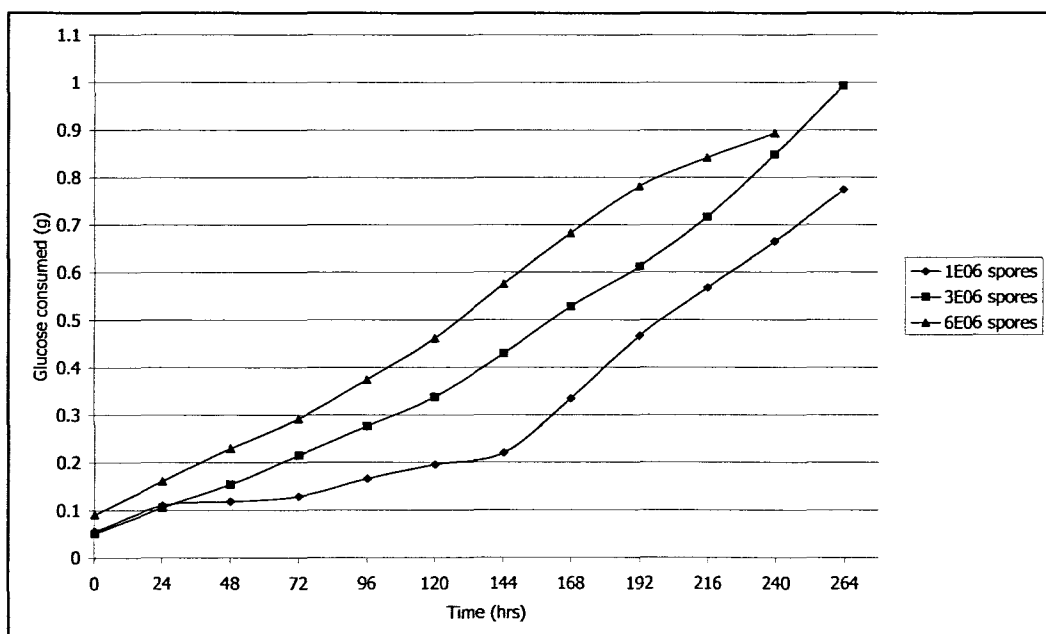
Figure 6.17: Accumulative glucose consumption profiles.
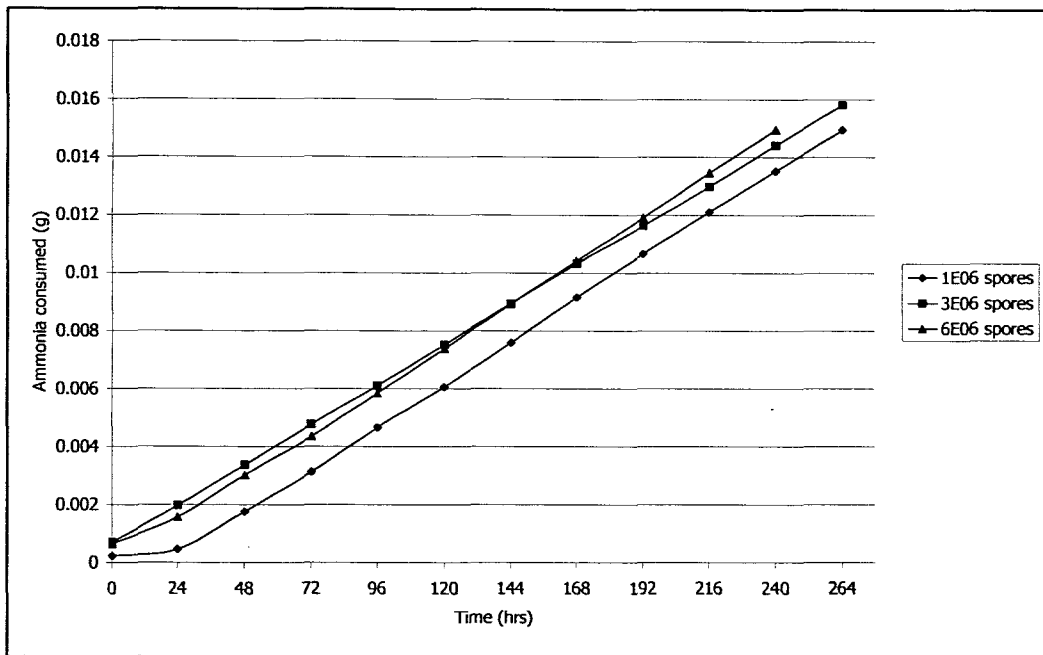
Figure 6.18: Accumulative ammonia consumption

6.2.5.2 Dry biofilm density and growth yield coefficient(s)

Dry biofilm density and biomass generated, increased with the amount of spores, which were used in the inoculation process, as shown in Table 6.1. The growth yield coefficient(s) are reduced, as more biomass was generated, even when substrate consumption increased. This implied that some of the glucose, which was consumed, was used for other biological phenomena than biomass generation in systems inoculated with higher spore concentrations. Glucose was identified as the primary substrate with growth limiting capabilities, thus making it suitable to use in the determination of growth yields coefficients.

Table 6.1: Growth yield coefficients.

Spore concentration per 40 ml	Total generated dry biofilm mass (g)	Dry biofilm density (g/m^3)	Growth yield coefficient (g biofilm per g glucose)
1 million (264 hrs)	0.203	1.16E06	0.262
3 million (264 hrs)	0.208	1.34E06	0.209
6 million (240 hrs)	0.183	1.17E06	0.205

The average growth yield coefficients were determined by using total generated dry biofilm mass for bioreactor systems which were inoculated with different amount of spores. The actual growth yield coefficient determined for the three million spore bioreactors was 0.209 g biofilm/g glucose, which was determined in section 6.2.3 as 0.202 g biofilm/g glucose, with a correlation coefficient of 0.96. This method was more robust compared to the graphical method. Other growth kinetic constants were not determined for bioreactors inoculated with one and six million spores as biofilm density was only determined at the end of the experiment.

6.3   *P. CHRYSOSPORIUM* BIOFILM STRUCTURE

The structure of biofilms in bioreactor systems has great importance as it affects substrate mass transfer across the surface of the biofilms. By clearly describing the morphology of the filamentous biofilm growing on the surface of the substratum, growth kinetics and other parameters can be better understood. The structure of *P. chrysosporium* biofilm immobilised in vertically orientated SFCMBR was described according to the different phases, as established in the growth kinetic section. As sufficient biofilm was not developed after 72 hrs of SFCMBR operation, the structural morphology was described in the SFCMBR systems, which operated beyond the lag phase. SEM photographs from different SFCMBR systems were used to evaluate the morphology of the biofilms.

6.3.1   Biofilm structure during the exponential phase

The biofilm in the exponential phase was determined between 72 and 120 hrs of operation. The mycelia near the substratum, was compact compared to that on the shell side, as shown in Figure 6.19. Some of the hyphae on the nutrient rich areas near the membrane surface, was completely septate, as growth of the lateral walls were meeting together, leaving minute pores at their tips, as shown in Figure 6.20. The structural format of mycelia was classified as vegetative, as most nutrients will be absorbed in this region, thus providing support for mycelia on the shell side. At this stage, reproductive propagules were not visible on the shell side where fertile mycelia were expected, due to limited nutrient availability as shown in Figure 6.21. In certain instances nutrient channels were evident between the compact-vegetative and aerial mycelia.

Membrane side, vegetative mycelia. (High nutrient area)

Shell side, aerial mycelia. (Limited nutrient area)
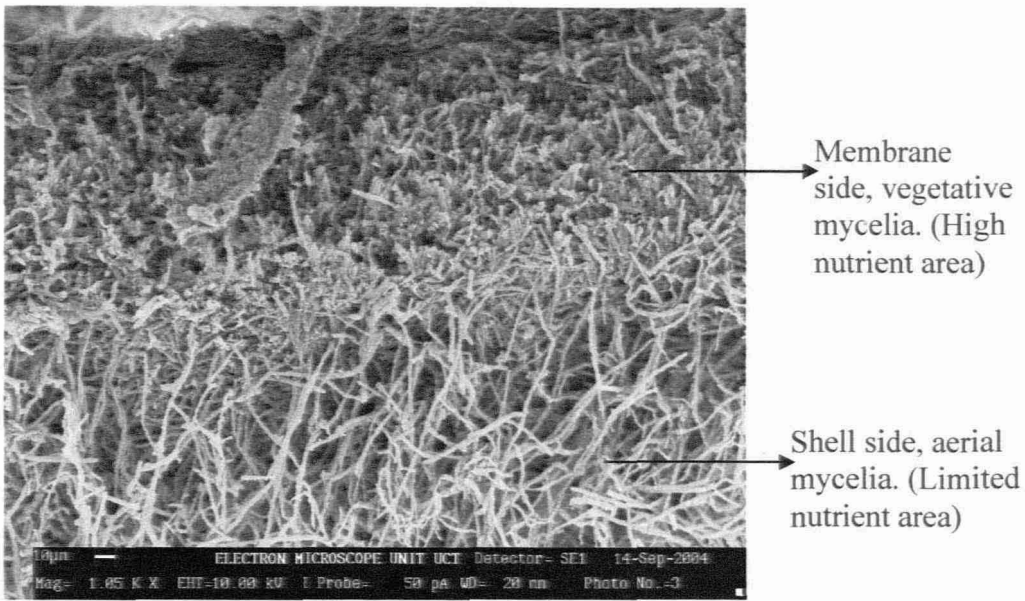
Figure 6.19: Biofilm differentiation during the exponential phase, showing vegetative and aerial mycelia.

Membrane side

Hyphae with complete septation
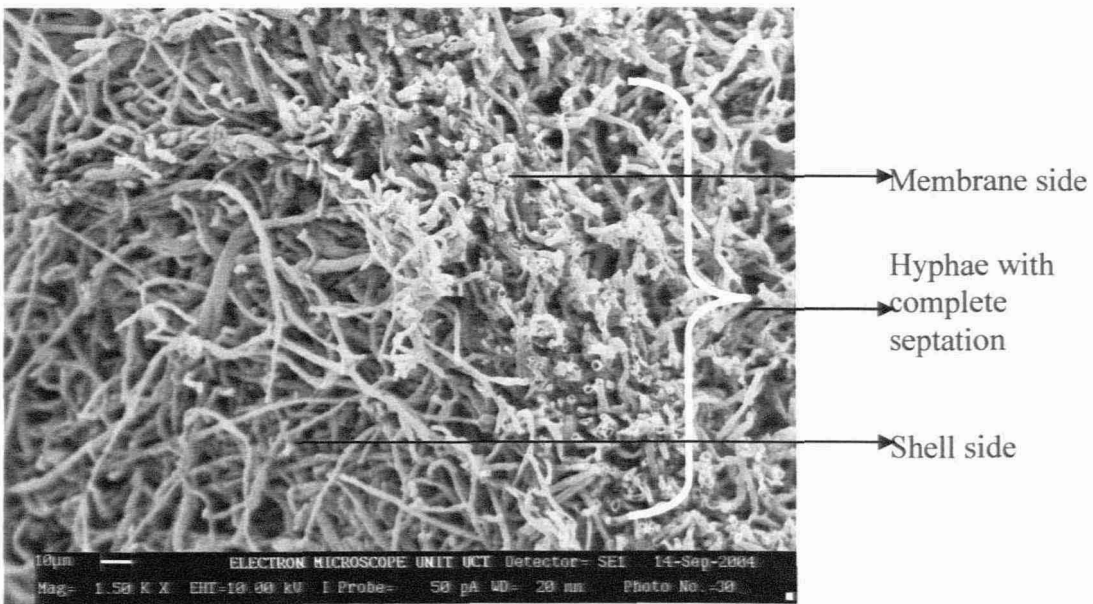
Shell side

Figure 6.20: Septate hyphae in the nutrient rich region near the substratum.
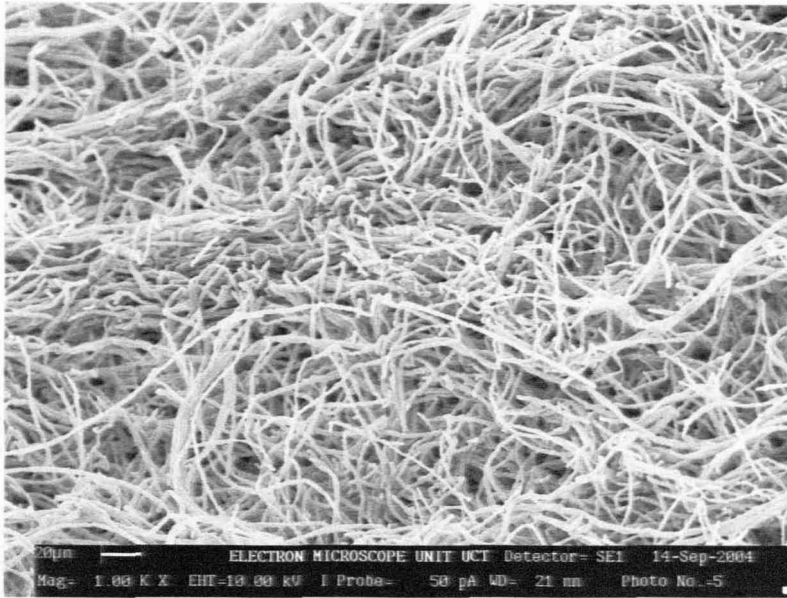
Figure 6.21: Mycelium structure on the shell side (extra-capillary space) of the bioreactor.

6.3.2   Biofilm structure during structural steady state

During the declining growth and structural steady state phases (120 to 216 hrs), fertile mycelia gave rise to reproductive propagules on the shell side, as shown in Figure 6.22.

Shell side mycelia with spore development
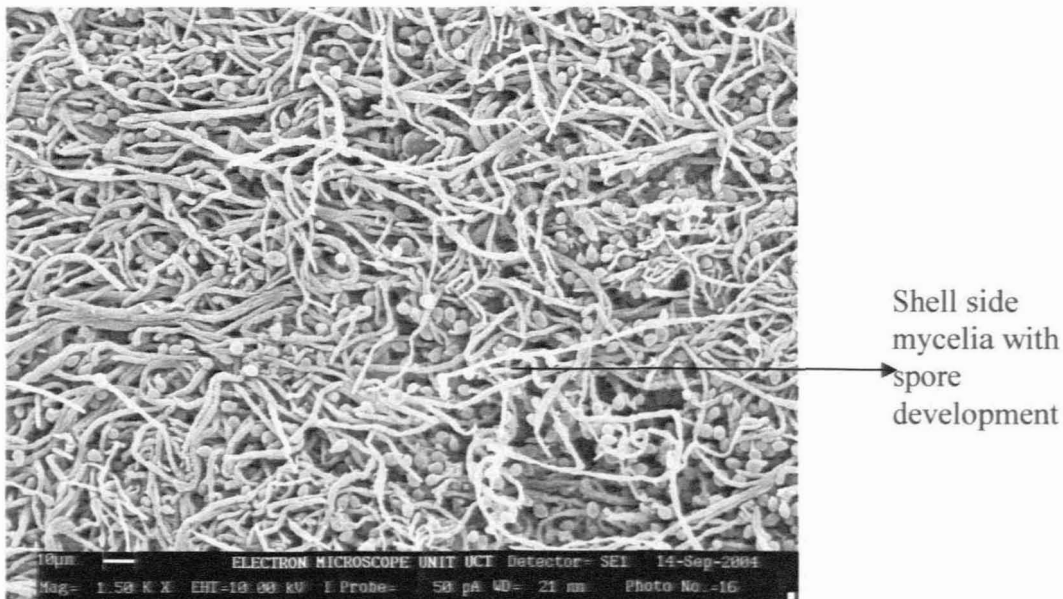
Figure 6.22: Fertile mycelia structure on the shell side with evident propagules on the end of hyphae.
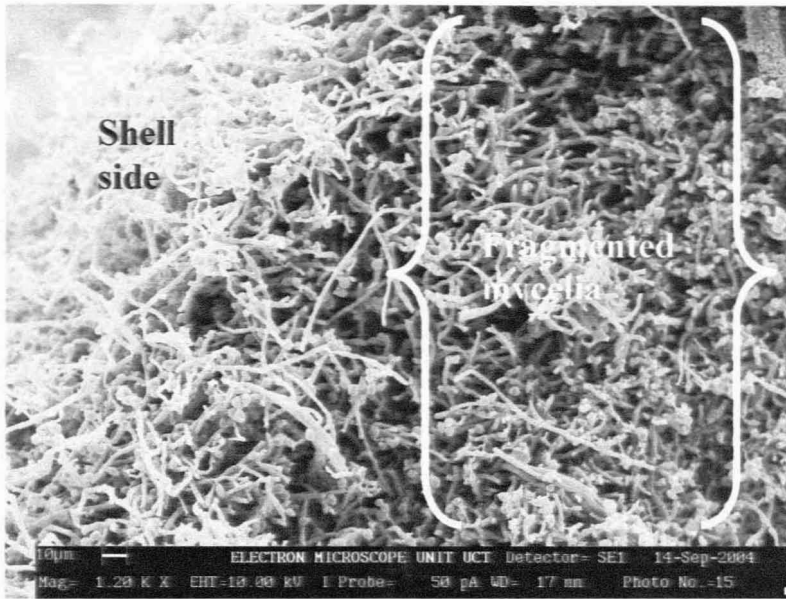
Figure 6.23: Segmented mycelia near the shell side.

A noticeable enlargement at the end of the hyphae was evident. Mycelia, which were further away from the substratum and closer to the shell side, were fragmented and compact-looking such as those near the substratum. This suggested that nutrient channels were established in this area, thus resulting in longer hyphael strands, which fragmented to adopt a vegetative state to absorb available nutrients, as shown in Figure 6.23. This clearly resulted in various successive growth cycles and thus achieved denser biofilms. The mycelium on the shell side, as shown in Figure 6.22, was weaved together and this resulted in limited oxygen diffusion through the biofilm, as shown in the oxygen mass transfer section. Oxygen flux, consumption and penetration depth was shown to be lower during this period (see Chapter 7).

6.3.3 Biofilm development after the primary growth cycle

This period was identified as being beyond 216 hrs of operation. During this period mycelia resembled the three categories of mycelia, which were identified as vegetative, aerial and fertile mycelia. Aerial mycelium appeared similar to vegetative mycelia, but was not as compact compared to vegetative mycelia near the substratum, as shown in Figure 6.24. Sporulation was evident as shown in Figure 6.25. It looked like some of the propagules produced, had germinated to provide another layer of mycelia on the shell side. The fertile mycelia appeared compact

97

compared to those identified in other periods. Upon physical inspection, it was observed that white layers of spores occurred on the outer surface of the biofilm during this period.
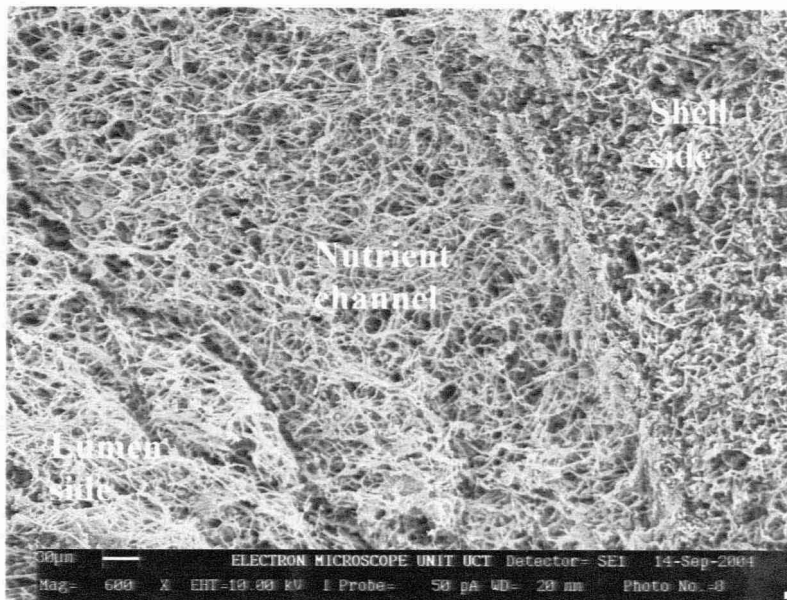
Figure 6.24: Mycelia on both the lumen and the nutrient channel showing compact hyphae, while highly fragmented hyphae on the shell side were observed.
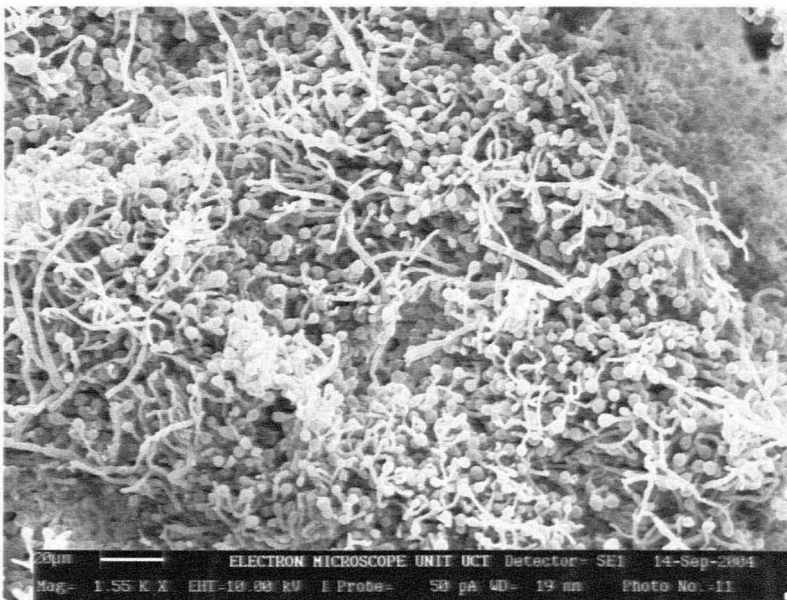
Figure 6.25: Fully developed propagules on the shell side of the biofilm.

6.4 MONITORING SFCMBR SYSTEMS OPERATION

The most important function of a membrane gradostat bioreactor with *P. chrysosporium* immobilised as a biocatalyst, is to produce enzymes which can then be used in various industrial applications such as bioremediation (explained in Chapter 1). During the operation of SFCMBR systems used in this study, both the pH and the redox potential were monitored in order to compare the biochemical make-up of the permeate. The average pH and redox potential was shown in Figures 6.26 and 6.27. Both *LiP* and *MnP* show unique characteristics, such as high redox potential and low pH optimum, as indicated by Oyadomari *et al.* (2003). By monitoring the pH and the redox potential, the researcher was able to indicate the possibility of enzyme production, even though enzyme activity was not quantified as this was not part of the study.
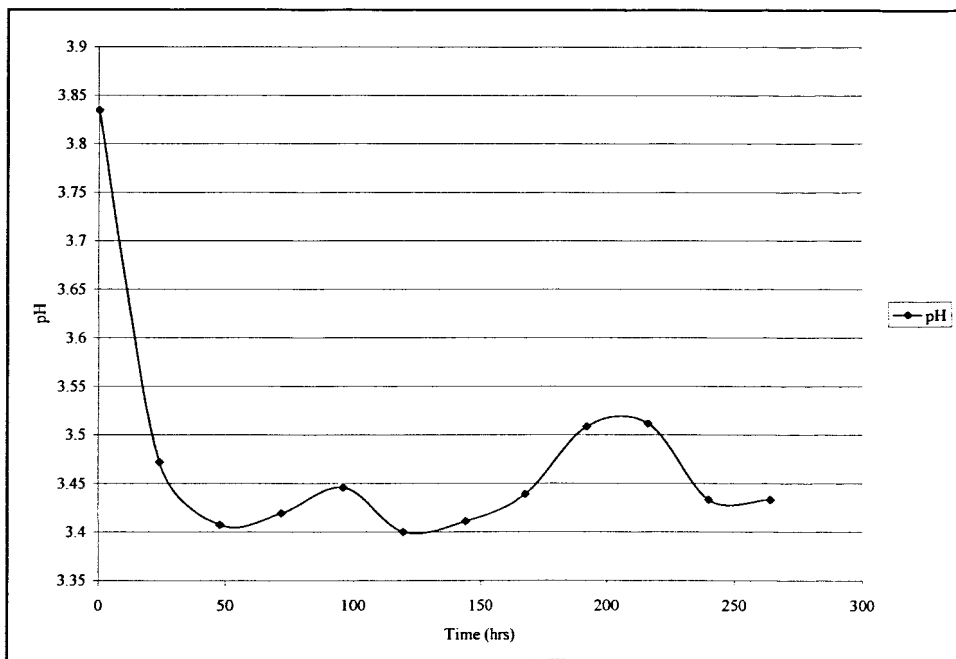
Figure 6.26: Average pH of permeate collected during the operation of SFCMBR systems operated over a period of 264 hrs.
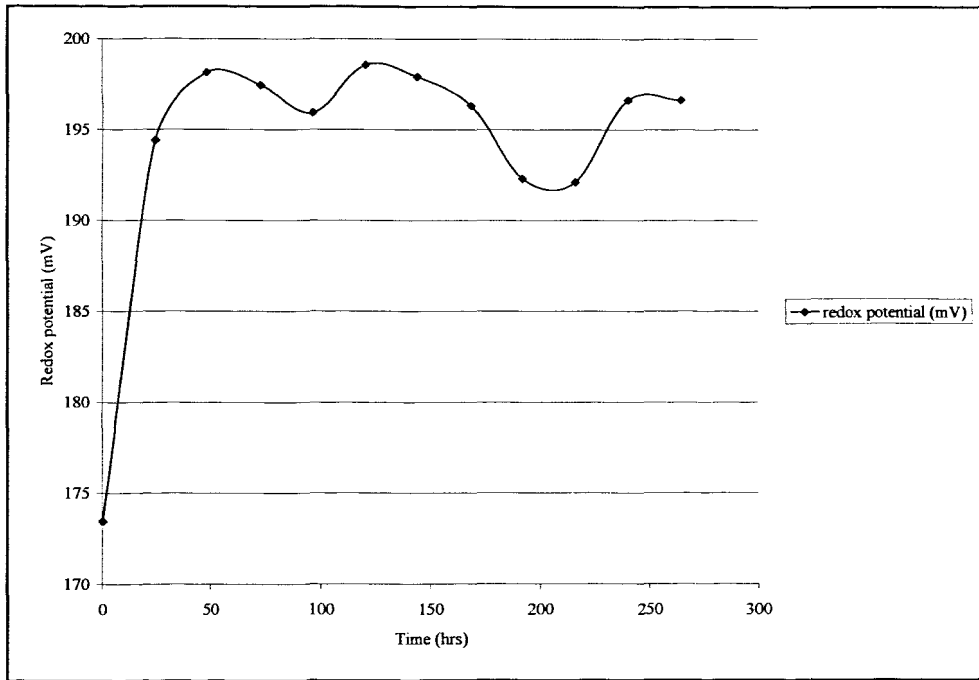
Figure 6.27: Average redox potential of permeate collected during the operation of SFCMBR systems operated over a period of 264 hrs.

CHAPTER 7 : MOMENTUM AND MASS TRANSFER

7.1 INTRODUCTION

Continuously operated hollow fibre membrane modules promise more rapid and constant performances as nutrients are supplied by pressure vessels and peristaltic pumps. In effectively designed membrane bioreactors, understanding the nature of momentum transfer of nutrients and solute patterns inside the membrane is essential, as this can affect the growth of biofilms. Pressure readings (taken using pressure transducers) were used to demonstrate how to model nutrient medium distribution in the lumen side of the membrane, from fundamental fluid dynamics laws.

The mass transfer of substrates can be modelled by using growth kinetic constants at different stages during the biofilm growth period. The transfer of substrates between phases is important in bioreactor systems, in which gases and fluids are involved. The designed bioreactor has both dissolved oxygen (DO) and glucose based nutrient medium transferred across the biofilm thickness. Mass transfer parameters/constants were evaluated in SFCMBR systems and were used to mathematically model the mass transfer of oxygen and glucose medium.

7.2 MOMENTUM TRANSFER IN THE SUBSTRATUM

A description of flow behaviour (momentum transfer) in membrane bioreactors is an important aspect of any bioreactor design. For all these bioreactors systems, where a biocatalyst is immobilised, the pressure drop and velocity data are of major importance. The analysis of nutrient flow behaviour in this study was more relevant to laminar flow in porous capillary membrane, where the dead-end filtration mode is applied. The pressure drop inside the membranes was determined to be proportional to the inlet flow rate as laminar flow was applied. This implies that the pressure drop was linked to the Poiseuilles law, while taking membrane characteristics into consideration.

7.2.1 Pressure profiles in SFCMBR systems

Pressure transducers were used to measure pressure along the lumen of the membrane in different SFCMBR systems, which operated at a dead-end filtration mode without an immobilised biofilm. The flow rate of the liquid medium was 1.67 ml/hr. The average pressure obtained along the membrane lumen (inlet and outlet) was 3.7 to 4.6 Pa, as shown in Figure 7.1. It was observed that during the initial stages (<400 minutes) of the operation, the inlet pressure (P_1) was higher compared to the outlet pressure (P_2). This period was classified as an unsteady state, as pressure readings were irregular, as the system adjusted itself to the operating conditions. After 6.5 hrs (>400 minutes), the outlet pressure (P_2) was observed to be higher than that of the inlet pressure (P_1). The overall pressure drop during the experiment was minimal, as expected in laboratory scale membrane bioreactors. Membrane permeability varied as it was seen with each bioreactor system. During the steady state operation of the bioreactors, a purging effect, shown with arrows, was identified. This was attributed to the polysulphone membrane's elasticity. As the pressure built up in the lumen, the membrane expanded to accommodate the incoming liquid medium to an extent that the pores in the lumen were big enough to purge sufficient liquid to release the pressure. This phenomenon was only identified during this study and needs to be verified.
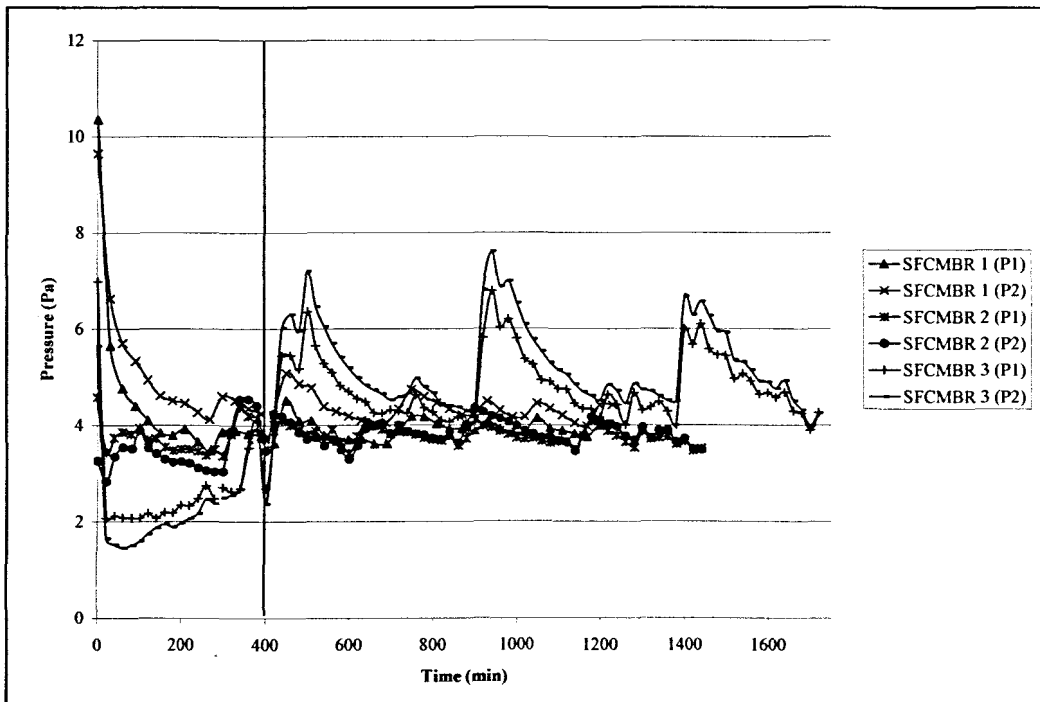
Figure 7.1: Inlet and outlet pressure profiles in vertical SFCMBR operated at 37 °C at a flow rate of 1.67 ml/hr.

7.2.2 Pressure drop modelling

The solutions for the first and second order differential equations (equations 3.18 and 3.19), for the pressure drop along the lumen of the membrane, were developed to be used for either an increase or decrease in pressure drop, by using the inlet pressure as a reference point. The solutions, which were obtained, included membrane characteristics, which the lumen pressure was dependent on. Table 7.1 shows results, which were obtained from different SFCMBR systems, which operated under the same conditions, in which inlet pressure (P_1) was used to determine exit pressure (P_2). The pressure drop models that were developed can be changed to suit operating conditions, for either unsteady or steady operation, by changing the overall arithmetic sign as follows: 1) for a pressure drop, a positive sign for the model was used; and 2) for an increase in pressure, a negative overall arithmetic sign was used. The accuracy of the models was determined by using a ratio between the modelled exit pressure and the experimental exit pressure (P_2). Higher accuracy was obtained for modelled pressure in both steady and unsteady state regions.

Table 7.1: Unsteady and steady state pressure transducer readings with modelled outlet pressure (modelled using mathematical models) and accuracy results.

Operating conditions	Unsteady state <400 minutes			Steady state >400 minutes		
Bioreactor	1	2	3	1	2	3
Measured P_1	4.52	3.74	2.69	4.12	3.77	4.30
Measured P_2	5.14	3.48	2.37	4.62	3.74	4.55
Modelled P_2	5.29	2.97	1.93	4.89	3.00	5.07
Accuracy	0.97	1.17	1.23	0.95	1.24	0.90

A permeability constant of 1E-12 m^2, as determined by Solomon (2001) was used for the modelling of the outlet pressure during this study. This value was a clear representative for all the capillary membranes, which were used in the study. To improve the accuracy of the results, individual membrane permeability should be determined in future studies.

7.2.3 Lumen velocity profiles development

The velocity profiles were developed for a system consisting of either a single fibre membrane or a multi-capillary membrane system, which was enclosed in a cylindrical cartridge. The profiles, which were developed, provided a description of flow in an average capillary membrane. The analysis of the velocity profiles were restricted to one SFCMBR system to demonstrate the profiles of a liquid medium, which was transported through the lumen of the membrane. Pressure readings from bioreactor #1 were used as an example to analyse the velocity profiles during the steady and unsteady state periods. In the analysis a constant shell side pressure equivalent to one atmosphere (101300 Pa), was used.

7.2.3.1 Axial velocity profile

The axial velocity profiles were analysed along the membrane radial length using equation 3.5 for both the steady and unsteady states' operating conditions, as shown in Figures 7.2 and 7.3. An inlet pressure (for the steady and the unsteady state), of 4.52 Pa and 4.12 Pa from bioreactor #1 was used for modelling axial velocity profiles for the unsteady state and steady state respectively. An inlet centre line velocity of 2.91E-04 m/s (calculated from volumetric flow rate), was used. From the profiles in Figure 7.2 it was observed that there was an increase in the axial velocity of the medium when the outlet pressure (P_2) was higher, compared to the inlet pressure (P_1) across the membrane. An increase in the axial velocity during the unsteady state period was obtained, compared to a decrease of the same magnitude during the steady state period. This effect was attributed to low membrane permeability where air was trapped in the lumen of the membrane, while the liquid medium flowing through the membrane was fed into the bioreactor system, which was operated in a dead-end filtration mode. This created an air-liquid medium build-up, thus effectively increasing the pressure during the unsteady state period. The steady state period showed a decrease in pressure along the membrane length which resulted in reduced velocity profiles along the length of membrane. The distribution in the liquid medium was fully developed thus resulting in higher inlet pressure (P_1), compared to outlet pressure (P_2).
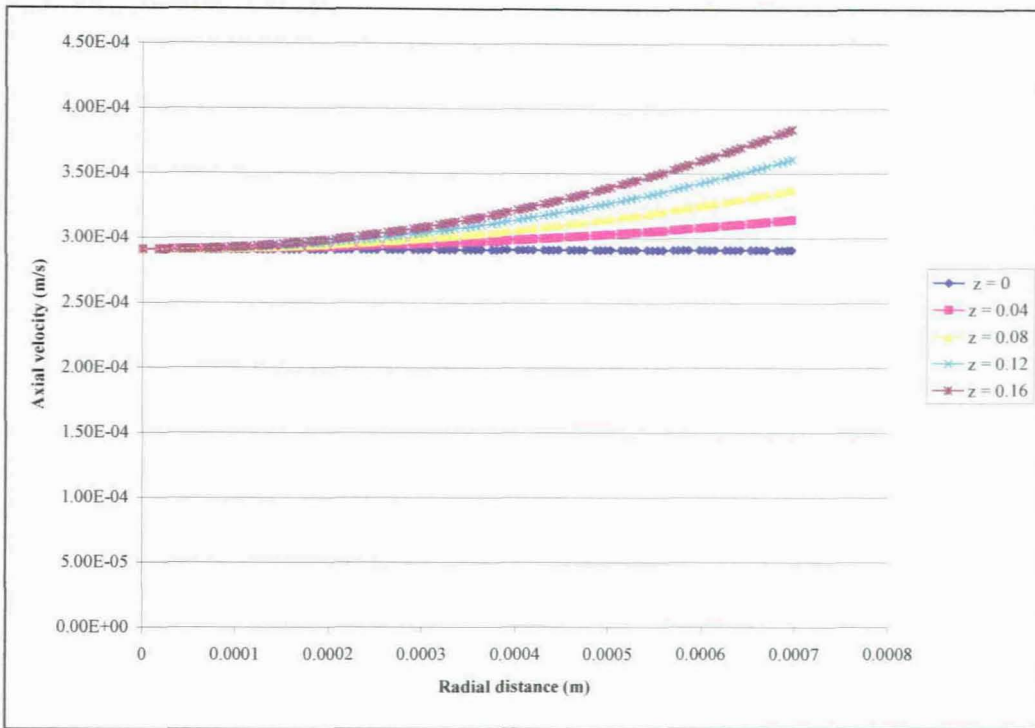
Figure 7.2: Unsteady state axial velocity profiles along the membrane radial distance using different axial lengths of the membrane.
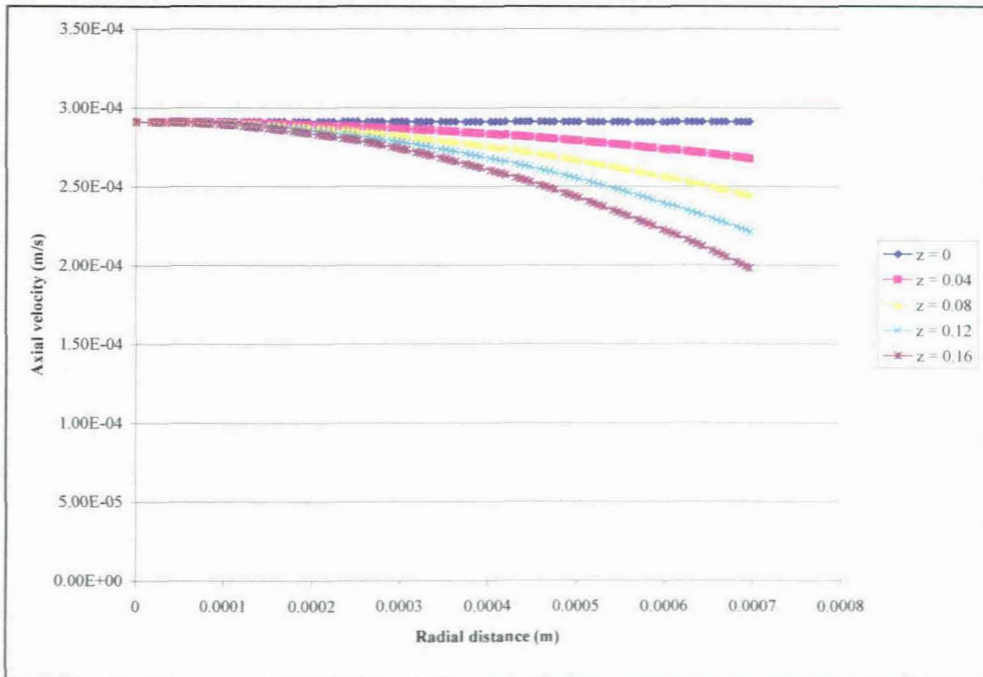
Figure 7.3: Steady state axial velocity profiles across the membrane radial distance using different axial lengths of the membrane.

7.2.3.2 Radial velocity profile

The radial velocity results were profiled across the membrane radial distance by using equation 3.7. The radial velocity at the centre of the membrane was set at 0 m/s (Kelsey *et al.*, 1990; Bruining, 1989), as shown in Figures 7.4 and 7.5. To evaluate the profiles, local pressures were used to evaluate the distribution of velocity at an axial length of 0 m and 0.16 m. In Figure 7.4, 4.52 Pa was used at an axial length of 0 m, while 5.14 Pa was at an axial length of 0.16m to profile radial velocities under unsteady state operating conditions. There was no change in the velocity profiles across the axial membrane length. The radial velocity at the lumen wall was quantified to be approximately 1.01E-07 m/s at any given length across the membrane. A reverse trend was shown in Figure 7.5, where negative velocity results were obtained for the steady state period.
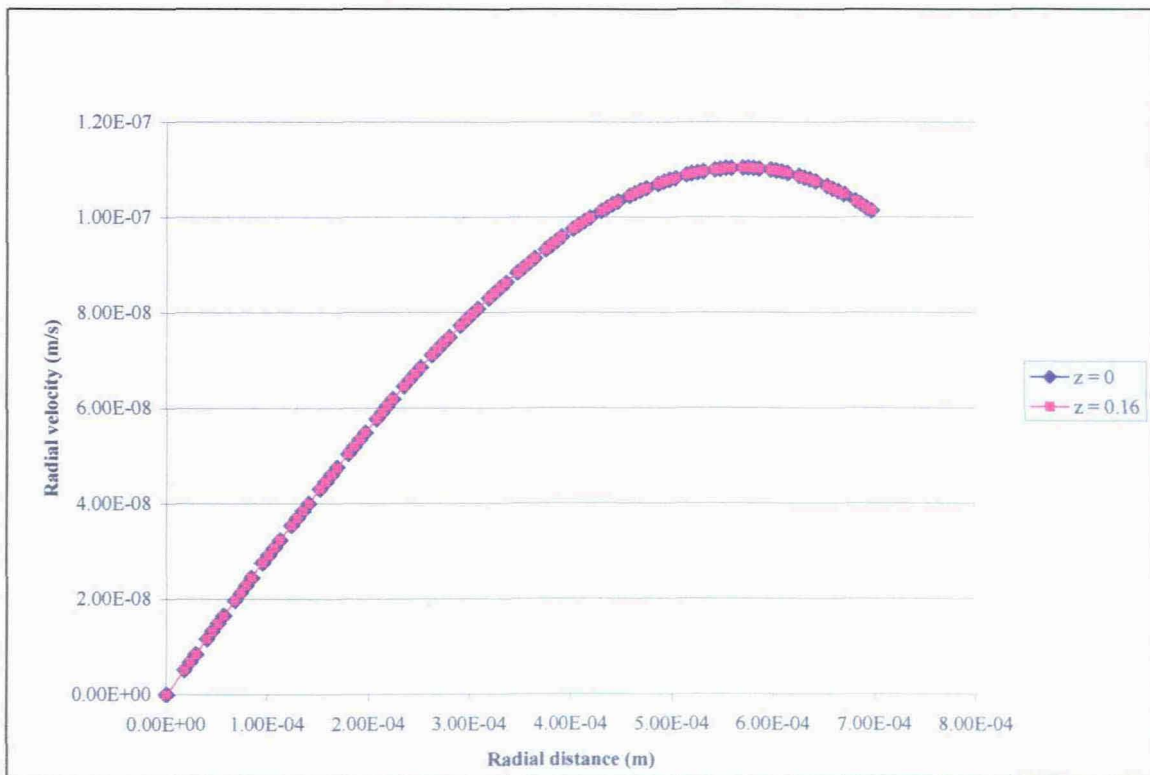
Figure 7.4: Radial velocity profiles across the membrane radial length at two different points across the length of the membrane (unsteady state).
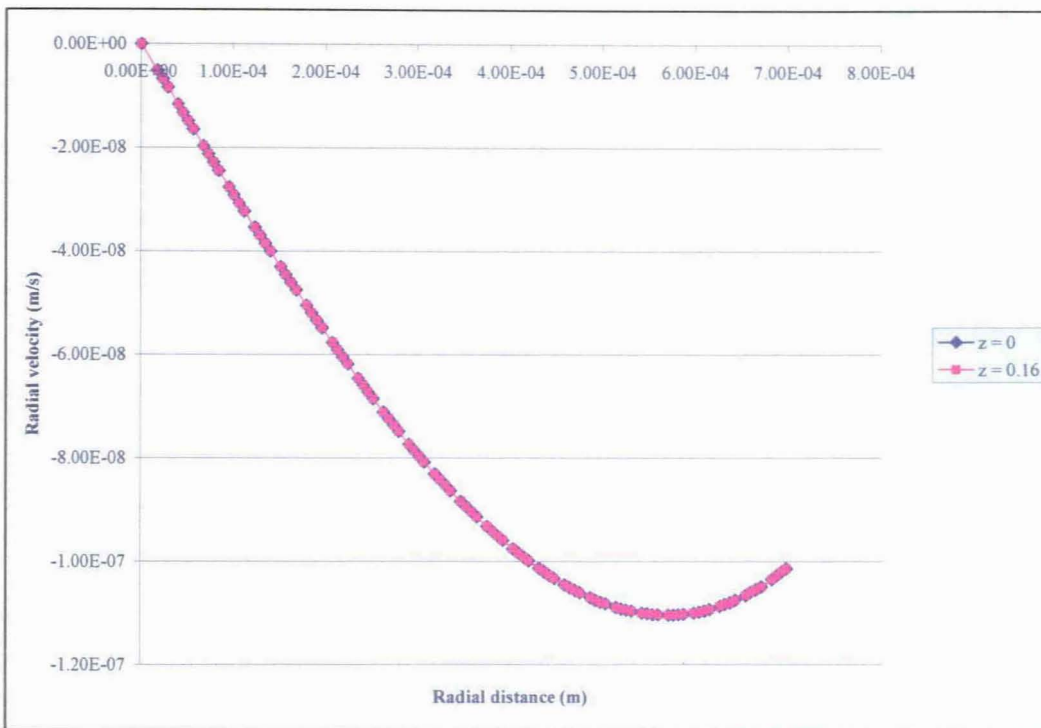
Figure 7.5: Radial velocity profiles across the membrane radial length at two different points across the length of the membrane (steady state).

7.3 OXYGEN MASS TRANSFER ACROSS THE BIOFILM

By assuming steady state conditions, the dissolved oxygen profiles, which were obtained by using an oxygen microsensor, were used in PROFILE 1.0 software, to determine the biological consumption for every measured point in the biofilm by using a one-dimensional mass conservation equation (equation 3.21), where the biofilm diffusivity was proportional to the product of biofilm porosity and molecular diffusivity. By using the software application, it was possible to locate the different zones of consumption and the resulting flux across the biofilm. High correlation coefficients ($R^2 > 0.90$) were considered when calculating mass transfer parameters. In the software calculation, more than 5000 steady state profiles were tested. Three oxygen profiles were measured from each of the SFCMBR systems taken off. Average profiles from each SFCMBR systems taken off, were used for calculations in this section.

7.3.1 Oxygen penetration depth

The oxygen penetration depth is an important control and design parameter for the performance of a fixed film bioreactor, as indicated by Freitas dos Santos *et al.* (1995) and Pavasant *et al.* (1996). The maximum average oxygen penetration depth obtained was 390 µm, with an average oxygen concentration of 0.09 g/m³. The penetration depth of oxygen obtained was in agreement with that of Lejeune and Baron (1997), who showed a penetration range of 0 to 350 µm. Figure 7.6 show oxygen profiles at various times during the development of the biofilm. The average penetration depth and oxygen concentration was determined from individually measured profiles.
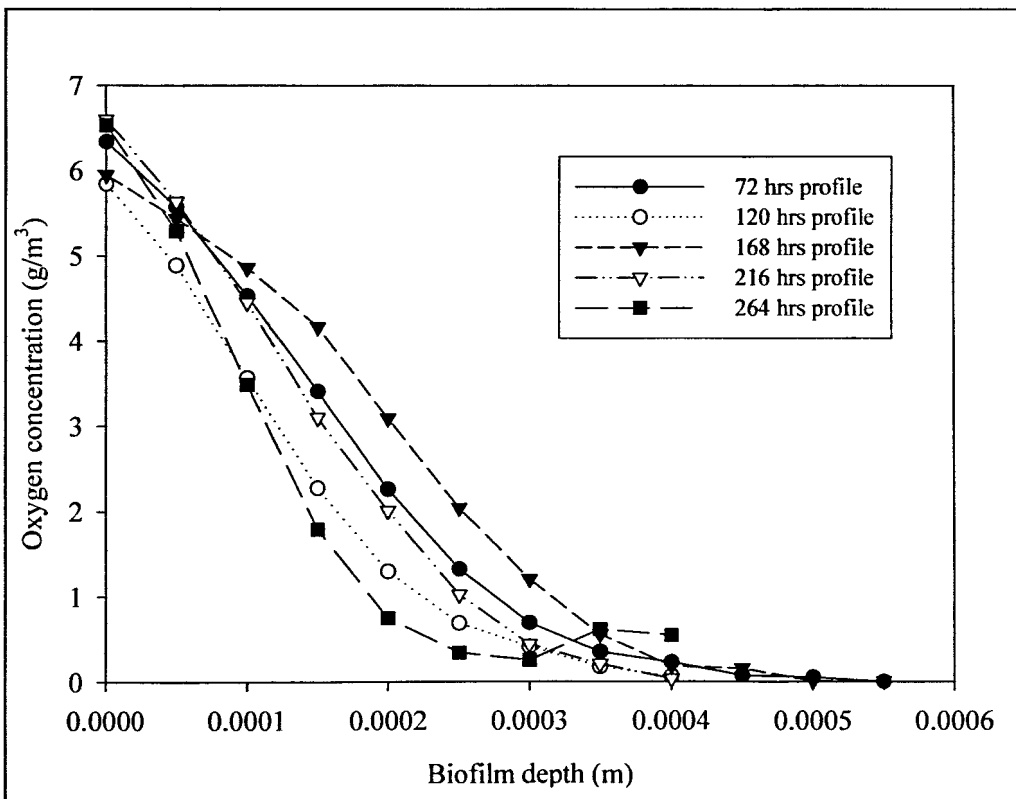
Figure 7.6: Average oxygen distribution measured in biofilms grown in bioreactors during different growth times.

7.3.2 Oxygen flux across the biofilm

The oxygen flux across the biofilm surface obtained from the PROFILE 1.0 software was plotted, as shown in Figure 7.7. As the biofilm grew, the structure became dense, which resulted in the biofilm becoming rough and this lead to a greater deviation in the flux values obtained. During the biofilm stationary phase at 168 hrs, (where fertile mycelia was visible on the shell side), the average flux obtained $(0.139 \text{ g/m}^2.\text{hr})$, was lower compared to other growth stages. One explanation was that the aerial mycelia strands began to compact as the rate of mycelia generation decreased, as shown in the growth kinetic section. During the exponential phase, the flux increased from 0.165 to $0.202 \text{ g/m}^2.\text{hr}$, as the biomass, which was generated, increased. At the start of the secondary growth phase, the flux increased from 0.238 to $0.295 \text{ g/m}^2.\text{hr}$ and the increase was 34% higher compared to that of the exponential phase.
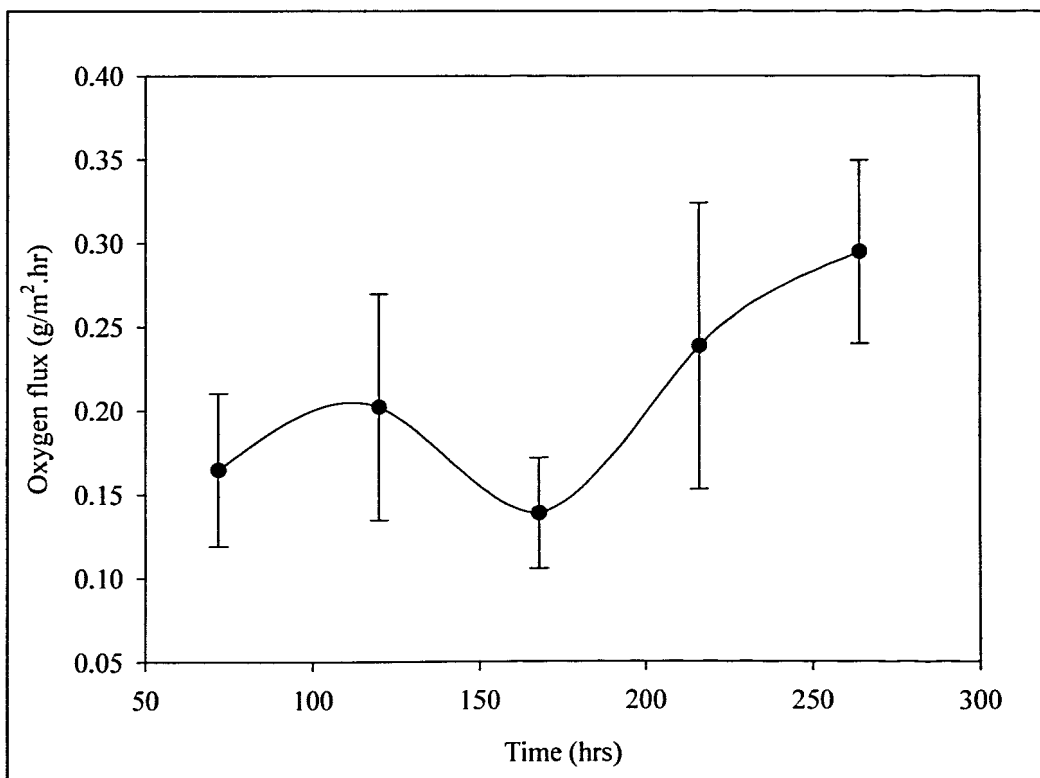
Figure 7.7: Oxygen flux across the biofilm surface at different growth stages.

7.3.3 Oxygen consumption rate

The consumption of oxygen was determined in different zones across the biofilm depth. The zones were classified by PROFILE 1.0 software, by changing consumption values with biofilm depth. The software finds the simplest consumption values, with the least number of descriptive variables to provide a good explanation for the measured oxygen profiles. Berg *et al.*'s, (1998) goal, when developing the Profile 1.0 software, was to find the combination of consumption rates that minimises the deviation between the calculated and the measured concentration profiles. For these reasons, the consumption data obtained was discussed under classified zones at different times and depth during biofilm development.

7.3.3.1 Oxygen consumption after 72 hrs of biofilm growth

During this period consumption of oxygen was divided into three zones, as shown in Figure 7.8. The first zone was classified as the zone of 180μm depth from the outside surface of the biofilm. It was observed that the average consumption was low (30.90 g/m^3.hr) in this zone, compared to the other two identified zones. Owing to the proximity of the zone to the shell side of the bioreactor system, the area was described as having a high oxygen flux, thus reducing the oxygen consumption rate. Aerial mycelia were shown not to be compact after 72 hrs of bioreactor operation. The second zone was identified as occurring between 180 to 350 μm in the biofilm. This was classified as a reaction zone during this particular period of bioreactor operation because high consumption rates of oxygen were quantified, averaging 777 g/m^3.hr. The third zone was closer to the substratum (>350 μm), with an average consumption rate quantified at 613 g/m^3.hr.
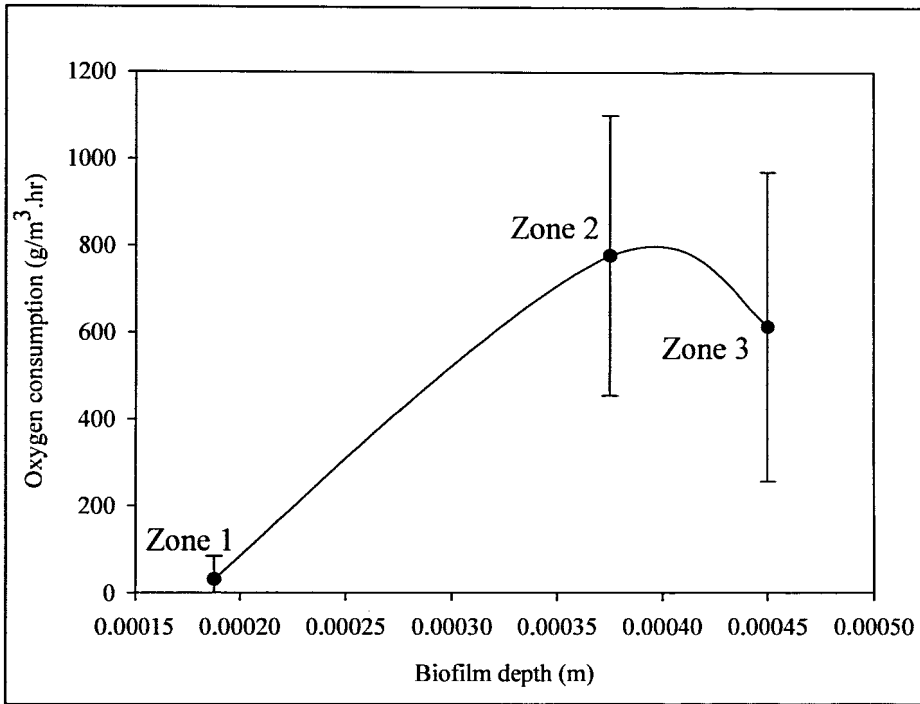
Figure 7.8: Average oxygen consumption profile in three different zones after 72 hrs of biofilm growth.

7.3.3.2 Oxygen consumption after 120 hrs of biofilm growth

Similar to the results obtained in section 7.3.3.1, consumption after 120 hrs of bioreactor operation was divided into three zones, as shown in Figure 7.9. The average oxygen consumption increased from 30.90 g/m^3.hr, (after 72 hrs of biofilm growth) to 298.7 g/m^3.hr (after 120 hrs of biofilm growth) in the first zone. This was attributed to an increase in flux and mycelia generation. This indicated that during the exponential phase, as the biofilm grew, more oxygen was used by the generated mycelia. Oxygen consumption in the reaction zone (zone 2), was calculated at 988.7 g/m^3.hr, which was determined as the highest compared to the other rates of consumption determined during the study. Near the substratum (zone 3), the consumption rates were determined at 561.7 g/m^3.hr, which was lower than that obtained in Figure 7.8.
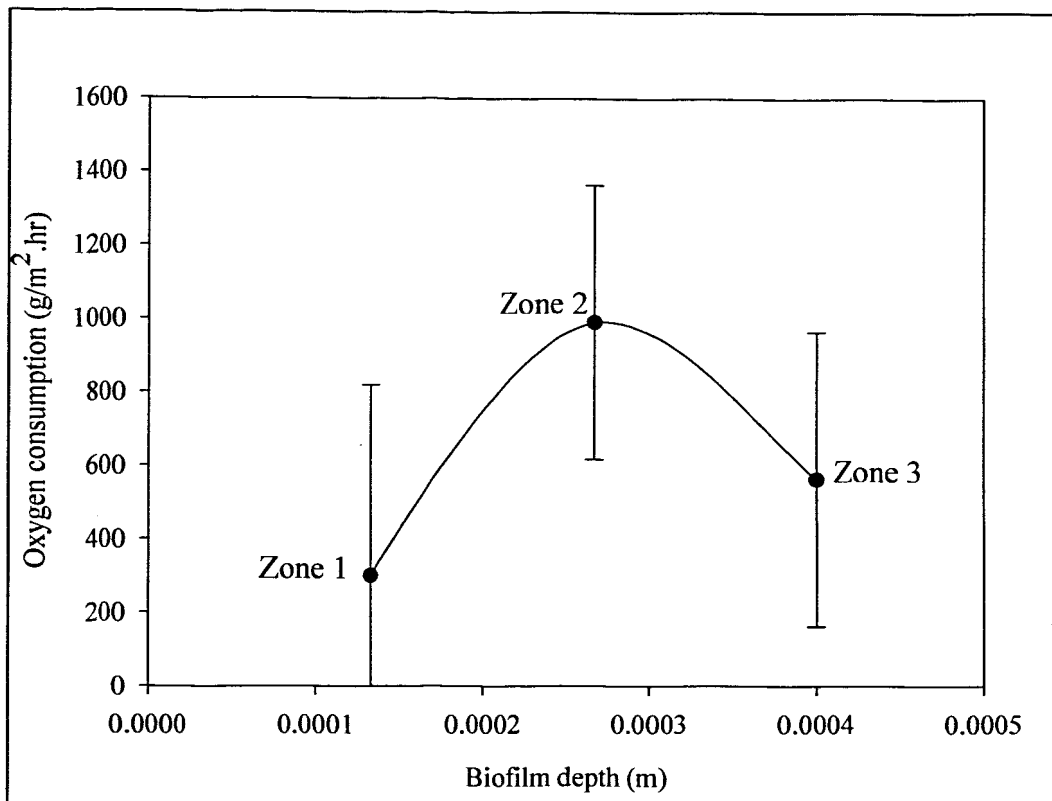
Figure 7.9: Average oxygen consumption profile in different zones after 120 hrs of biofilm growth.

7.3.3.3 Oxygen consumption after 168 hrs of biofilm growth

This period was classified as the deceleration phase, where the biofilm goes through a period in which there was a reduction in the generation of the new haphae strands. The oxygen flux across the outside surface of the biofilm was determined to be very low, thus affecting the consumption. The PROFILE 1.0 software divided the dissolved oxygen profiles into two consumption zones. The two consumption zones were classified at depths of 0 to 290 μm and 290 to 450 μm in the biofilms. The rate of consumption was 140.7 g/m^3.hr in the first zone, while in zone two, consumption was at an average of 505.1 g/m^3.hr, as shown in Figure 7.10.
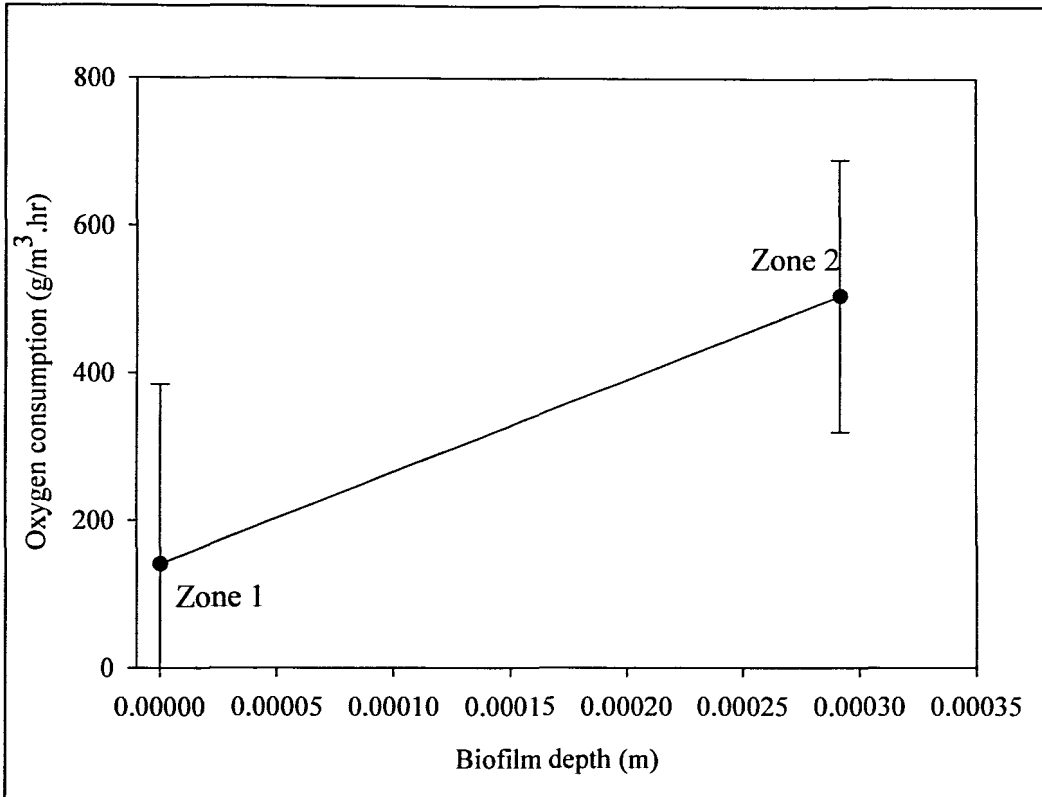
Figure 7.10: Average oxygen consumption after 168 hrs of biofilm growth in two different zones.

7.3.3.4 Oxygen consumption after 216 hrs of biofilm growth

After the structural steady state, where new mycelia were not generated, the average profiles were divided into two consumption zones similar to those determined in section 7.3.3.3. The profile was divided into two zones, namely 0 to 200 μm and 200 to 400 μm, as shown in Figure 7.11. The average consumption was 589.2 g/m^3.hr in the first zone and 838.6 g/m^3.hr in the second zone.
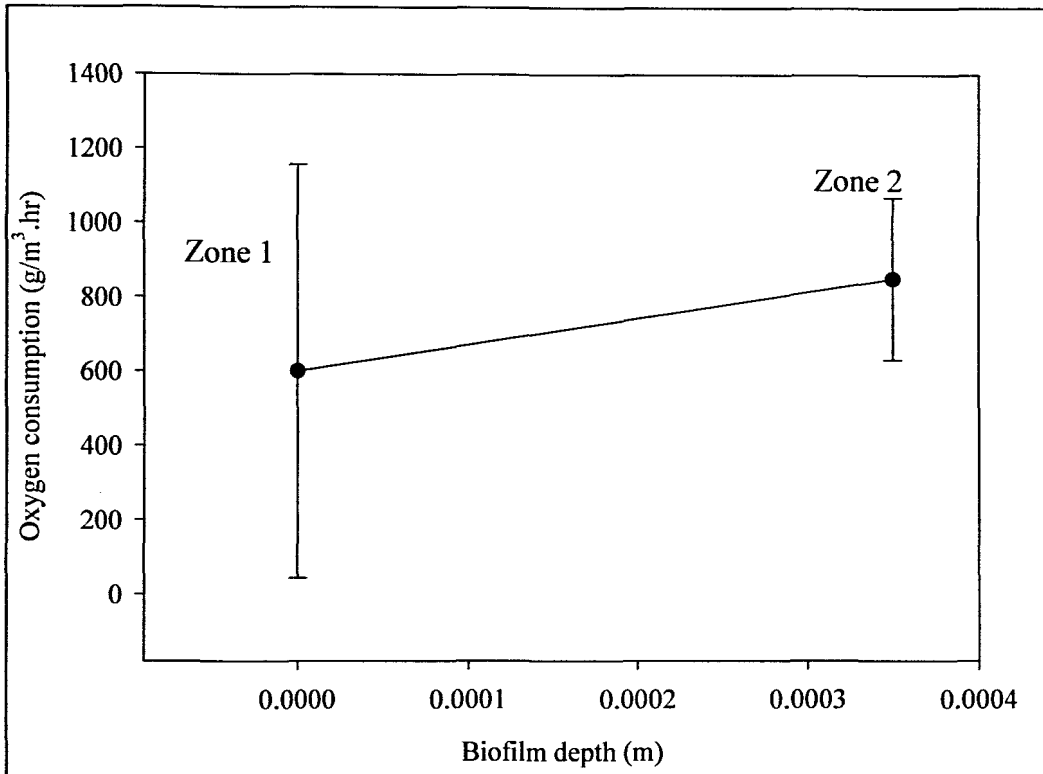
Figure 7.11: Average oxygen consumption after 216 hrs of biofilm growth in two different zones.

7.3.3.5 Oxygen consumption after 264 hrs of biofilm growth

After 216 hrs of bioreactor operation, the biofilm was into its secondary growth phase. The oxygen flux was determined to be at its highest during this period. This increased the consumption of oxygen, as all the profiles were determined to have one consumption zone across the biofilm. The highest rate of consumption was determined as 1099 g/m^3.hr, while quantified at a low of 578.4 g/m^3.hr in the third profile. Figure 7.12 showed an average consumption of 918.5 g/m^3.hr across the biofilm (0 to 400 µm).
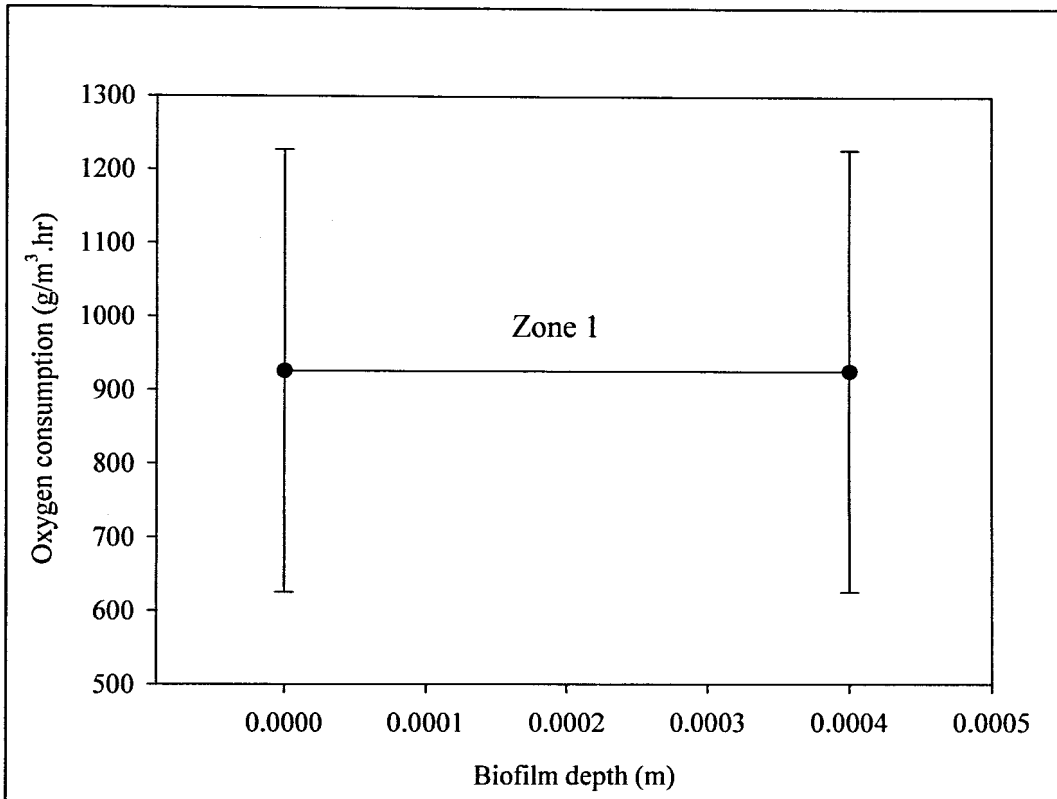
Figure 7.12: Average oxygen consumption after 216 hrs of biofilm growth in two different zones.

7.3.4 External mass transfer coefficient

The mass transfer coefficient was determined by using the oxygen flux values obtained in 7.3.1, which used the external liquid film (bulk) concentration and the biofilm surface concentration. The external mass transfer coefficient was calculated by dividing the flux with the difference between the external liquid film and the biofilm surface oxygen concentration (i.e. illustrated in equation 2.17). The lowest average mass transfer coefficients were obtained at 120 hrs and 264 hrs as the biofilm was in its exponential phase during this period. The values, which were obtained showed a high variability because the values were highly dependent on the characteristics of the shell side biofilm surface (classified as aerial mycelia), which varied from individual bioreactors. The obtained values can be used for modelling flux across a *P. chrysosporium* biofilm surface at different times during the biofilm growth. The mass transfer coefficient values ranged from 0.131 to 0.602 m/hr, as in Figure 7.13.
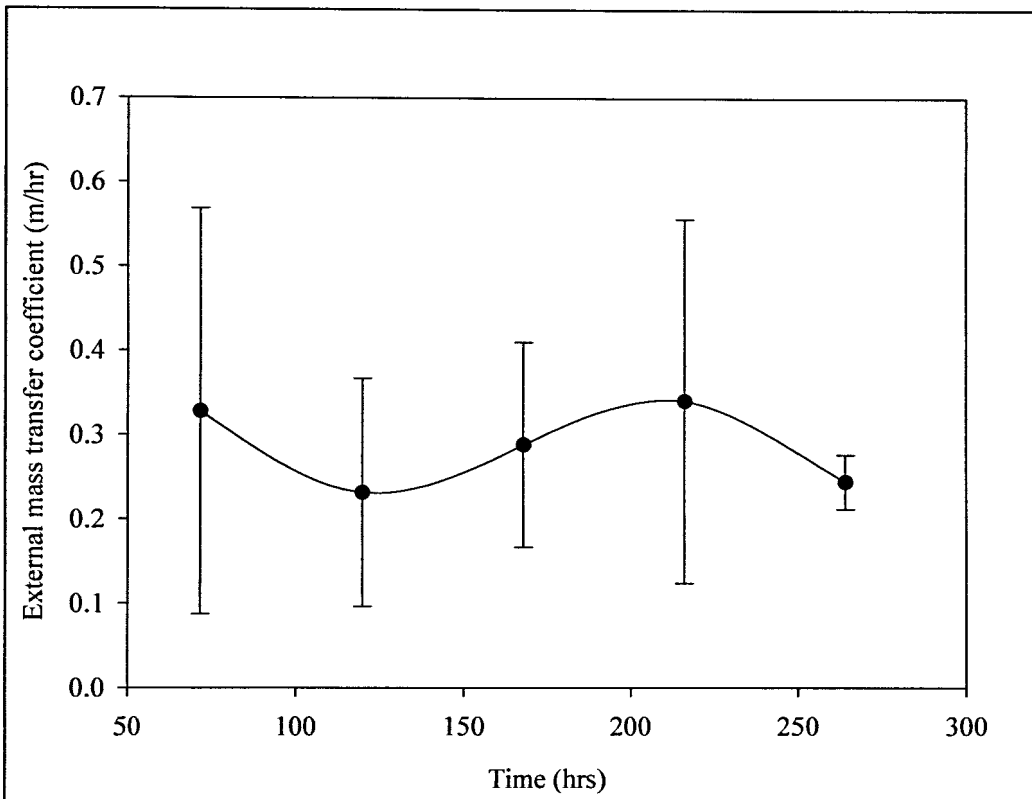
Figure 7.13: External mass transfer coefficient, β profile.

7.3.5 Oxygen based Monod saturation constant

The distribution of oxygen in biofilms was modelled by using the Monod saturation constant, K_m, as it was assumed that oxygen consumption was, through a biological reaction, based on Monod's kinetic equation. The oxygen-based Monod's saturation constant was determined as indicated in section 3.3. The saturation constant increased in the primary exponential phase (72 to 120 hrs) from 0.767 g/m^3 to 2.07 g/m^3, as shown in Figure 7.14. As shown previously also, oxygen flux increased during this period. During the secondary exponential growth phase a different trend was established where the saturation constant reduced from 1.92 g/m^3 (216 hrs) to 1.1 g/m^3 (264 hrs). The average saturation constant was determined as 0.567 g/m^3 during the biofilm's structural steady state.

116
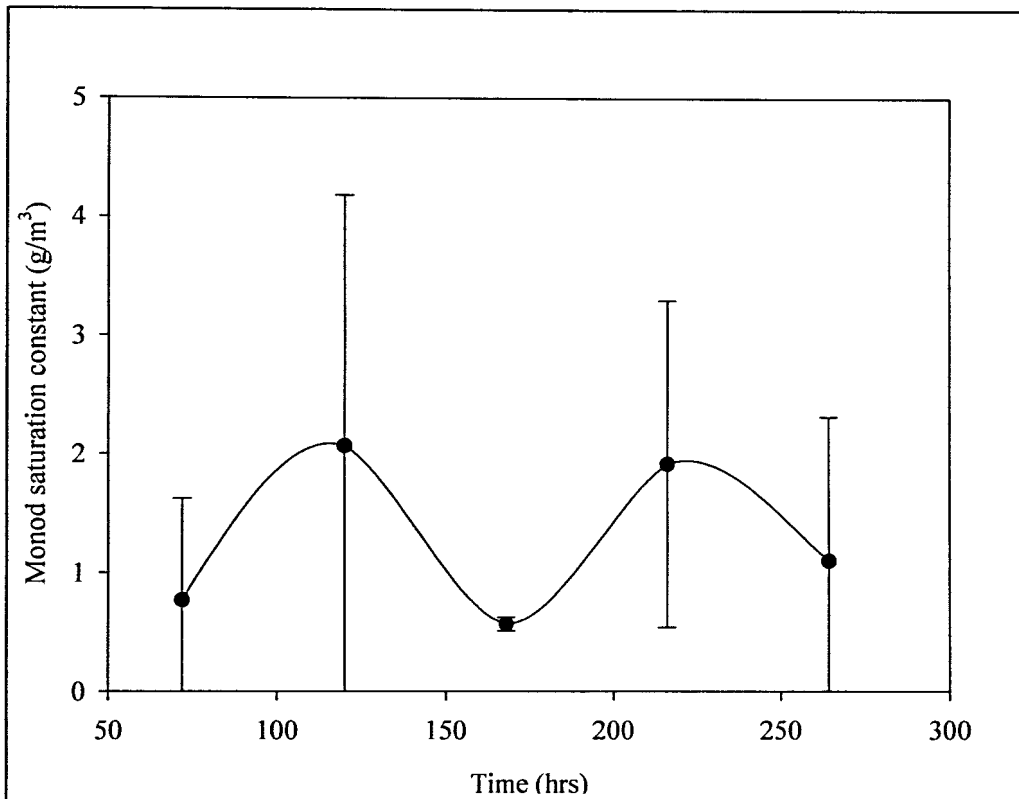
Figure 7.14: Oxygen based Monod's saturation constants at different times during biofilm development.

7.3.6 Biofilm diffusion coefficient and kinetic parameter, $D_f/k_{O_2}X$

In Figures 7.15 and 7.16 the kinetic parameter, $D_f/k_{O_2}X$, and the biofilm diffusion coefficient, D_f, were plotted over a period of 216 hrs. The kinetic parameter, $D_f/k_{O_2}X$, decreased when the biofilm was in its primary and secondary exponential phases, as shown in Figure 7.15. The kinetic parameter was determined as explained in section 3.3. In the first exponential phase (72 to 120 hrs), the average kinetic parameter decreased from 1.1E-8 m^6/g to 5.3E-9 m^6/g. The highest average kinetic parameter of 1.3E-8 m^6/g was obtained at 168 hrs, which was then reduced to 4.7E-9 m^6/g, as the biofilm approached its secondary exponential phase.

117
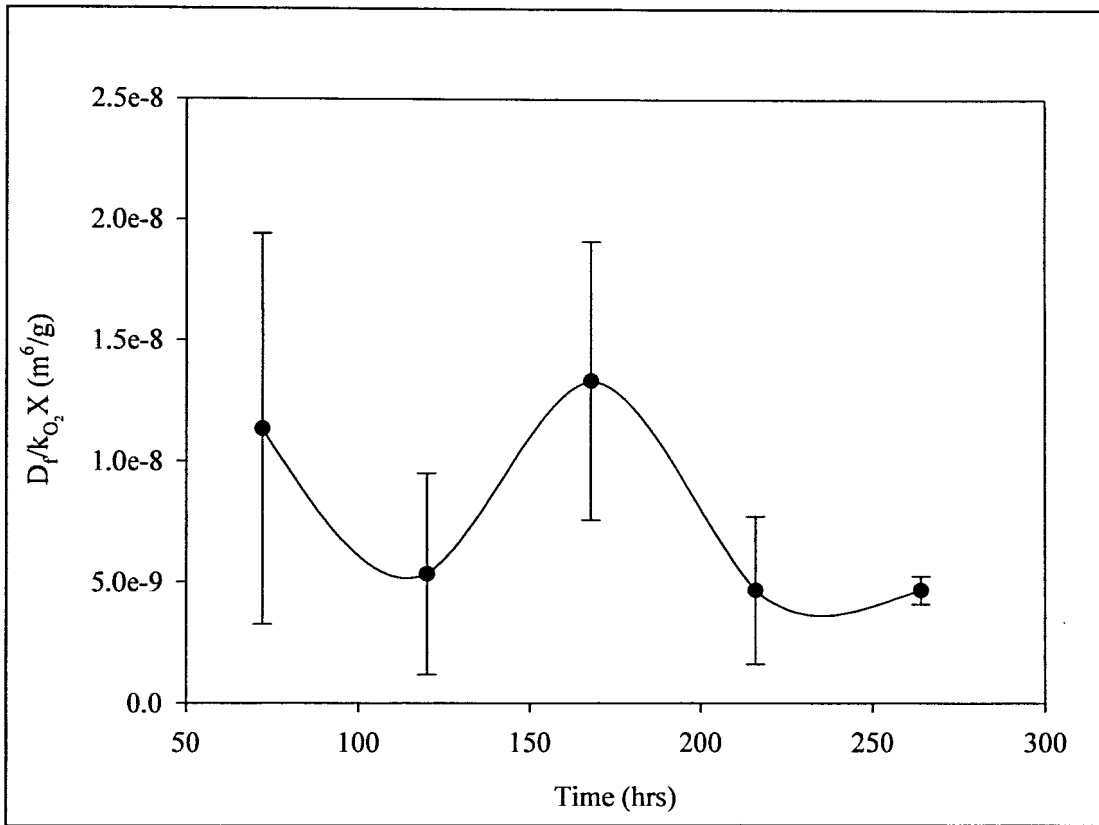
Figure 7.15: The kinetic parameter, D_f/kX profile.

The diffusion coefficient was calculated by using equation 2.17, where the product between the flux and the penetration depth was divided by the difference in the oxygen concentration at the biofilm surface and at the penetration depth. The trend, which was obtained, showed similar characteristics with the flux profile, as shown in Figure 7.16. The biofilm's average diffusion coefficient increased with the increase in flux during both the primary and the secondary exponential phases. The lowest average biofilm diffusion was obtained at 168 hrs with the value of 1.03E-5 m^2/hr.

In the periods 72 hrs to 120 hrs, the average biofilm diffusivity increased from 1.13E-5 m^2/hr to 1.27E-5 m^2/hr, while after the structural steady state it increased from 1.03E-5 m^2/hr to 1.54E-5 m^2/hr. In general, the average biofilm diffusivity, which was obtained during the study correlated to the oxygen diffusivity values listed in Table 2.1. At a temperature of 40°C, oxygen diffusivity of 1.17 E-5 m^2/hr in Table 2.1, was closely related to diffusivities obtained from the bioreactors, which were operated in an incubator at 37 °C.
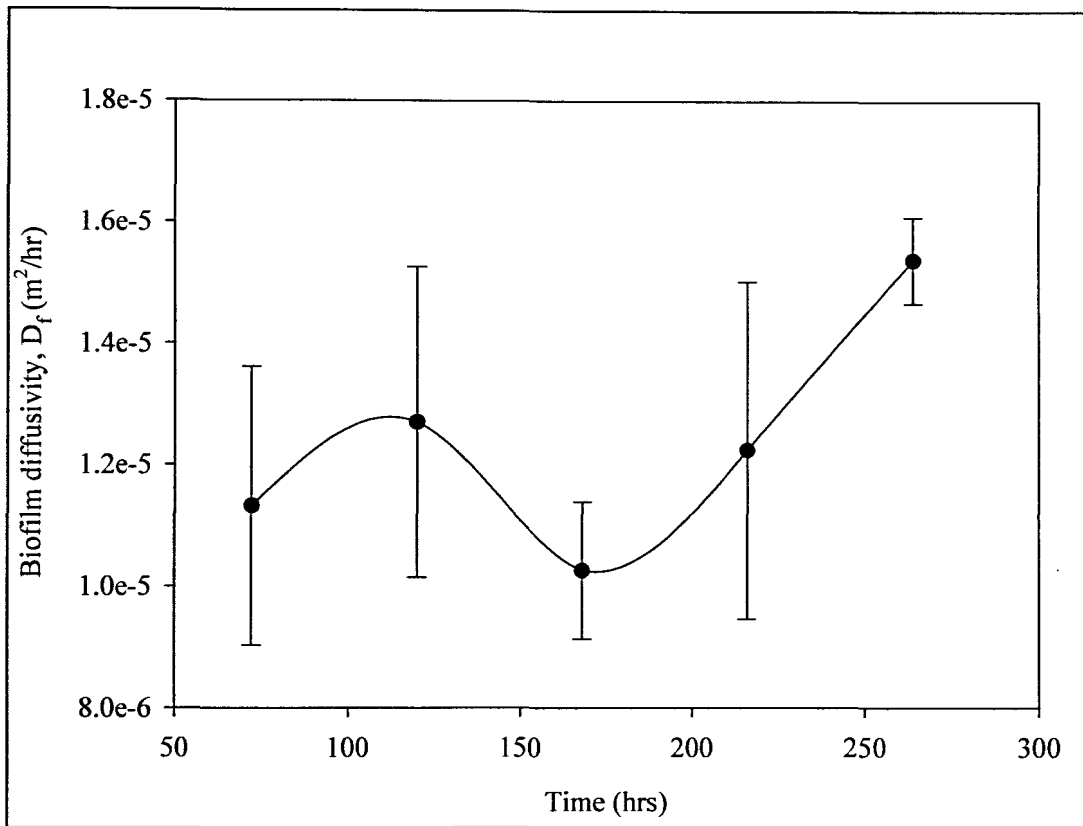
Figure 7.16: Biofilm diffusion coefficient determined during different stages of biofilm development.

7.3.7 Mathematical model for oxygen distribution across *P. chrysosporium* biofilm

By using methods as explained in the mathematical model section, dissolved oxygen parameters were determined from oxygen profiles in SFCMBR systems. By using equation 3.26 and the predetermined parameters, oxygen models can be developed, which simulate oxygen profiles in biofilms. Table 7.2 shows parameters, which can be used to simulate oxygen profiles.

Table 7.2: Kinetic parameters used for oxygen distribution simulation

Growth phases	Kinetic parameters		Biofilm depth
	$k_{O_2} X / D_f$	K_m	(m)
Lag (0 to 72 hrs)	1.33E08	0.77	0.00039
Exponential (72 to 168 hrs)	1.67E08	1.13	0.00039
Steady State (168 to 216 hrs)	2.25E08	1.19	0.00039

These parameters can be used to model oxygen profiles during different phases of biofilm development. The modelled oxygen profiles, as shown in Figure 7.17, are a representation of dissolved oxygen profile at different stages during biofilm development. The models may be used to describe a dissolved oxygen profile in bioreactor systems, where *P. chrysosporium* is immobilised on a substratum, while air is fed into the extra capillary space as a source of oxygen.
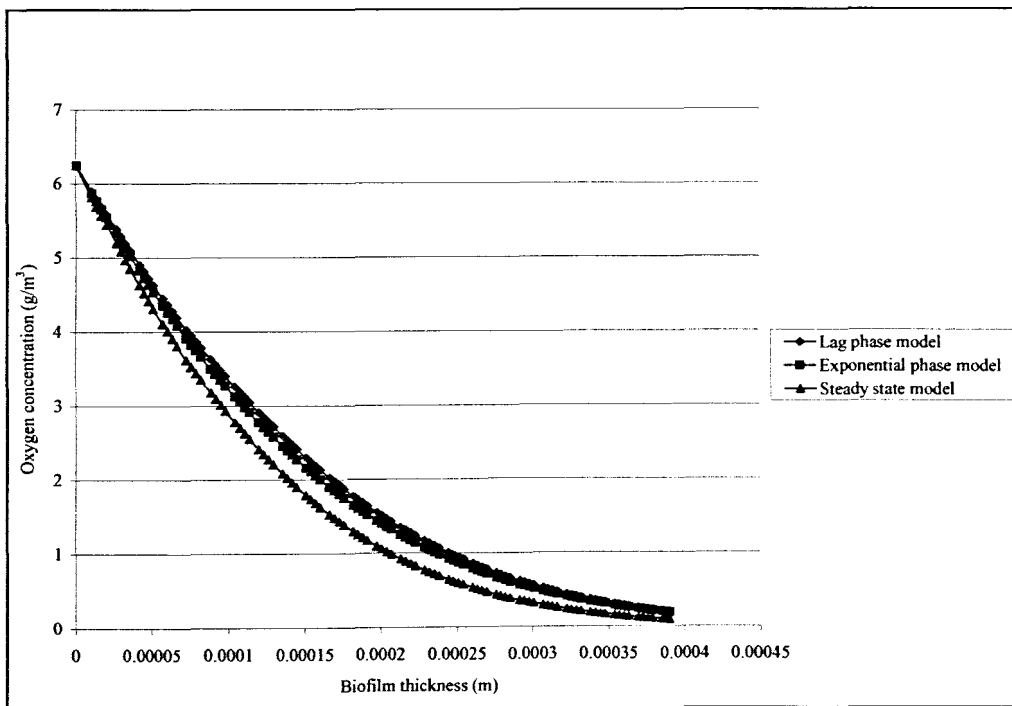
Figure 7.17: Dissolved oxygen diffusion models across *P. chrysosporium* biofilm during different growth phases.

7.4   NUTRIENT MASS TRANSFER ACROSS THE BIOFILM

The hydrogen peroxide microsensor was calibrated by using a standard curve method. A standard addition of 0.3774 g/L was used and the current generated for the solution was recorded, as shown in Figures 7.18. A signal generated from traces of hydrogen peroxide in any medium can be matched to the standard curve, whilst obtaining corresponding hydrogen peroxide concentration. The resultant calibration curve, which was obtained, was not linear as expected, resulting in a lower signal response at higher hydrogen concentrations.
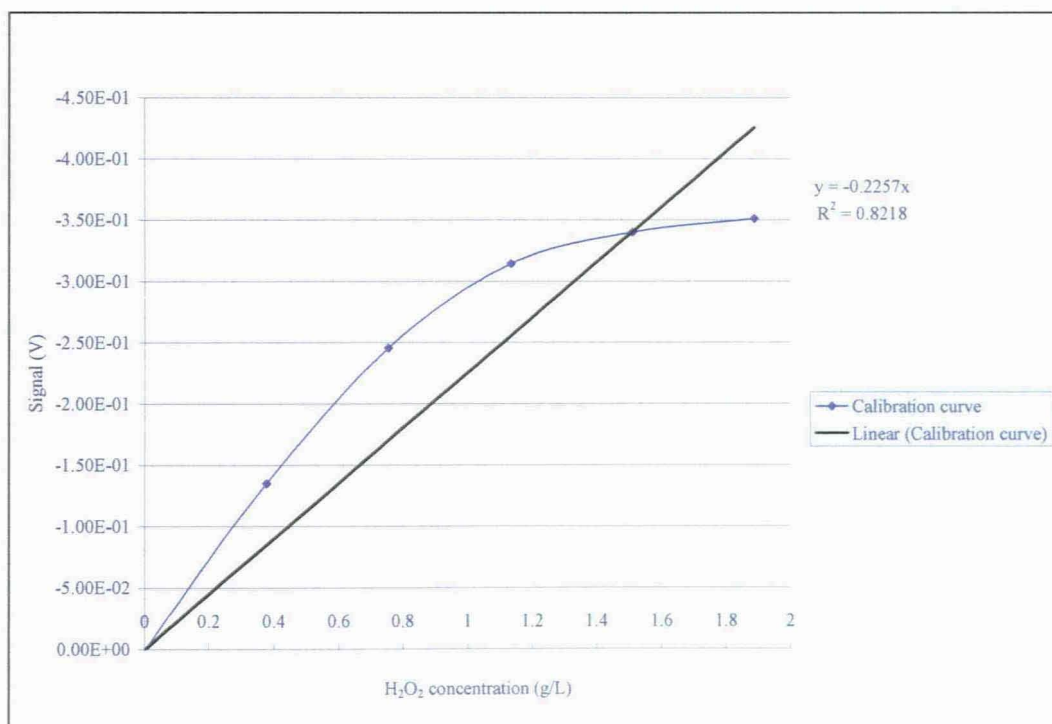
Figure 7.18: Hydrogen peroxide microsensor calibration curve obtained by using an external calomel electrode and a picoammeter.

7.4.1   Measuring hydrogen peroxide profiles across the biofilm

After several experiments where hydrogen peroxide was fed to the biofilm through the lumen of the membrane to establish nutrient gradients across the biofilm, a negative signal was not obtained as expected with hydrogen peroxide solutions (shown in Figure 7.19). The same procedure was undertaken at room temperature with flow rates, which range from 1.67 ml/hr

(operating flow rate when nutrient medium was fed to the bioreactor system) to 7 ml/hr over a period of 24 hrs with similar results obtained during the exercise. This was attributed to two aspects. Firstly, the hydrogen peroxide solution was not stable in a water medium and, secondly, the presence of ligninolytic enzymes in the biofilm structure might have degraded the available hydrogen peroxide.
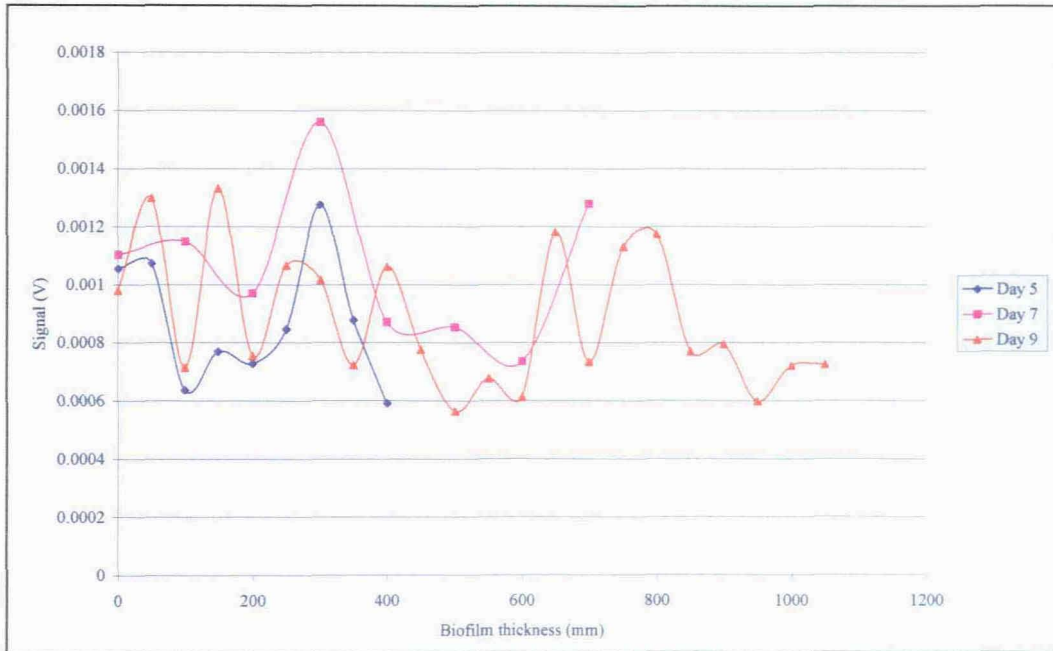
Figure 7.19: Hydrogen peroxide mass transfer across the biofilm.

CHAPTER 8 : MCMBR SYSTEM COMMISIONING

8.1   INTRODUCTION

Three MCMBR systems were operated over a period of 11 days to evaluate their operational capacity while monitoring substrate consumption and enzyme production. The permeate pH and redox potential was monitored daily and compared to results, which were obtained in the SFCMBR systems operated over the same period of time. Dissolved oxygen distribution was measured on different membranes and compared to models developed in Chapter 7. As enzymes were produced by *P. chrysosporium*, a laboratory application investigation was performed where permeate that was produced was added to olive oil wastewater to evaluate the degradation of phenols. In these MCMBR systems, fourty-five million spores (three million spores per membrane) were used in the immobilisation process.

8.2 MULTI-CAPILLARY MEMBRANE BIOREACTOR SYSTEM OPERATION

8.2.1 Bioreactor monitoring

The measurement of redox potential and pH was essential to measure as explained in section 5.2.5, in order to monitor the biochemical properties of permeate collected from the MCMBR systems. The redox potential of permeate collected was above 200 mV in the early stages (day 1 to 5) of the MCMBR systems operation, with biofilm growth visible after 24 hrs of operation. This was not observed when operating SFCMBR systems, where the redox potential above 200 mV was obtained after 3 to 4 days of operation. Figures 8.1 and 8.2 show redox potential and pH readings respectively obtained from individual bioreactors. The values of the redox potential from permeate decreased with time, while pH values increased in the same period (see Figure 8.1 and 8.2). In SFCMBR systems, the redox potential increased with operational time, with pH values decreasing.

In the period 0 to 6 days, the average redox potential was above 200 mV and decreased to below 200 mV in the period 6 to 11 days. The average pH values obtained after 6 days of MCMBR operation were above 3.8, with values below that obtained in the period 0 to 6 days.
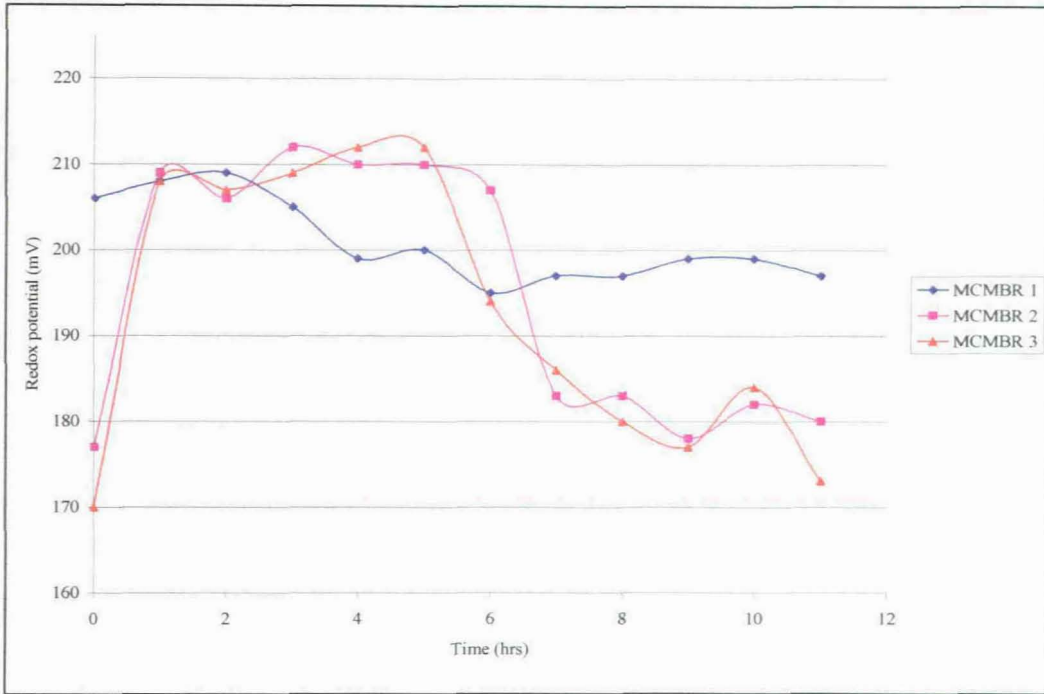
Figure 8.1: Redox potential readings obtained from MCMBR systems operated simultaneously.
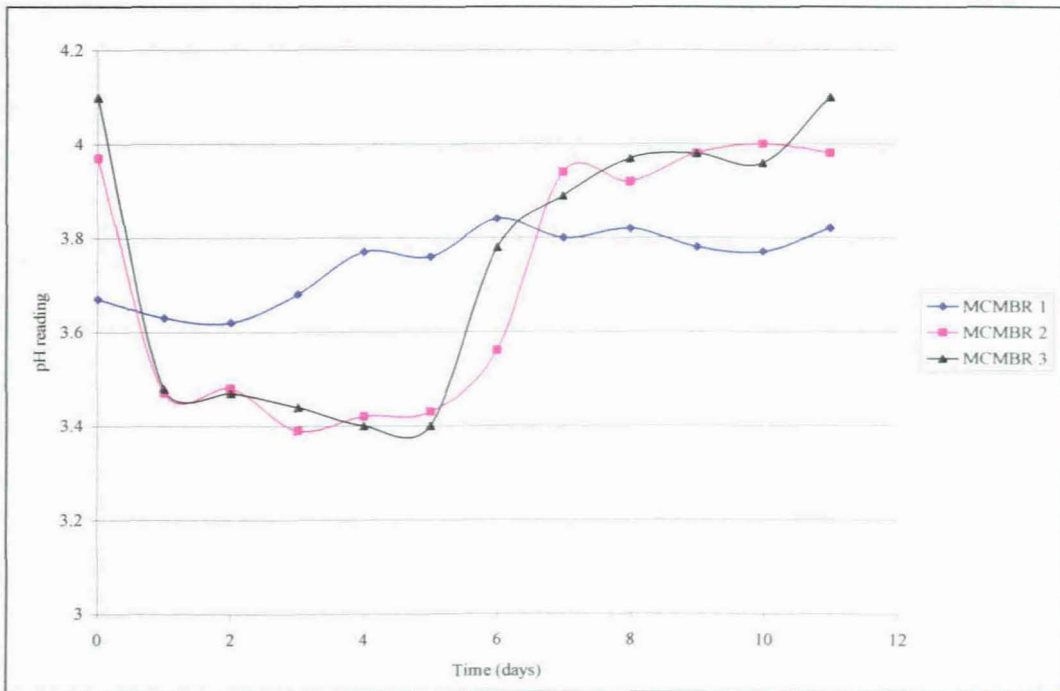
Figure 8.2: pH readings obtained from MCMBR systems operated simultaneously.

8.2.2 Substrate consumption

8.2.2.1 Glucose consumption

Approximately 3.47 g/day of glucose was supplied to each MCMBR system operating in an incubator set at a temperature of 37 °C. This was calculated by determining the concentration in the feed and by multiplying the amount of nutrient medium supplied (0.3 L/day) to the systems. Figure 8.3 shows the daily consumption of glucose over a period of 11 days. On average 1.46 g/day of glucose supplied to the MCMBR was consumed which represented over 40% of the glucose supplied. From this determination, it was observed that glucose usage was generally higher in MCMBR systems compared to SFCMBR systems. Initially (period 0 to 1 days), about 60% of the glucose, which was supplied was consumed as the immobilised spores germinated. After day 1, a thin layer of biofilm was visible on most of the membranes in the MCMBR systems, while in SFCMBR systems, biofilm visibility was on day 3.
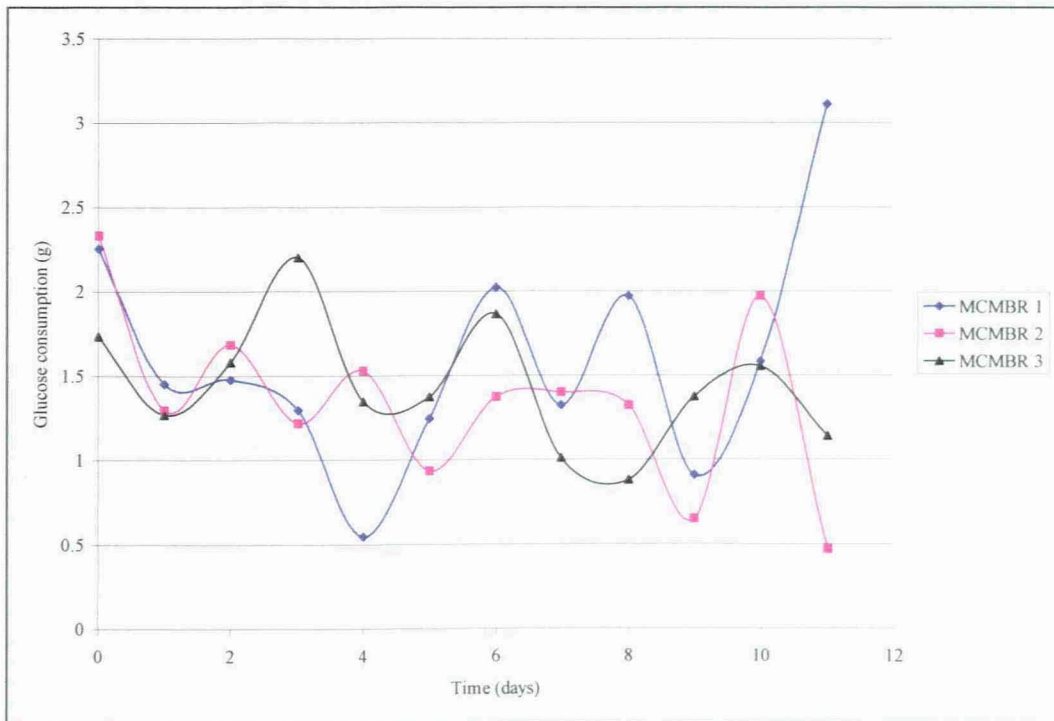
Figure 8.3: Glucose consumption in MCMBR system operated over a period of 11 days.

8.2.2.2 Ammonia consumption

Ammonia consumption was calculated by multiplying the calculated ammonia concentration in permeate by the volume of permeate collected daily (0.3 L/day), and then subtracting from the amount of ammonia in the feed. About 0.0117 g/day of ammonia was supplied to the MCMBR systems. On average, above 90% of the ammonia supplied to the MCMBR was consumed during the period 0 – 6 days with lower consumption determined thereafter, as shown in Figure 8.4.
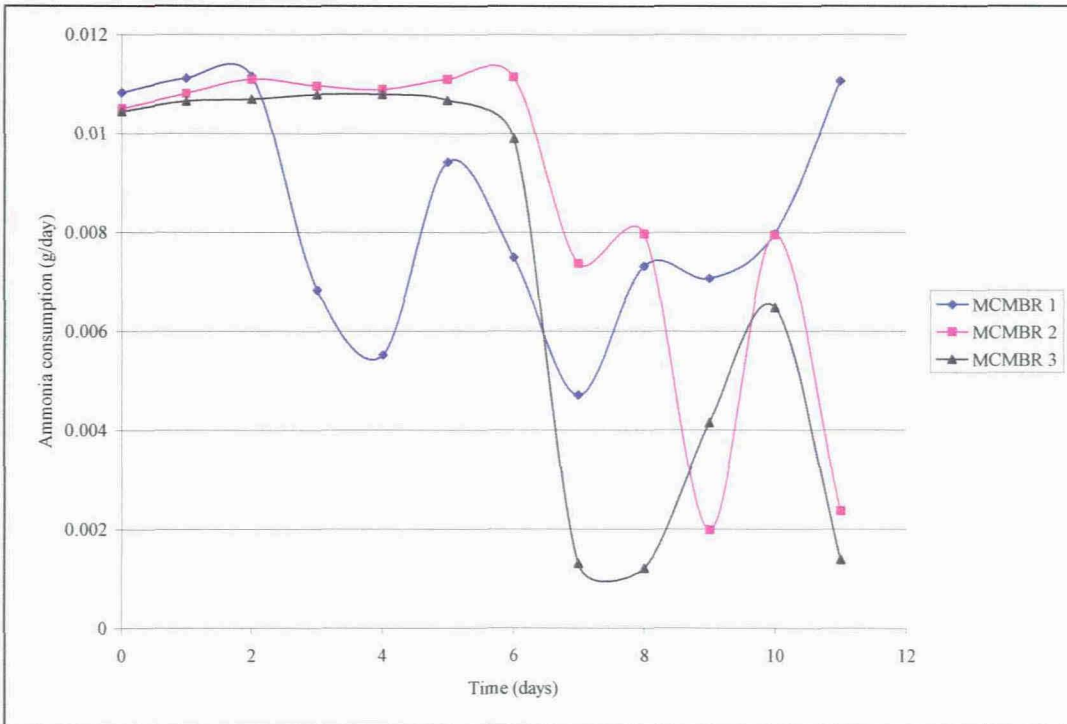
Figure 8.4: Daily ammonia consumption determined from MCMBR systems operated simultaneously.

8.2.3 Oxygen mass transfer across the biofilm

The dissolved oxygen distribution in the immobilised biofilm was determined by using an oxygen microsensor from three randomly selected membranes in each of the MCMBR systems. As the MCMBR systems were operated and dismantled after a period of 11 days (264 hrs), a model was plotted using equation 3.25 (with modelling kinetic constants for 168 to 216 hrs, as listed in Table 7.2) to evaluate the difference between the described model and experimental

profiles, as shown in Figure 8.5. It was observed that the model values were generally lower at different depths compared to the obtained experimental values. This was attributed to the configuration of the MCMBR systems with a bigger extra capillary space, as the kinetic constants used in the model were obtained from SFCMBR systems.
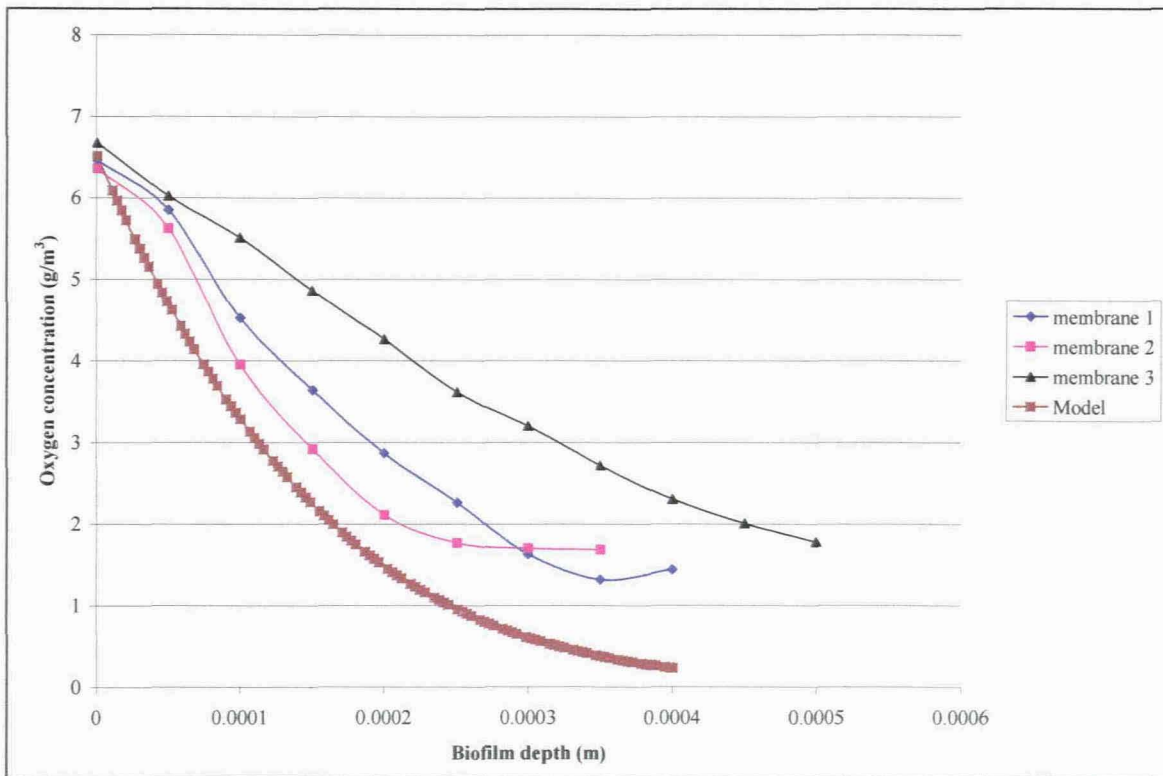
Figure 8.5: Oxygen distribution in *P. chrysosporium* biofilm from randomly selected membranes from three different MCMBR systems.

8.2.4 Enzyme activity

8.2.4.1 *Lignin peroxidase (LiP)* activity

All three MCMBR systems showed *LiP* production in the range of 0 to 74 U/L during the period of operation. In the period of 0 to 5 days, *LiP* activity was higher (Area A) compared to the later stages of operation (7 to 11 days, Area B). In all the bioreactor systems, *LiP* activity was low on day 6, as shown in Figure 8.6. It was shown that in the period of 0 to 5 days, permeate, which was produced had high redox potential and ammonia consumption was shown to be high, thus

resulting in higher enzyme production. Lower redox potential and ammonia consumption during a period of 7 to 11 days was shown to hamper reasonable *LiP* production.
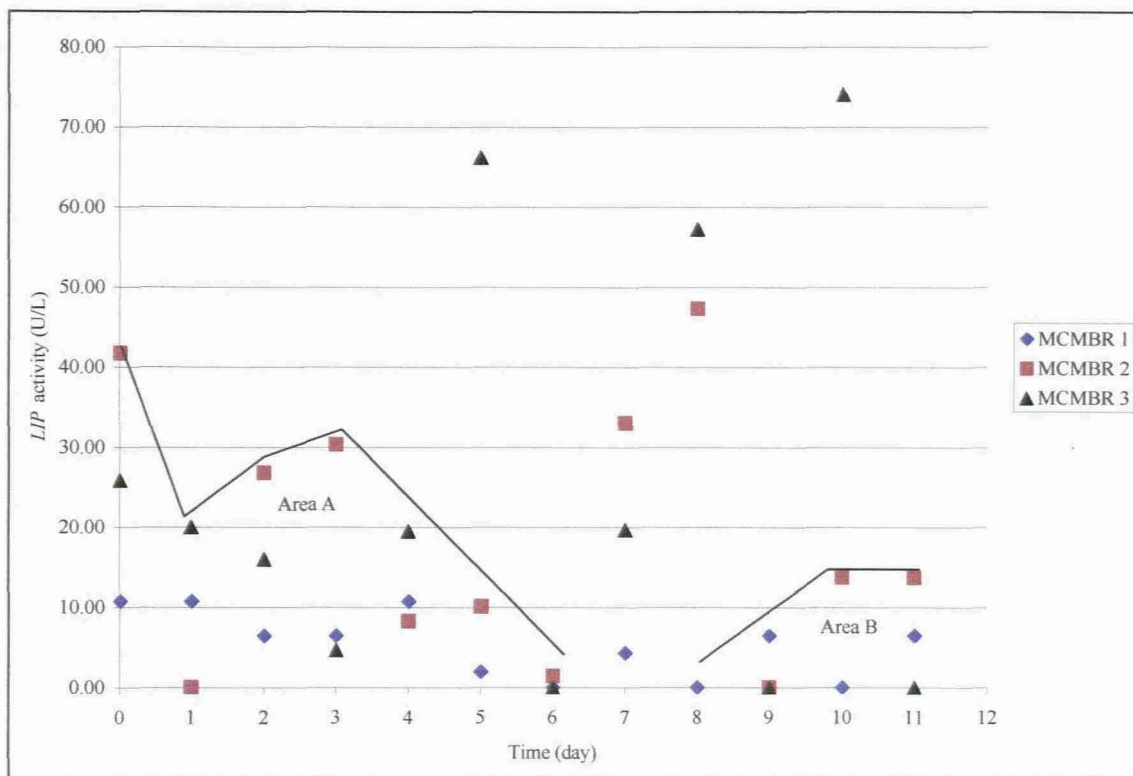
Figure 8.6: Average *Lignin Peroxidase (LiP)* activity from the three MCMBR systems. Area A: high *LiP* production; and Area B: low *LiP* production.

8.2.4.2 *Manganese Peroxidase (MnP)* activity

On average, lower *MnP* (lower than 5 U/L over a period of 11 days) production was obtained in MCMBR systems #1 and #2, as shown in Figure 8.7. MCMBR 3 showed lower *MnP* production during earlier stages of operation with the highest (*MnP* activity above 15 U/L) obtained in the periods 6, 7 and 11 days. The results showed that the biofilm was not starved of its nutrient source, as 300 ml/day of nutrients were supplied to the MCMBR systems, thus resulting in lower *MnP* production. It appeared that operating conditions were suited for *LiP* production compared to *MnP* production.
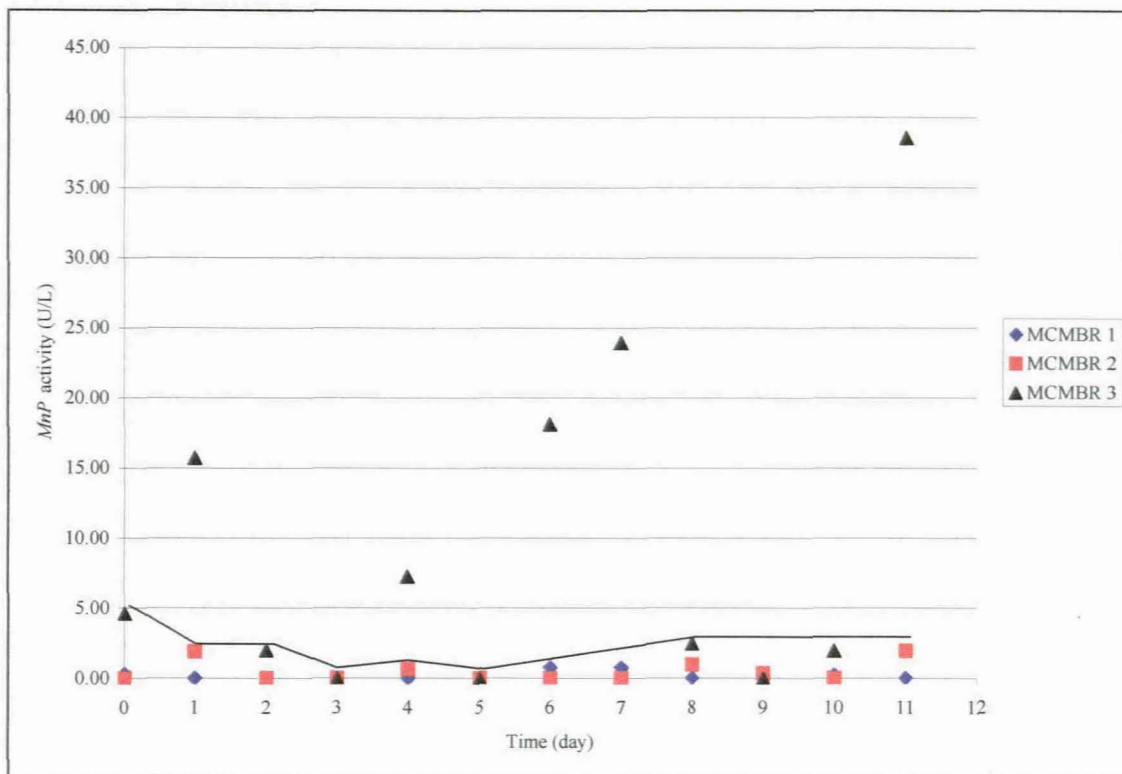
Figure 8.7: Average *Manganese Peroxidase (MnP)* activity from the three MCMBR systems.

8.3 MCMBR SYSTEM APPLICATION

The ability to biodegrade various aromatic compounds by ligninolytic enzymes produced by *P. chrysosporium* fungi is widely studied by various researchers (Walsh, 1998; Griselda & Eduardo, 1990; Tien, 1987; Livernoche *et al.*, 1981). The enzymes are reported to degrade a broad spectrum of structurally diverse compounds, including phenolic compounds. To validate what was indicated in literature by researchers, laboratory application investigations had to be undertaken by using permeate with redox potential above 200 mV (day 2) from MCMBR system #1. Olive wastewater from an olive mill, which was rich with phenol content, was deemed to be suitable for the experiment. The permeate sample and olive wastewater were mixed in volumetric ratio's of 50:50 and 25:75 in four volumetric flasks, namely R1, R2, R3 and R4 with magnetic stirrers.

A Merck® phenol cell test kit was used to determine the phenol content at the beginning of the experiment and in 24 hour periods thereafter. Sulphuric acid (200 µL, which acts as a catalyst),

129

was dispensed into a glass cell in which 10ml of deionised water was added to dilute the acid. A micro-spoon of reagents Ph-1K and Ph-2K was added to the diluted acid solution in the glass cell. The prepared permeate mixture(s) (200 µL) was added to the glass cell, where a reaction took place. The glass cell was then used to determine the amount of phenol content in the solution by using a spectroquant analyser.

The investigation focused on the extracellular enzyme degradation of phenolics available in wastewaters by using permeates from the MCMBR system. The results showed a significant reduction in phenol content for the different permeate-wastewater ratio by using permeates from the identified system. The average phenol content after 24 hrs was in the range of 30 mg/L, which was reduced to below 10 mg/L average phenol content after 72 hrs. This was a 66.7% reduction in the phenol content, as shown in Figure 8.8.
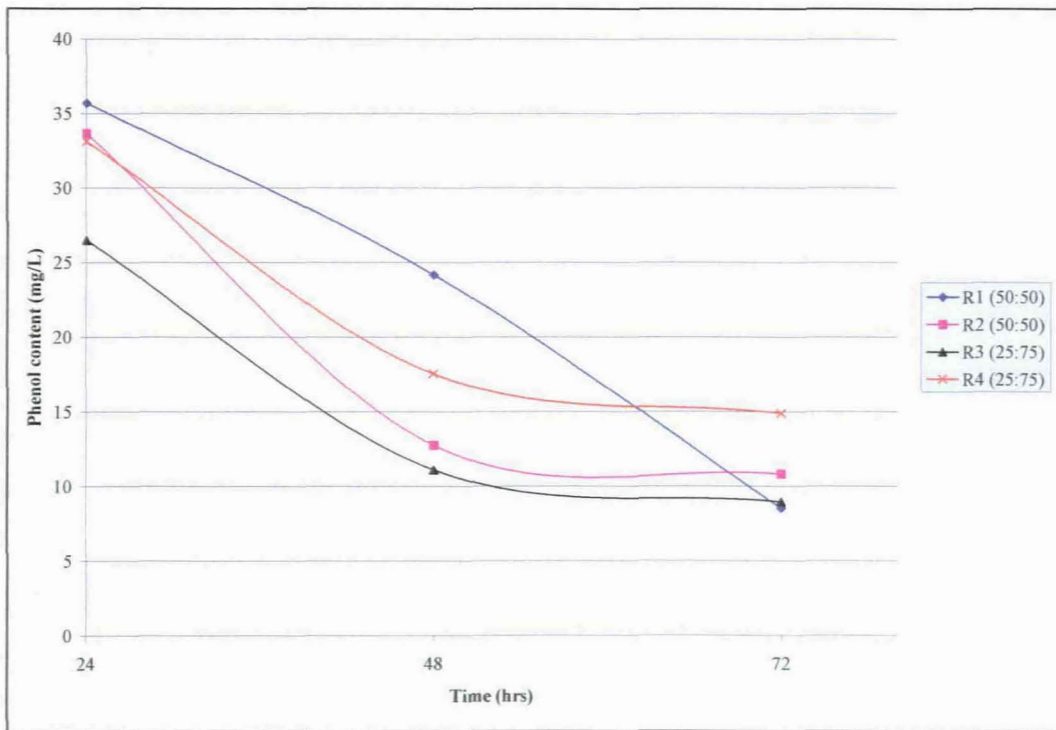
Figure 8.8: Phenol reduction results using permeate from one of the MCMBR systems.

CHAPTER 9 : CONCLUSION

9.1   QUANTIFYING GROWTH KINETICS OF *P. CHRYSOSPORIUM*

The dry biofilm density curve was simulated by using a growth rate constant of 0.035 hr^{-1} with an initial density of 5.33E04 g/m^3, which was used in the simulation. The primary growth phase occurred during a period of 168 hrs after which a steady state phenomena was observed, where biofilm dry mass did not increase at an average density of 9.7E05 g/m^3. A secondary growth phase occurred after 216 hrs, as was observed by Kirk *et al.* (1978) in flasks, which contained 21% oxygen. Daily glucose and ammonia consumption was monitored to determine consumption rates. Different rates of glucose consumption were established, which were consistent with different growth phases determined by the dry biofilm density model. An average glucose consumption of 94.7 g/m^3.hr was established, which was determined to be higher compared to TFBR, which used the same nutrient medium. After a period of 48 hrs, an average of 90% of all ammonia supplied to the SFCMBR systems was consumed compared to 15% of the glucose consumed. The consumption rate of ammonia was determined as 1.46 g/m^3.hr over a period of 264 hrs.

The linearization techniques (Lineweaver-Burk and Eadie-Hofstee plots) were used to evaluate different kinetic constants from accumulative glucose and ammonia consumption data at different stages during the biofilm development. The Lineweaver-Burk plot achieved higher correlation coefficients when used over the entire experimental period, while the Eadie-Hofstee plot was suitable during the initial stages of glucose consumption. The substrate utilisation rate during the primary growth phase was 185 g/m^3.hr with 56.97 g/m^3.hr, which was obtained by using the Eadie-Hofstee plot during the lag phase.

Ammonia utilisation was determined as 4.6 g/m^3.hr by using the Lineweaver-Burk plot over the primary growth phase and 1.43 g/m^3.hr by using the Eadie-Hofstee plot during the lag phase. The Monod's saturation constants based on substrate consumption was determined by using linearization plots with higher correlation coefficients. The glucose based Monod's saturation constants was determined as 1.12E04 g/m^3 for the entire primary growth phase (0 to 264 hrs) and 2.16E03 g/m^3 for the initial stages (0 to 72 hrs) of biofilm development. The ammonia based

131

Monod's saturation constants were determined as 1 g/m^3 over the primary growth phase (0 to 216 hrs), compared to 0.32 g/m^3 obtained during the lag phase (0 to 72 hrs).

The average growth yield coefficients of glucose and ammonia were determined as 0.202 and 41.36 g biofilm/ g glucose, respectively. The values obtained were dependent on the consumption rates of individual substrates of which 15% of glucose and 84% of ammonia supplied to the SFCMBR systems was consumed when 3 million spores were used for inoculation. The basic growth of *P. chrysosporium* was determined to follow a logistic growth curve, with primary and secondary growth phases as determined by various researchers who used batch-system bioreactors. During the primary phase, the glucose based growth yield coefficient was determined as 0.299 g biofilm/ g glucose and as 0.230 g biofilm/ g glucose during the secondary growth phase.

The maximum specific growth rate was determined as 4.75E-03 hr^{-1} from the primary (glucose) substrate consumption data. The value obtained was small compared to the value of the reaction rate constant obtained in section 6.2.1, which lead to a new approach, where the actual values from simulated density data were used to quantify the maximum specific growth rate. The maximum specific growth rate was determined from the steepest slope when the logarithmic modelled biofilm density was plotted against time and was found to be 0.032 hr^{-1}. The value of the growth rate constant was determined to be equivalent to the maximum specific growth rate. The biofilm's specific growth rate decreased with an increase in biofilm density. The Monod's saturation constant determined at 0.0163 hr^{-1}, (which is equivalent to half the value of the specific growth rate), was 2.77E03 g/m^3. Glucose and ammonia consumption are dependent on the biomass, which is generated by using different spore concentrations. The rate of glucose and ammonia consumption increased with increasing spore concentration inoculated on the membranes. In SFCMBR systems, which were inoculated with one million spores, a lag phase of 24 hrs was observed in terms of ammonia consumption.

The rate of glucose consumption increased between 72 to 240 hrs in different SFCMBR systems inoculated with different spores. SFCMBR systems, which were inoculated with higher spore concentrations, generated biofilms that were heavier and which had high density values. Low growth yield coefficients were observed in biofilms with high densities as substrates can be utilized for other biological processes.

The mycelia in the exponential phase consisted of hyphae situated in nutrient rich areas and was classified as vegetative. The reproductive propagules (spores) were not visible during this stage. The declining growth phase was characterised by hyphael strands, which were compact in the extracapillary space, resulting in reduced flux and other mass transfer processes. Longer strands of hyphae had fragmented and adopted a vegetative state as new nutrient channels were developing. A limited amount of propagules were seen during this stage. Mycelia developed after the primary growth phase contained visible propagules in the extracapillary phase. The fertile mycelia were compact with fragmented haphae.

9.2   MOMENTUM AND SUBSTRATE MASS TRANSFER

An average pressure of 3.7 to 4.6 Pa was obtained in SFCMBR systems, which operated in dead-end filtration mode. As steady state operation was established after 400 minutes of operation with the outlet pressure (P_2) higher than the inlet pressure (P_1). The modelled pressure drop and increase (modelled using the inlet pressure to predict the outlet pressure) was used in velocity profile development. The arithmetic sign was changed to suit the modelling conditions (pressure drop and increase), with higher accuracy achieved in both the unsteady and steady state.

From Bioreactor #1's pressure results (illustrated in Table 7.1); it was apparent that a decrease in axial velocity during the steady state period was determined with negative radial velocity. During the unsteady state operation, an increase in axial pressure at the outlet was recorded, resulting in increased velocity profiles across the membrane radial length at different points along the length of the membrane. The average radial velocity at the lumen wall was estimated at 1.01E-07 m/s during this period.

The average flux across the biofilm increased from 0.165 to 0.202 $g/m^2.hr$ during the exponential phase of the primary growth phase compared to 0.238 to 0.295 $g/m^2.hr$, which was obtained for the exponential phase in the secondary growth phase. The flux was determined to be low (0.139 $g/m^2.hr$) during the deceleration phase in the primary growth phase. The oxygen consumption rate was classified under different zones during biofilm development. The number of zones decreased from three to one as the biofilm grew older.

After 72 hrs of SFCMBR operation, the average consumption was 30.90 $g/m^3.hr$ in the first zone (classified as the region where aerial mycelia was dominant), 777 $g/m^3.hr$ in the second zone and 613 $g/m^3.hr$ in zone three (near the substratum). Oxygen consumption rates in the first zone increased from 30.90 to 298.7 $g/m^3.hr$ after 120 hrs of biofilm growth. After 120 hrs of biofilm growth, the consumption of oxygen was divided into three zones. In the second zone consumption was determined as 988.7 $g/m^3.hr$ and 561.7 $g/m^3.hr$ near the substratum. During the period of 72 to 120 hrs of biofilm growth, zone two was classified as the reaction zone, since higher consumption rates were established in this zone.

After 168 to 216 hrs of biofilm growth, two consumption zones were established. The consumption zones were determined at biofilm depths of 0 to 290μm and 290 to 450μm. The consumption rate was 3.55E-14 $g/m^3.hr$ in the first zone and 546.7 $g/m^3.hr$ in the second zone. After the structural steady state (216 hrs), consumption was 589.2 $g/m^3.hr$ in the first zone while in the second zone it was determined as 883.8 $g/m^3.hr$. In the secondary growth phase (obtained after 264 hrs of biofilm), only one zone across the biofilm was identified with an average oxygen consumption of 578.4 $g/m^3.hr$.

External mass transfer coefficients were generally lower during both the primary and secondary exponential phases. The values ranged from 0.131 to 0.602 m/hr. The average oxygen penetration depth was 390□m with oxygen based Monod's saturation constant at its lowest (0.567 g/m^3) during the biofilm's structural steady state. Increasing saturation constants were obtained during the exponential phases in the primary and secondary phases.

The Kinetic parameter, $D_f/k_{O_2}X$ was the highest at 1.3E-08 m^6/g during the deceleration phase (168 hrs) and decreased during exponential phases of the primary and secondary growth phases.

The average kinetic parameter decreased from 1.1E-08 to 5.3E-09 m^6/g during the period 72 to120 hrs and 4.7E-09 m^6/g at 216 hrs. The biofilm diffusion coefficient increased during the two identified exponential phases from 1.13E-05 to 1.27E-05 m^2/hr during the period 72 to 120 hrs, while in secondary exponential phase (168 – 264 hrs) the diffusivity increased from 1.03E-05 to 1.54E-05 m^2/hr. The diffusivity obtained during the study compared fairly to the diffusivity values listed in Table 2.1. Oxygen profiles may be modelled by using kinetic parameters, as shown in Table 7.2.

The hydrogen peroxide sensor was successfully calibrated with a decrease in the signal, which was obtained at higher concentrations of 1.6 to 1.8 g/L. It was established that the hydrogen peroxide, which was used to profile nutrient medium distribution across the biofilm surface, was not suitable due to its instability in water. It was concluded that the ligninolytic enzyme trapped in the matrix of the biofilm, degraded the available hydrogen peroxide, resulting in an ineffective profiling of nutrients gradients.

9.3   MEMBRANE BIOREACTOR SYSTEM COMMISIONING

A high redox potential above 200mv and low ph readings were obtained while monitoring the MCMBR system during the early stages of operation, with biofilm visibility obtained after day 1. Lower redox potential readings were observed after day 6. Both ammonia and glucose consumption varied during the operation of the MCMBR systems. A higher consumption of glucose was determined compared to the consumption rates obtained in SFCMBR. On average, 1.5 g/day of glucose was consumed. Higher ammonia consumption was quantified in the early stages (0 to 6 days) of MCMBR's operation with a lower consumption obtained thereafter (6 to 11 days)

The oxygen distribution model plotted, which used kinetic constants listed in Table 7.2, was not descriptive of experimental values obtained due to the difference in the MCMBR system configuration (larger extra capillary space) compared to SFCMBR system (which were used to obtain the kinetic constants). The MCMBR system used in the study was determined to be suitable for *LiP* than *MnP* production. Higher *LiP* activity was obtained during the period of 0 to 5 days, with *MnP* activity determined under 5 U/L during the same period. In the later stages (7 to 11 days) of the MCMBR system operation, lower *LiP* activity averaging 10 U/L was

135

determined. *LiP* production was favourable in the MCMBR systems, which were used in the study.

Wastewater containing phenols was used to evaluate the effectiveness of the bioreactor systems used in this study, by using permeate obtained during the operation. The overall reduction of phenols was 66.7% in both SFCMBR and MCMBR systems, with an initial phenol content of approximately 30 mg/L.

BIBLIOGRAPHY

Asenjo, J.A. & Merchuk, J.C. 1995. *Bioreactor system design*. New York: Marcel Dekker.

Asther, M., Lesage, L., Drapron, R., Corrieu, G. & Odier, E. 1988. Phospholipid and fatty acid enrichment of *Phanerochaete chrysosporium* INA-12 in relation to ligninase production. *Applied Microbiology and Biotechnology*. 27: 393 – 398.

Barclay, C.D., Legge, R.L. & Farquhar, G.F. 1993. Modelling the growth kinetics of *Phanerochaete chrysosporium* in submerged static culture. *Applied Environmental Microbiology*. 59 (6): 1887 – 1892.

Berg, P., Risgaard-Petersen, N. & Rysgaard, S. 1998. Interpretation of measured concentration profiles in sediment pore water. *Limnology and Oceanography*. 43 (7):1500 – 1510.

Bonnarme, P. & Jefferies, T.W. 1990. Mn(II) regulation of lignin Peroxidase and manganese dependent Peroxidase from lignin degrading white rot fungi. *Applied Environmental Microbiology*. 56 (1): 210 – 217.

Bosco, F., Ruggeri, B. & Sassi, G. 1996. Experimental identification of a scalable reactor configuration for lignin peroxidase production by *Phanerochaete chrysosporium*. *Journal of Biotechnology*. 52: 21 – 29.

Bruining, W.J., 1989. A general description of flows and pressures in hollow fibre membrane modules. *Chemical Engineering Science*. 44(6):1441 – 1447.

Bumpus, J.A. & Aust S.D. 1987. Biodegradation of environmental pollutants by the white rot fungus *Phanerochaete chrysosporium*. Involvement of the lignin degrading system. *Bioassays*. 6: 166 – 170.

Buswell, J.A. & Odier, E. 1987. Lignin biodegradation. *Critical Reviews of Biotechnology*. 6: 1 – 60.

Ceribasi, I.H. & Yetis, U. 2001. Biosorption of Ni (II) and Pb (II) by *Phanerochaete chrysosporium* from a binary metal system-Kinetics. *Water Research.* 27: 15-20.

Costerton, J.W., Lewandowski, Z., DeBeer, D., Caldwell, D., Korber, D. & James, G. 1994. Minireview: Biofilms, the customised micronich. *Journal of Biotechnology.* 176 (8): 2137 – 2142.

De Beer, D. Stoodley, P. & Lewandowski, Z. 1994. Liquid flow in heterogeneous biofilms. *Biotechnology Bioengineering.* 44: 636 – 641.

De Beer, D. & Schramn, A. 1999. Microenvironments and mass transfer phenomena in biofilms studied with micro-sensors. *Water Science Technology.* 39 (7): 173 – 178.

Doseretz, C.G., Chen, H-C., & Grethlein, H.E. 1990. Effect of environmental conditions on extracellular protease activity in ligninolytic cultures of *Phanerochaete chrysosporium. Applied environmental microbiology.* 56(2): 395 – 400.

Faison, B.D. & Kirk, T.K. 1985. Factors involved in the regulation of ligninase activity in *Phanerochaete chrysosporium. Applied environmental microbiology.* 49(2): 299 – 328.

Fane, A.G., Chang, S. & Chardon, E. 2002. Submerged hollow fibre membrane module-design options and operational considerations. *Desalination* 146: 231 – 236.

Fenn, P., Choi, S. & Kirk, T.K. 1981: Ligninolytic activity of *Phanerochaete chrysosporium*: Physiology of suppression by ammonia and l-glutamate. *Archives of Microbiology.* 130: 66 – 71.

Fenn, P. & Kirk, T.K. 1981: Relationship of nitrogen to the onset and suppression of ligninolytic activity and secondary metabolism in *P. chrysosporium. Archives of Microbiology.* 130: 59 – 65.

Flickinger, M.C. & Drew, S.W. 2004. *Encyclopaedia of bioprocess technology.* Vol. 1. New York: John Wiley.

Fogler, H.S. 1999. *Elements of chemical reaction engineering*. 3rd ed. Upper Saddle River, New Jersey: Prentice Hall.

Forney, L.J., Reddy, C.A. & Pankratz, H.S. 1982. Ultrastructural localisation of hydrogen peroxide production in ligninolytic Phanerochaete chrysosporium cells. *Applied Environmental Microbiology*. 44. 732 – 736.

Frank-Kamenetskii, D.A. 1969. *Diffusion and heat transfer in chemical kinetics*. New York. Plenum Press.

Freitas dos Santos, L.M. & Livingston, A.G. 1995. Novel membrane bioreactor for detoxification of VOC wastewaters: Biodegradation of 1, 2-dichloroethane. *Water Research*. 29 (1): 179 – 194.

Garcin, C.J. 2002. Design and manufacture of a membrane bioreactor for the cultivation of fungi. Unpublished MSc thesis, Rhodes University: Grahamstown.

Glen, J.K & Gold, M.H. 1988. Manganese Peroxidase from *Phanerochaete chrysosporium*. *Methods in Enzymology*. 161: 258 – 265.

Gold, M.H., & Alic, M. 1993. Molecular biology of the lignin degrading basidiomycete *Phanerochaete chrysosporium*. *Microbiology Reviews*. 57(3): 605 – 622.

Govender, S. 2000. Optimisation studies on a membrane gradostat bioreactor for ligninase production using white rot fungi. Unpublished M-Tech thesis, ML Sultan Technikon: Durban, R.S.A.

Govender, S., Jacobs, E.P., Leukes, W.D., Odhav, B. & Pillay, V.L. 2004. Towards an optimum spore immobilisation strategy using *Phanerochaete chrysosporium*, reverse filtration and ultrafiltration membranes. *Journal of Membrane Science*. 238: 83 – 92.

Griselda, G.D. & Eduardo, A.T. 1990. Screening of white rot fungi for efficient decolourisation of bleach pulp effluent. *Biotechnology Letters*. 12 (11): 869 – 872.

Hibiya, K., Nagai, J. & Tsuneda, S. 2003. Simple prediction of oxygen penetration depth in biofilms for wastewater treatment. *Biochemical Engineering Journal.* 19 (1): 61 – 68.

Howell, J.A., Sanchez, V. & Field, R.W. 1993. *Membranes in bioprocessing: Theory and application.* Cambridge: Chaplan and Hall.

Jacobs, E.P. & Leukes, W.D. 1996. Formation of an externally unskinned polysulphone capillary membrane. *Journal of Membrane Science.*121: 149 – 157.

Jacobs, E.P. & Sanderson, R.D. 1997. Capillary membrane production development. Report to the WRC by the institute of polymer science. WRC Report No. 632/1/97.

Jeffries, T.W., Choi, S. & Kirk, T.K. 1981: Nutritional regulation of lignin degradation by *P. chrysosporium. Applied Environmental Microbiology.* 42: 290-296.

Kelsey, L.J., Pillarella, M.R. & Zydney, A.L. 1990. Theoretical analysis of convective flow profiles in a hollow fibre membrane bioreactor. *Journal of Membrane Science.* 130: 3211 – 3220.

Khodui, R.S. & Tien, M. 1994. Kinetic analysis of lignin peroxidase: explanation of the mediation phenomenon by veratryl alcohol. *Biochemistry.* 33: 4225 – 4230.

Kirk, T.K., Schultz, E., Connors, W.J., Lorenz, L.F. & Zeikus, J.G. 1978. Influence of culture parameters on lignin metabolism by *Phanerochaete chrysosporium. Archives of Microbiology.* 117: 277 – 285.

Kirkpatrick, N. & Palmer, J.M. 1987. Semi-continuous ligninase production using foam-immobilised *Phanerochaete chrysosporium. Applied Microbiology Biotechnology.* 27: 129 – 133.

Kuwahara, S.W., Glenn, J.K., Morgan, M.A., & Gold, M.H. 1985. Separation and characterization of two extracellular H_2O_2 dependent oxidases from ligninolytic cultures of *Phanerochaete chrysosporium. FEBS LETTERS.* 169: 247 – 250.

Leisola, M., Ulmer, D.C. & Fiechter, A. 1984: Factors affecting lignin degradation in lignocelluloses by *P. chrysosporium*. *Archives of Microbiology.*137: 171-175.

Lejeune, R. & Baron, G.V. 1997. Simulation of growth of a filamentous fungus in 3 dimensions. *Biotechnology and Bioengineering.* 53: 139 – 150.

Leukes, W.D., Jacobs, E.P., Rose, P.D., Sanderson, R.D. & Burton, S.G. 1996. Secondary metabolite production. R.S.A patent 95/7366. U.S.A patent 08/705,624. E.P.O patent 963606333.4.

Leukes, W. 1999. Development and characterization of a membrane gradostat bioreactor for the bioremediation of aromatic pollutants using white rot fungi. Unpublished PhD thesis, Rhodes University: Grahamstown.

Lewandowski, Z., Webb, D. & Hamilton, M. 1999. Quantifying biofilm structure. *Water Science Technology.* 39 (7): 71 – 76.

Lewandowski, Z. & Beyenal, H. 2001. Limiting-current microelectrodes for quantifying mass transport dynamics in biofilms. *Methods in Enzymology.* 337: 339 – 359.

Lewandowski, Z. & Beyenal, H. Mass transport in heterogeneous biofilms. In: Wuertz, S., Bishop, P.L. and Wilderer, P.A. (eds) *Biofilms in water treatment.* IWA Publishing, London. 2003, pp 147 – 175.

Linko, S. 1992. Production of *Phanerochaete chrysosporium* Lignin Peroxidase. *Biotechnology advance.* 10. 191 – 236.

Livernoche, D., Jurasek, L., Desrochers, M. & Veliky, I.A. 1981. Decolourization of a Kraft mill effluent with fungal mycelium immobilised in calcium alginate gel. *Biotechnology Letters.* 3 (3): 701 – 706.

Martin, W. 2000. Recovery of impregnated gold from waste mine timber through biological degradation. Unpublished M-Tech thesis, Cape Technikon: Cape Town.

Murga, R., Steward, P.S. & Daly, D. 1995. Quantitative analysis of biofilm thickness variability. *Biotechnology and Bioengineering*: 45. 503 – 510.

Oyadomari, M., Shinohara, H., Johjima, T., Wariishi, H. & Tanaka, H. 2003. Electrochemical characterization of lignin Peroxidase from the white rot basidiomycete *Phanerochaete chrysosporium. Journal of Molecular Catalysis B: Enzymatic*: 21. 291 – 297.

Pavasant, P., Freitas dos Santos, L.M., Pistikopoulis, E.N. & Livingston, A.G. 1996. Prediction of optimal biofilm thickness for membrane attached biofilms growing in an extractive membrane bioreactor. *Biotechnology and Bioengineering*. 31: 913 – 921.

Perie, F.H. & Gold, M.H. 1991. Manganese regulation of manganese peroxidase expression and lignin degradation by the white rot fungus *Dichomitus squalen. Applied Environmental Microbiology*. 57: 2240 – 2245.

Perry, R.H & Green, D.W. (Ed) 1997. *Perry's chemical engineering's handbook.* 7th ed. New York: McGraw-Hill.

Poulos, T.L. & Kraut, J. 1980. The stereochemistry of peroxidase catalysis. *Journal of Microbiology*. 45: 8199 – 8205.

Revsbech, N.P. 1989. An oxygen microelectrode with a guard cathode. *Limnology and Oceanography*. 34: 472 – 476.

Ryan, D.R., Russel, A.K., Leukes, W.D., Rose, P.D. & Burton, S.G. 1998. Suitability of a modified capillary membrane for growth of fungal biofilms. *Desalination*. 115 (3): 307 – 312.

Scott, K. 1996. *Handbook of industrial membranes.* Oxford: Elsevier Advanced Technology.

Sheldon, M.S. & Small, H.J. 2005. Immobilisation and biofilm development of *Phanerochaete chrysosporium* on polysulphone and ceramic membranes. *Journal of Membrane Science*. 263: 30 – 37.

Shuler, M.L., & Kargi, F. 1992. *Basic concepts: Bioprocess engineering*. Englewood Cliffs, New Jersey: Prentice-Hall.

Solomon, M. 2001. Membrane bioreactor production of Lignin and Manganese peroxidase of *Phanerochaete chrysosporium*. Unpublished MTech thesis, Cape Technikon: Cape Town.

Street, R.L., Watters, G.Z. & Vennard, J.K. 1996. *Elementary fluid mechanics*. 7th ed. New York: John Wiley.

Tharakan, J.P., & Chau, P.C. 1986. Operation and pressure distribution of immobilized cell hollow fibre bioreactors. *Biotechnology and Bioengineering*. 28: 1064 – 1071.

Tien, M. & Kirk, T.K. 1984. Lignin degrading enzyme from *Phanerochaete chrysosporium*: Purification, characterization, and catalytic properties of a unique H_2O_2-requiring oxygenase. *Proc. Natl. Acad. Sci.* USA 81: 2280 – 2284.

Tien, M. 1987. Properties of ligninase from *Phanerochaete chrysosporium* and their possible applications. *Critical Reviews of Microbiology*. 15 (2): 141 – 167.

Tien, M. & Kirk, T.K. 1988. Lignin peroxidase of *Phanerochaete chrysosporium*. *Methods in Enzymology*. 161: 238 – 249.

Treybal, R.E. 1980. *Mass transfer operations*. 3rd ed. New York: McGraw-Hill.

Venkatadri, R. & Irvine, R.L. 1993. Cultivation of *Phanerochaete chrysosporium* and production of lignin peroxidase in novel biofilm reactor system: Hollow fibre reactor and silicon membrane reactor. *Water Research*. 27(4): 591 – 596.

Viana, M., Jouannin, P. & Chulia, D. (2002). About pycnometric density measurements. *Talanta*. 57 : 583 – 593.

Walsh, G. 1998. Comparison of pollutant degrading capacities of strain of *Phanerochaete chrysosporium* in relation to physiological differences. Unpublished Honours Thesis. Rhodes University, Grahamstown.

Wariishi, H. Valli, K.& Gold, M.H. 1992. Mn(II) oxidation by MnP from the basidiomycete *Phanerochaete chrysosporium*: Kinetic mechanism and role of chelators. *Journal of Biological Chemistry.* 267: 23688 – 23695.

Waterland, L.R., Robertson, C.R. & Michaels, A.S. 1975. Enzymatic catalysis using asymmetric hollow fibre membranes. *Chemical Engineering Communication.* 2: 37-47.

Yetis, U., Doleka, A., Dilek, F.B. & Ozcengiz, G. 2000. The removal of Pb(II) by *Phanerochaete chrysosporium. Water Research.* 34: 4090 – 4100.

Young, D.F., Munson, B.R., & Okiishi, T.H. 1997. *A brief introduction to fluid mechanics.* New York: John Wiley.

Yoon, S-H, Kim, H-S, & Yeom, I-T. 2004. Optimization model of submerged hollow fibre membrane modules. *Journal of Membrane Science.* 234: 147 – 156.

Zapanta, L.S. & Tien, M. 1997. The roles of veratryl alcohol and oxalate in fungal lignin degradation. *Trends in Biotechnology.* 53: 93 – 102.

Zhang, T.C. & Bishop, P.L. 1994. Density, porosity and pore structure of biofilms. *Water Research.* 28 (11). 2267 – 2277.

APPENDIX A: GROWTH AND MAINTANENCE OF THE FUNGUS

A1:   Preparation of the growth medium (spore inducing media)

The method for preparation of the growth medium was taken from Tien and Kirk (1988).

Add the following ingredients in order into a 1000ml Schott bottle.

Glucose	10g
Malt extract	10g
Peptone	2g
Yeast extracts	2g
Asparagine	1g
KH_2PO_4	2g
$MgSO_4.7H_2O$	1g ($MgSO_4 = 2.05g$)
Agar-agar	20g
Thiamin-HCl	1mg

Make up to 1000ml mark with distilled water, close the cap and shake to dissolve powder. Cover with tinfoil to prevent contamination and put a piece of heat detecting tape (Autoclave tape) on the foil to prepare for autoclavation. If no cap is available, cover the opening with non-absorbent cotton wool and then wrap it with tinfoil. Label the bottle with the present date, your name and the description of the contents and place into autoclave for 20 minutes at 121 ^{0}C to ensure sufficient sterilisation. The water level in the autoclave chamber must cover the bottom. After removing from the autoclave allow the content to cool down to a workable temperature before casting into the Petri dishes.

A2: Casting of the agar slants

Petri dishes:

Working under a laminar flow hood and using the flaming technique (flame after opening and before closing the bottle). Fill each Petri dish with the still hot agar by opening the lid only as far as necessary and pour agar evenly into it until the bottom of the dish is about 1cm thick. Flame the agar flask outlet before and after the agar is poured onto a Petri dish to avoid any possible transferred contamination. Leave the lids slightly open for a while to prevent moisture forming (condensation) underneath the lids. After the agar has cooled down sufficiently, it will become stiff with a consistency of jelly. Now you can proceed with the inoculation of *Phanerochaete Chrysosporium* spores.

Roux bottles:

Working under an operating laminar flow hood and using the flaming technique, fill each Roux bottle with about 250ml still hot agar. Cover the tops with non-adsorbent cotton wool and leave bottles slightly elevated for air circulation. Allow the agar to cool down for a few hours; it will be stiff as jelly and ready for inoculation.

A3:   Inoculation *Phanerochaete chrysosporium* on the agar slants
Petri dishes:

Work under an operating laminar flow hood and clean the surface thoroughly with 70% ethanol to avoid contamination. A platinum rod is used as the tool to transfer spores. Flame the tool under a Bunsen burner and cool it down by dipping it into the fresh agar located on the rim of the Petri dish. Cut out a square piece (about 1cm) of the inoculation culture and place in the middle of the fresh Petri dish and cover the lid. Continue until all the Petri dishes are inoculated. Store the Petri dish upside down and incubate at 37 ^{0}C for approximately seven days until spores are ready. Label with your name and present date.

Roux bottles:

Working under an operating laminar flow and using the flaming technique, cut out a square piece (about 1cm) with a flamed object and place in the middle of the Roux bottle and cover with cotton wool. Store the Roux bottle lying on its side with the top slightly elevated and incubate at 37 0C for approximately seven days until spores are ready. Label with your name and present date.

A4:   Spore solution preparation

Autoclave the following equipment:
- 1000ml distilled water in a Schott bottle
- 20ml syringe with glass wool
- 250ml flask

Always work under a laminar flow hood and work as clean, considerate and careful as possible to avoid any form of contamination. Take all the above-mentioned precautions to ensure maximum sterility.

Pour 5ml cooled sterile distilled water into each Petri dish containing spores and mycelium, under sterile conditions, close the lid and shake the water in rotational movements for one minute, to ensure that all spores are in solution. Transfer the washing solution from the Petri dishes into a sterile 100ml Schott bottle, repeat this three to four times on one agar slant. Continue with this procedure until you have enough spore solution. The bottle now contains a spore/mycelium solution.

A5: Separation of spores from mycelium

Heat sterilise (autoclave) a sterile syringe with glass wool for 15 minutes. Filter the solution through a 0.22μm sterile filter using the sterile syringe with glass wool, into a 250ml flask.

A6: Determination of spore purity and concentration

Spore purity

Under sterile conditions pipette a small drop of spore solution onto a slide, cover it with a cover slip and observe with a light microscope at x100 magnification. Uniform oval spores with a small size distribution and no or very few visible mycelium pieces should be seen.

Spore concentration

The spore solution concentration is determined by measuring absorbance at 650nm with a spectrophotometer. The spectrophotometer should be switched on at least 30 minutes before it is used in a fixed wavelength mode. The UV and visible lights should be switched on. Ordinary plastic cuvettes are used for the spore solution concentration. According to Tien and Kirk (1988) an absorbance of $1.0cm^{-1}$ is approximately, 5×10^6 spores/ml.

- Pour distilled water into a plastic corvette and place into the spectrophotometer.
- Blank the spectrophotometer by clicking on the word blank in the bottom left corner of the screen.

- Repeat two or three times until the absorbance reads close to 0.
- Replace the blank with a quartz corvette filled with spore solution. (NB: Do not leaf the cover open for too long).
- Click on "Read sample" at the top of the screen.
- Read of the absorbance and write it down (e.g. 0.0741).

To obtain a million spores (example):

An absorbance of, $1 = 5 * 10^6$ spores/ml

i.e. $0.0741 = x$

$\therefore$ $x = \dfrac{0.0741 * (5 * 10^6)}{1} = 3.7 * 10^5$ Spores/ml

Therefore: $3.7 * 10^5$ Spores for every 1ml

i.e. $1 * 10^6$ Spores for every 2.7ml

Dissolve 2.7ml of the spore solution into 250ml sterilised distilled water. This solution will be used for inoculation of the reactor.

APPENDIX B: PREPARATION OF THE NUTRIENT SOLUTION

B1:   Trace element stock solution

Dissolve 1.5g Nitrilotriacetate in 800ml-distilled water. After dissolving the nitrilotriacetate completely, adjust the pH to 6.5 with 1M KOH (8g/500ml). Add each component sequentially.

$MgSO_4$	3g	($MgSO_4.7H_2O$ = 6.14g)
$MnSO_4$	0.5g	($MnSO_4.H_2O$ = 0.56g)
NaCl	1g	
$FeSO_4.7H_2O$	0.1g	
$CoCl_2$	0.1g	($CoCl_2.6H_2O$ = 0.187g)
$ZnSO_4.7H_2O$	0.1g	
$CuSO_4$	0.1g	
$AlK(SO_4)_2.12H_2O$	0.01g	
H_3BO_3	0.01g	
$Na_2MoO_4.2H_2O$	0.01g	

Make up to 1L with autoclaved distilled water. Filter sterilise the solution into an autoclaved bottled using a 0.22μm filter. Filter sterilize through 0.22μm filter into sterile bottle and store at 4 ^{0}C. This solution should be light yellow.

B2:   Basal III medium stock solution

KH_2PO_4	20g	
$MgSO_4$	5g	
$CaCl_2$	1g	($CaCl_2.2H_2O$ = 1.32g)
Trace element solution	100ml	(See B1 above)

Make up to 1L with autoclaved distilled water. Filter sterilize through 0.22μm filter into sterile bottle and store at 4 ^{0}C.

B3:   10% Glucose stock solution

Glucose   100g

Make up to 1L with autoclaved distilled water. Autoclave for 20 minutes and store at 4 ^{0}C.

B4:   0.1M 2, 2-dimethylsuccinate stock solution (pH 4.2)

2, 2-dimethylsuccinate 13.045ml in 1L autoclaved distilled water.

Calculated as follows:

If powder:

Mw   =   146 g/mol

Moles =   mass/Mw

0.1M   =   mass/146.1

Mass   =   0.1*146.1 = 14.61 g (put into 1L)

If Liquid:

If density   =   1.12 g/mol

               =   Mass/volume

Volume   =   14.61/1.12

               =   13.045 ml (put into 1L)

Autoclave for 20 minutes and store at 4 ^{0}C.

B5:   Thiamin-HCL (Do not autoclave)

Thiamin-HCl   100 mg/l stock

Filter sterilize through 0.22μm filter into sterile bottle and store at 4 ^{0}C.

B6:   Ammonium tartrate

Ammonium tartrate   8g

Make up to 1L with autoclaved distilled water. Autoclave for 20 minutes and store at 4 ^{0}C.

B7:   0.4M Veratryl alcohol (light sensitive)

Veratryl alcohol   2.907ml in 1L

Calculated as follows;

If powder:

Mw   =   168.19 g/mol

Moles =   mass/Mw

0.02M =   mass/168.19

Mass   =   3.3638 g (put into 1L)

If Liquid:

If density   =   1.157 g/mol

               =   mass/volume

Volume   =   2.907 g/ml (put into 1L)

Filter sterilize through 0.22μm filter into sterile bottle and store at 4 ^{0}C (Store in dark place when not in use).

B8:   Nutrient medium composition

Basal III medium   100ml

10% glucose stock solution   100ml (Carbon source)

0.1M 2, 2-dimethylsuccinate   100ml (Growth enhancer)

Thiamin-HCL   10ml (Vitamin)

Ammonium tartrate   25ml (Nitrogen source)

| 0.4M Veratryl alcohol | 100ml (Growth enhancer) |
| Trace elements | 60ml |

Make up to 1L with autoclaved distilled water.

Points to remember:

- When dispensing culture media, always use sterile measuring cylinders and dispense into sterile containers.
- Always use autoclaved-distilled water.
- All stock solutions should be sterilised before the time. It is therefore not necessary to autoclave the nutrient media again after it is made up.
- Nutrient medium must be kept at 4 ^{0}C if not in use.

APPENDIX C: LIGNINOLYTIC ENZYME ASSAYS

C1: Lignin Peroxidase Assay

Lignin Peroxidase activity was determined spectrophotometrically at 25 ^{0}C using veratryl alcohol as the substrate (Tien and Kirk, 1998). The activity was measured by determining the rate of oxidation of veratryl alcohol to veratraldehyde. This was monitored at 310nm. The alcohol exhibits no absorbance at 310nm whereas the aldehyde absorbs strongly. The extinction coefficient used for veratraldehyde was 9300$M^{-1}.cm^{-1}$. Use is made of this property in a continuous in a continuous spectrophotometer assay. Activity is expressed in U.L^{-1}, where 1 unit = 1μmol/min.

Prepare the following stock solutions

10 mM Veratryl Alcohol

- Transfer 1.454ml into 1L distilled H_2O.
- Store at 4 ^{0}C in a dark container when not in use.

Calculated as follows:

If powder:

Mw	=	168.19 g/mol
Moles	=	mass/Mw
0.01M	=	mass/168.19
Mass	=	1.6818 g (put into 1L)

If Liquid:

If density	=	1.157 g/mol
	=	Mass/volume
Volume	=	1.454 ml (put into 1L)

250mM Tartaric acid

- Add 9.43g to 80ml distilled H_2O.

- Using 1M NaOH, adjust pH to 2.5 (i.e. add 40 g/L NaOH to distilled water to make 1M NaOH).

- Make up to 250ml volume.

- Store at 4 ^{0}C.

Calculated as follows:

Mw	=	150 g/mol
0.25 M	=	0.250 mol/L
(150 g/mol*0.25 mol/L)	=	37.725 g/L
Required	=	9.43 g/ 250ml

5mM Hydrogen Peroxidase (H_2O_2)

- Made up fresh every time

- Light sensitive; do not leave standing in direct sunlight for extended periods of time.

- 50 μL of 30% H_2O_2 in a 100ml flask and make up to volume.

Assay material and method

	Blank	Sample
10mM Veratryl alcohol	200 μL	200 μL
250mM Tartaric acid	200 μL	200 μL
Distilled water	520 μL	220 μL
Enzyme solution		300 μL
5mM H_2O_2	80 μL	80 μL
Total	**1000 μL**	**1000 μL (1) ml**

Note: Add everything into the Eppindorf tube except the H_2O_2, which is added just before assaying.

Spectrophotometer settings:

- Kinetics mode
- UV light switched on
- Read at 310nm for 5 minutes at 10 seconds intervals
- Factor: 1075.3
- Temperature: 25 ^{0}C
- Extinction coefficient: 9300 $M^{-1}.cm^{-1}$

Calculation of activity

- The objective is to get a reading in units per litre, where 1 unit = 1µmol substrate converted per minute (mM/min.L).

- Take your absorbance readings and a plot a graph showing absorbance versus time.

- The initial slope, $\dfrac{dA}{dt}$ will give you the value for initial rate of reaction.

- To convert this into $\dfrac{dC}{dt}$, use Lambert-Beer method and divide by the extinction coefficient E, which is 9300 $M^{-1}.cm^{-1}$. This gives a value in mol/min.L.

- Moles are now changed to micromoles by multiplying by 10^6. This gives micro-moles/min.L, which equals 1 unit; therefore the answer is now in units per litre.

- Now you have to consider sample handling. First, you need to account for dilution in your assay. If you used 200µl of enzyme sample solution in a 2ml reaction volume, this constitutes a dilution of 1 in 10. You therefore have to multiply your answer by 10.

- If you have concentrated your sample by using cut off tubes, you have to divide by your concentration factor. If you fill your cut off tubes initially with 3ml and you have 0.5ml concentration enzyme solution left, your factor would be 6

- As a guideline, if you have not concentrated your sample, then multiply your $\dfrac{dA}{dt}$, readings in minutes by 1075.3.

Therefore: *activity* $(U/L) = \left[\dfrac{\dfrac{dA}{dt} * (dilution \quad factor)}{extinction \quad coefficient} \right] * 60 * 10^6$

C2:   Manganese Peroxidase assay

Castillo, M.D.; Stenstrom, J. and Ander, P. 1994. Determination of Manganese Peroxidase activity with 3-Methyl-2-benzothiazolinone Hydrazone and 3-(Dimethylamino) benzoic acid. *Analytical Biochemistry*, 218(2):399-404)

This assay is based on the oxidative coupling of 3-methyl-2-benzothiazolinone hydrazone (MBTH) and 3-(dimethylamino)benzoic acid (DMAB). The reaction of MBTH and DMAB in the presence of H_2O_2, Mn^{2+} and *MnP* gives a deep purple-blue colour with a broad absorption band with a peak at 590 nm. The extinction coefficient (EC) is high (53 000 $M^{-1}cm^{-1}$), so low *MnP* activities can be detected. *Lignin Peroxidase* and laccase, usually present in cultures of white rot fungi, gave little or no interference at the concentrations tested. However, slight interference from very high *LiP* activity may occur at very low *MnP* activity.

Prepare the following solutions and store in the fridge

1.   0.7 mM MBTH (3-methyl-2-benzothiazolinone hydrazone)
0.038 g of MBTH in 250 ml of distilled water.

2.   9.9 mM DMAB (3-dimethylamino benzoic acid)
0.41 g of DMAB in 250 ml distilled water.

3.   3 mM MnSO$_4$
0.051 g of MnSO$_4$ in 100 ml distilled water

4.   0.5 mM H$_2$O$_2$
5.68 µl of H$_2$O$_2$ in 100 ml distilled water

5.   1M Sodium succinate buffer (pH 4.5)

- Add together 2M succinic acid and 2M sodium hydroxide.

- 2M succinic acid: 11.809g succinic acid in 50ml distilled H_2O

- 2M sodium hydroxide: 4g of sodium hydroxide in 50ml distilled H_2O.

6.   1M Sodium Lactate buffer (pH 4.5)

- Add together 2M lactic acid and 2M sodium hydroxide

- 2M lactic acid: 10.68 ml lactic acid in 50ml distilled H_2O

- 2M sodium hydroxide: 4g of sodium hydroxide in 50ml distilled H_2O.

Spectrophotometer settings:

Kinetics mode

UV and visible light switched on

Temperature 25°C

Read at 590 nm for 1 minutes (60 seconds) at 0.5 sec intervals

Activity is calculated the same as explained before.

APPENDIX D: GLUCOSE AND AMMONIUM ASSAYS

D1: Glucose assay using Roche ® D-Glucose kit (Cat No: 10 716 251 035)

Dissolve contents of one bottle 1 (ATP) with 45ml sterile distilled water. Store in fridge. Bring to 20- 25 °C before use

Procedure for assay

Pipette into cuvettes	Blank	Sample
Solution 1	1.0 ml	1.000 ml
Sample solution	----	0.100 ml
distilled water	2.000 ml	1.900 ml
Mix**, read absorbance's of the solutions (A_1) after approximately 3 min and start reaction by addition of:		
Suspension 2	0.020 ml	0.020 ml
Mix **, wait for the end of the reaction (approximately 10-15 min) and read absorbance's of the solutions (A_2).		

- Pipette 1000 µl (1 ml) of bottle 1 solution into two plastic cuvettes, namely B (blank) and S (sample)

- Dilute the permeate sample, by adding 10 µl of permeate to 990 µl of sterile distilled water (Dilution factor = 100)

- Add 100 µl of diluted permeate into the S (sample) cuvettes. To test nutrient solution add 100 µl of diluted nutrient into the S (sample cuvettes)

- Add 1900 µl of sterile distilled water to S (sample) and 2000 µl of sterile distilled water into B (blank). Close and mix. Bring samples to 20-25°C before use.

- Read absorbancy (A1) of the blank and samples against water in a 1 cm (10mm) light path at 340 nm

- Add 20 µl (0.02 ml) of bottle 2 (solution of enzyme, Hexokinase) into both cuvettes (B and S) and mix. Wait until the reaction has stopped (10 – 15 min) and read absorbencies (A2).
- Determine the absorbance differences (A2 – A1) of the blank and sample
- Use the equation below to evaluate the glucose concentration:

NB: If the sample has been diluted during the preparation, the result must be multiplied by the dilution factor F

$$c(g/l) = \frac{V \times Mr \times F}{\varepsilon \times d \times v \times 1000} \times \Delta A \qquad \text{Where: } \Delta A = (A_2 - A_1)_{sample} - (A_2 - A_1)_{blank}$$

Dilution table

Estimated amount of D-glucose per litre measurements at different absorbencies		Dilution with water	Dilution factor
340 or 334 nm	365 nm		
<0.5 g	<1 g	--	1
0.5-5g	1-10 g	1 + 9	10
5-50 g	10-100g	1 + 99	100
>50 g	>100 g	1 + 999	1000

D2:   Ammonia Assay using Merck Spectroquant NH4+ kit (Cat No: 1.00683.0001)

Method

Ammonium nitrogen NH_4-N occurs partly in the form of ammonium ions and partly as ammonia. A pH-dependent equilibrium exists between the two forms. In strong alkaline solutions NH_4-N is present almost entirely as ammonia. This reacts with hypochlorite ions to form monochloramine, which in turn reacts with a substituted phenol to form a blue indophenol. This is then determined photometrically.

Wavelength	Measuring range	Number of determinations
712	2.0 - 150 mg/L NH$_4$-N	95
	2.6-193 mg/L NH$_4^+$	

Preparation

- Analyse immediately after sampling

- The pH must be within the range 4 – 13. Adjust if necessary, with a sodium hydroxide solution or sulphuric acid. Adjust, if necessary, with sodium hydroxide solution or sulphuric acid.

- Check the ammonium content with the spectroquant Ammonium Test. Samples containing more than 193 mg/L NH$_4^+$ must be diluted with distilled water.

- Filter turbid samples.

- Decompose or extract solid sample materials by an appropriate method

Procedure

Preparation of measurement sample for measuring range of 2 – 75 mg/l NH$_4$-N (2.6-96.6 mg/l NH$_4^+$)

Reagent NH$_4$-1	5 ml	Pipette into a test tube
Pretreated sample (20-30°C)	0.2 ml	Add using pipette and mix
Reagent NH$_4$-2	1 level blue microspoon in cap of bottle	Add and shake **vigorously until the reagent is completely dissolved**
Leave to stand for 15 min, then fill the measurement sample into a 10-mm cell and measure in the spectroquant or in a photometer at 712 nm		

Note
- Due to the strong temperature dependence of the colour reaction, the temperature of the reagents should be between 20 and 30 °C.

- Certain photometers may require a blank (preparation as per measurement sample, but with distilled water instead of sample).

- For photometric measurement the cells must be clean. Wipe if necessary with a clean cloth.

- Measurement of turbid solutions gives false-high readings.

- Ammonium-free samples turn yellow on addition of reagent NH_4-2.

- The colour of the measurements solution remains stable for at least 60 min after the end of the reaction time stated above.

- In the event of ammonium concentrations exceeding 2500 mg.L^{-1}, other reaction products are formed and false-low readings are yielded. In such cases it is advisable to conduct a plausibility check of the measurement results by diluting the sample (1:10; 1:100).

Calculation

$$NH_4^+ (mg/L) = 1.2877(NH_4 - N/mg/L) + 0.0247$$

APPENDIX E: DETAILED MATHEMATICAL MODELS

E1: Mathematical modelling of nutrient flow behaviour in vertically placed polysulphone hollow fibre membranes.

Conditions:

1. Flow behaviour is assumed to be a convective process only, as nutrient supply is by a peristaltic pump.

2. The models to be developed will provide description of flow through some average fibre in a vertically placed multi capillary membrane bioreactor.

Continuity equation in cylindrical coordinates:

$$\frac{d\rho}{dt} + \frac{1}{r}\left[\frac{d(r\rho u_r)}{dr}\right] + \frac{1}{r}\left[\frac{d(\rho u_\theta)}{d\theta}\right] + \frac{d(\rho u_z)}{dz} = 0$$

For steady or unsteady flow were the flow is uncompressible with constant density while considering axial (z-direction) and radial (r-direction) flow only, the equation above is reduced to,

$$\frac{du_z}{dz} + \frac{1}{r}\left[\frac{d(ru_r)}{dr}\right] = 0 \qquad \text{(Continuity equation)}$$

In terms of the cylindrical polar coordinates the Navier-Stokes equation can be written as (z/axial direction),

$$\rho\left(\frac{\partial u_z}{\partial t} + u_r\frac{\partial u_z}{\partial r} + \frac{u_\theta}{r}\frac{\partial u_z}{\partial \theta} + u_z\frac{\partial u_z}{\partial z}\right) = -\frac{\partial P}{\partial z} + \rho g_z + \mu\left[\frac{1}{r}\frac{\partial}{\partial r}\left(r\frac{\partial u_z}{\partial r}\right) + \frac{1}{r^2}\frac{\partial^2 u_z}{\partial \theta^2} + \frac{\partial^2 u_z}{\partial z^2}\right]$$

The above equation is considered to be the governing differential equation of motion for incompressible, Newtonian fluids flowing in the axial direction between two parallel plates.

162

Considering our system (vertically placed hollow fibre membranes) the following conditions will prevail,

1. $\dfrac{du_z}{dt} = 0$ (Steady laminar flow through fibres)

2. $\dfrac{du_z}{d\theta} = 0$; $\dfrac{du_r}{dr} = 0$ $u_r = 0$ (Bulk flow in the z direction only)

3. $\dfrac{du_z}{dz} = 0$ (Reduction of continuity equation, considering condition 2 above)

4. $\rho g_z \approx 0$ (The hydrostatic pressure in single capillary membrane systems operated at dead-end filtration mode is negligible compared to gauge pressure)

The equation is reduced to, $0 = -\dfrac{dP}{dz} + \mu\left[\dfrac{1}{r}\dfrac{d}{dr}\left(r\dfrac{du_z}{dr}\right)\right]$

The momentum equation can be rearranged as,

$$\dfrac{dP}{dz} = \mu\left[\dfrac{1}{r}\dfrac{d}{dr}\left(r\dfrac{du_z}{dr}\right)\right] \qquad \text{(Momentum balance equation)}$$

Solution to the momentum equation:

$$u_z = \left(\dfrac{dP}{dz}\right)\dfrac{r^2}{4\mu} + C_1 \ln r + C_2$$

Physical conditions :

Fibre centre ($r = 0$)	Lumen ($r = R_L$)
$\dfrac{du_z}{dr} = 0$ (u_z is finite, no slip conditions for viscous fluids)	$u_z = 0$

Then $C_1 = 0$ and $C_2 = -\dfrac{R_L^2}{4\mu}\left(\dfrac{dP}{dz}\right)$

The solution of the momentum equation is: $u_z = \dfrac{1}{4\mu}\left(r^2 - R_L^2\right)\left[\dfrac{dP}{dz}\right]$

Differential format:

Also $\dfrac{du_z}{dr} = \dfrac{r}{2\mu}\left[\dfrac{dP}{dz}\right]$ (Evaluated at different z values)

Solution to the continuity equation:

$$\frac{du_z}{dz} + \frac{1}{r}\frac{d(ru_r)}{dr} = 0$$

Therefore: $\quad d(ru_r) = \left[\dfrac{d}{dz}\left[-\dfrac{1}{4\mu}\left(r^2 - R_L^2\right)\left(\dfrac{dP}{dz}\right)\right]r\right]dr$

The solution: $u_r = -\dfrac{1}{16\mu}\left(r^3 - 2rR_L^2\right)\dfrac{d^2P}{dz^2}$

Differential format:

$\dfrac{du_r}{dr} = \dfrac{1}{16\mu}\left(2R_L^2 - 3r^2\right)\dfrac{d^2P}{dz^2}$ (Evaluated at different z values)

From literature: $u_r = \varepsilon u_m = \hat{K}_p(P - P_s)$ at $r = R_L$

Were ε is the porosity of the lumen and u_m is the radial velocity in the fibre matrix.

At $r = R_L$: $u_r = \dfrac{R_L^3}{16\mu}\dfrac{d^2P}{dz^2}$

Therefore: $u_m = \dfrac{R_L^3}{16\mu\varepsilon}\dfrac{d^2P}{dz^2}$

Then across the thickness of the fibre matrix (l_m)

$\dfrac{du_m}{dl_m} = \dfrac{R_L^3}{16\mu\varepsilon}\dfrac{d^2P}{dz^2}$ (Evaluated at different z values)

Solution to the second-order differential equation:

From flow behaviour modelling, the axial velocity profile is given by:

$$u_z = \frac{1}{4\mu}\left(r^2 - R_L^2\right)\left(\frac{dP}{dz}\right)$$

The volumetric flow rate can be found by integrating the velocity profile throughout the cross section of the membrane,

$$Q = \int_A u_z\, dA$$

The differential area in cylindrical coordinates (r→θ plane) $\therefore dA = r\,dr\,d\theta$.

$$Q = \int_0^{2\pi}\left(\int_{r=0}^{r=R} u_z r\,dr\right)d\theta$$

Of which the solution is: $\dfrac{dP}{dz} = \left(\dfrac{8Q\mu}{\pi R_L^4}\right)$

At $r = R_L$: $u_r = \dfrac{R_L^3}{16\mu}\dfrac{d^2P}{dz^2} = \hat{K}_p(P - P_S)$

165

Therefore: $\dfrac{d^2 P}{dz^2} = \omega(P - P_S)$ were $\omega = \dfrac{16\mu\hat{K}_p}{R_L^3}$

The solution of the second order differential equation in terms of complimentary function and particular integral is:

$$P = Ae^{-\sqrt{\omega}z} + Be^{-\sqrt{\omega}z} + P_S$$

With initial conditions: $P(z = 0) = P_1$ & $\dfrac{dP}{dz}(z = 0) = 0$

The solution of constants A and B are:

$$A = \frac{1}{2}(P_1 - P_S) \quad A = B$$

Therefore: $P = (P_1 - P_s)\cosh(\sqrt{\omega}z) + P_S$

Differential format:

$$\frac{dP}{dz} = (P_1 - P_s)\sqrt{\omega}\, \sinh(\sqrt{\omega}z)$$

$$\frac{d^2 P}{dz^2} = (P_1 - P_s)\omega\cosh(\sqrt{\omega}z)$$

E2: Simple simulation of oxygen profiles in *P. chrysosporium* biofilms (Similar to that of Hibiya *et al.*, 2003)

Simulation:

The oxygen distribution in biofilms was simulated with a Monod equation with regard to oxygen consumption through chemical/biological reaction. The calculation is as follows: the mass balance equation for oxygen in the biofilm is,

$$\frac{dC_{O_2}}{dt} = D\left(\frac{d^2C_{O_2}}{d\delta^2}\right)_f - \frac{k_{O_2}XC_{O_2}}{K_m + C_{O_2}}$$

Where C_{O_2} is the oxygen concentration, t the time, D the effective diffusion coefficient of oxygen in the biofilm, δ the distance from the biofilm surface, k_{O_2} the reaction rate constant, K_m the Monod saturation constant, and X the dry density of the biofilms. At steady state $\left(\dfrac{dC_{O_2}}{dt} = 0\right)$ were the consumption rate equals to the diffusion rate, the equations becomes,

$$D\left(\frac{d^2C_{O_2}}{d\delta^2}\right)_f = \frac{k_{O_2}XC_{O_2}}{K_m + C_{O_2}}$$

The inverse of the above equation will result in the following linear expression,

$$\left(\frac{d^2C_{O_2}}{d\delta^2}\right)_f^{-1} = \left(\frac{DK_m}{k_{O_2}X}\right)\frac{1}{C_{O_2}} + \frac{D}{k_{O_2}X}$$

Where the value of K_m, can be calculated, by dividing the slope by the intercept.

Experimental profiles:

By experimentally measuring the oxygen distribution in any biofilm at different depths using an oxygen microsensor, the experimental profile will best be fitted by an exponential equation with the format,

$$C = a_4 e^{-a_5 \delta}$$

The above equation can be differentiated twice to obtain a second order deferential equation,

$$\left(\frac{d^2 C_{O_2}}{d\delta^2} \right) = a_4 a_5 e^{-a_5 \delta}$$

Then
$$\left(\frac{d^2 C_{O_2}}{d\delta^2} \right)^{-1} = \frac{1}{a_4 a_5^2 e^{-a_5 \delta}}$$

By plotting $\dfrac{1}{a_4 a_5^2 e^{-a_5 \delta}}$ againstError! Objects cannot be created from editing field codes., a straight line was obtained at lower oxygen concentrations compared to high oxygen concentrations. The gradient of the trend-line (at low oxygen concentrations) $\dfrac{DK_m}{k_{O_2} X}$ was divided by the interceptError!

Objects cannot be created from editing field codes., obtaining K_m .

Note: High correlation coefficients ($R^2 = 0.9999$) of the trend-line are required to get more accurate simulation results.

Evaluation:

Using the sets of parameters $\dfrac{D}{k_{O_2} X}$ and K_m which were computed as described previously, the first derivative of oxygen concentration in the biofilm can be expressed as,

$$\frac{dC_{O_2}}{d\delta} = -\sqrt{2\frac{k_{O_2}X}{D}\left(C_{O_2} - K_m Ln\left(\frac{K_m + C_{O_2}}{K_m}\right)\right)}$$

The equation above was derived from equation 2.16 developed by Frank-Kamenetskii (1969). The following is an example of a first order differential equation program, which can be used to evaluate the simulation curve.

E3:   Modelling mass transfer through *P. chrysosporium* biofilm:

Nutrient flow behaviour in the biofilm matrix, constitute three distinct areas that are classified as constituents of mass transfer phenomena. The areas are, 1) Convective nutrient transport closer to the substratum (Membrane), as nutrient medium was supplied by a peristaltic pump, 2) Diffusion, which occurs further away from the substratum surface and 3) biological reaction which was assumed to follow Monod's equation.

Treybal (1980) has shown that flow of a component in terms of 1) diffusion, 2) convection, 3) rate of generation and 4) accumulation, in three dimensional coordinates is given by equation 3.26. (As generated from a substrate mass balance with a reaction).

$$u_x\frac{\partial C_s}{\partial x} + u_y\frac{\partial C_s}{\partial y} + u_z\frac{\partial C_s}{\partial z} + \frac{\partial C_s}{\partial \theta} = D\left(\frac{\partial^2 C_s}{\partial x^2} + \frac{\partial^2 C_s}{\partial y^2} + \frac{\partial^2 C_s}{\partial z^2}\right) + r_B \quad 9.1$$

Where r_B is the biological generation.

$\dfrac{\partial C_s}{\partial \theta}$ Is the accumulation of the substrate.

Equation 3.26 was adjusted for substrate flow through a fungus matrix situated in a vertical position. The following general conditions were considered:

3. Substrate consumption was in terms of biological reaction, therefore,

$$r_B = -\frac{k_s X C_s}{K_m + C_s}$$

4. Mass transfer was one-dimensional (z direction, i.e. across the biofilm) and there was no accumulation of substrate in the biofilm, therefore $\dfrac{\partial C_s}{\partial \theta} = 0$.

The equation was then reduced to,

$$u_z \frac{\partial C_s}{\partial z} = D\left(\frac{\partial^2 C_s}{\partial z^2} \right) - \frac{k_s X C_s}{K_m + C_s} \qquad\qquad 9.2$$

Two distinctive regions were identified in the biofilm. The two regions were classified as, 1) Convection dominant area and 2) Diffusion dominant area. Mass transfer in the two regions was modelled using different mathematical models for simplicity.

Convection dominant area

The maximum rate of flux in the absence of diffusion limitations was given by equation 3.28, developed from equation 3.27.

$$-\frac{dC_s}{dz}\bigg|_{z=\delta} = u_z \frac{k_s X C_s}{K_m + C_s} \delta \qquad\qquad 9.3$$

Experimental concentration profiles were evaluated across a certain biofilm thickness and parameters such as the Monod's saturation constant were evaluated (similar to the oxygen profiles) and then used in the simulation model by using a first order differential solver to obtain appropriate curves.

Diffusion dominant area

Equation 3.28 is then reduced to,

$$D\frac{d^2C_s}{dz^2}\bigg|_{z=\delta} = \frac{k_s X C_s}{K_m + C_s} \qquad\qquad 9.4$$

The equation was evaluated similar to oxygen concentration profile using the mass balance equation (Equation 2.15) developed by Frank-Kamenetskii (1969).

APPENDIX F: MICROSENSOR OPERATION

a)   Polarising the picoammeter:

Channel 1 of the Unisense pA 2000 picoammeter was used. The 'Diplay' selector was turned to 'Pol 1' and adjusted to -0.80V using the polarisation control. The 'Display' selector was turned to 'signal 1' and then the 'Gain' screw was completely turned counter-clockwise. The display signal was then adjusted to zero on the 'offset' dial and left for 24 hours to stabilise.

b)   Connecting the oxygen microsensor:

The BNC of the microsensor was connected, which contains connections for both the reference and sensing cathodes, to the input terminal of the picoammeter, and then the yellow cathode was connected to the guard terminal first and the signal on the display was monitored.

c)   Pre-polarisation of the microsensor:

Before the sensor was polarised, the electrolyte will contain oxygen. This oxygen must be consumed by the sensing cathode and the guard cathode before stable operation of the sensor is possible. The sensor was secured and adjusted such that the tip was immersed in continuously aerated water (obtained by bubbling air from and aquarium pump through the water). The sensor was polarised until it has exhibited a stable signal for 10 minutes.

Calibration of the microsensor:

- **Concentration reading (0%)** – The oxygen microsensor was placed in an anoxic solution (Sodium ascorbate and NaOH, both to final concentrations of 0.1 mol/L), which acts as a strong oxygen reducing agent. The tip of the microsensor was placed in this solution for 5 minutes, and the signal obtained was the zero setting for the oxygen concentration.

- **Concentration reading (100%)** – The sensor tip was placed in the calibration solution (nutrient medium), which was aerated by bubbling industrial oxygen. After 5 minutes of vigorous bubbling, the oxygen was turned off and the signal obtained was noted as a calibration value for 100% oxygen. Then the sensor was ready for use.

General use: Oxygen microsensor:

1. Turn on the power switch on the picoammeter
2. Check that the "GAIN" screw is turned fully counter clockwise.
3. Check polarisation voltage. The value should be -0.80 V. If not this value correct using "VOLT" screw and "POLARITY" switch.
4. Put the "DISPLAY" knob to "SIGNAL". The reading on the LCD display should be 0.00 before connecting the sensor, if not adjust to zero with the "OFFSET" screw at "200 nA" range.
5. Connect the sensor leads to the meter in the following order: 1) Connect black wire to "INPUT". 2) Connect yellow wire to "GUARD".
6. Polarise the sensor by putting in continuously aerated water. When polarisation is initiated, the signal will be very high and then drop rapidly over the first few minutes. There after the signal will drop slowly.
7. Turn the "RANGE" to "2000 pA". The signal should stabilise (positive on the LCD display.)
8. Perform calibration according to protocol.
9. Sensor is ready for use.

General use: Hydrogen Peroxide microsensor:

10. Turn on the power switch n the picoammeter
11. Check that the "GAIN" screw is turned fully counter clockwise.
12. Check polarisation voltage. The value should be +0.80 V. If not this value correct using "VOLT" screw and "POLARITY" switch.
13. Put the "DISPLAY" knob to "SIGNAL". The reading on the LCD display should be 0.00 before connecting the sensor, if not adjust to zero with the "OFFSET" screw at "10 000 nA" or Higher range. i.e 10 μA.

14. Connect the sensor leads to the meter in the following order: 1) Connect platinum wire (anode) to "INPUT". 2) Connect SCE (standard calomel electrode) to "GUARD" i.e this is an external reference. Calomel is a solution of Hg_2Cl_2.

15. Polarise the sensor by putting in continuously aerated water. When polarisation is initiated, the signal will be very high and then drop rapidly over the first few minutes. There after the signal will drop slowly.

16. Turn the "RANGE" to "10 μA". The signal should stabilise (negative on the LCD display).

17. Perform calibration according to protocol. The relationship between the current and the amount of HP in solution must be generated for each electrode. Once the current produced in the test sample can be related to the concentration of HP in solution.

18. Sensor is ready for use.

APPENDIX G: EXAMPLE OF IN/OUTPUT FILES FOR PROFILE 1.0 SOFTWARE

H1: INPUT FILE

1. The input file used in Profile 1.0 software using Microsoft® Notepad

Interpretation of Oxygen profile (Reactor 1-72 hrs)

0	depth at top
0.00045	depth at bottom
5	maximum number of equally spaced zones in interpretation
4	type of boundary condition
6.500632794	concentrations at the top
0.000	flux at the bottom
1.161e-5	Diffusion of oxygen in nutrient medium at 37 °C
1	expression for biofilm diffusivity
6.500632794	concentration at x = start
-1.0e+20	minimum consumption
0.0	maximum consumption rate
0.001	maximum deviation (%)

0.01 level of significance in the F statistics

Depth [m]	Fi	DB	Alfa	Oxygen concentration (g/m^3)
0	0.8	0	0	6.500632794
0.00005	0.8	0	0	5.166305533
0.0001	0.8	0	0	3.846087472
0.00015	0.8	0	0	2.654867818
0.0002	0.8	0	0	1.745832176
0.00025	0.8	0	0	1.100840147

175

0.0003	0.8	0	0	0.642291125
0.00035	0.8	0	0	0.31294207
0.0004	0.8	0	0	0.112591421
0.00045	0.8	0	0	0.013423897

2. The first output file obtained from the Profile 1.0 program

Name of input file: Interpretation of oxygen profile (Reactor 1-72 hrs).txt

Name of output file: Results Reactor 1-72 hrs

Input read from file - the calculation begins.

Zones	SSE	R**2	Zones: 2	3	4	5
1	.1216E+00	.9974 ----	.005	.001	.000	.000
2	.4275E-01	.9991 ---------	.007	.000	.000	
3	.1430E-01	.9997 ---------------	.000	.001		
4	.8850E-03	1.0000 ---------------	.000			
5	.9837E-03	1.0000				

The F statistics suggest 4 zones. Choose the number of zones for further

calculations: 4

Zones	SSE	R**2	Zones: 3	2	1
4	.8850E-03	1.0000 ----	1.000		
3	.8842E-03	1.0000 ---------	.000		

2   .8594E-01   .9982 ---------------- .106

1   .1216E+00   .9974

The F statistics suggest 3 zones. Choose the number of zones in

final result: 3

The calculation is done -   113857 steady state profiles are tested.

Calculated concentration at top   :   .6501E+01

Calculated concentration at bottom: .3191E-01

Calculated flux at top   :   .2014E+00

Calculated flux at bottom   :   .0000E+00

Depth integration of production   :   -.2014E+00

Depth integration of irrigation   :   .0000E+00

Depth integration of production and irrigation in each zone:

Zones	Production	Irrigation
1	-.1043E-01	.0000E+00
2	-.1006E+00	.0000E+00
3	-.9039E-01	.0000E+00

3. The second output file obtained from the Profile 1.0 program

Depth [m]	Fi	DB	Alfa	Oxygen conc.	IRRIGATION	PRODUCTION	
.0000E+00	.8000E+00	.0000E+00	.0000E+00	.6501E+01	.0000E+00	.0000E+00	
.0000E+00	.8000E+00	.0000E+00	.0000E+00	.6501E+01	.0000E+00	-.9271E+02	
.1575E-04	.8000E+00	.0000E+00	.0000E+00	.6075E+01	.0000E+00	-.9271E+02	
.3375E-04	.8000E+00	.0000E+00	.0000E+00	.5593E+01	.0000E+00	-.9271E+02	
.5175E-04	.8000E+00	.0000E+00	.0000E+00	.5115E+01	.0000E+00	-.9271E+02	Zone 1
.6975E-04	.8000E+00	.0000E+00	.0000E+00	.4640E+01	.0000E+00	-.9271E+02	
.8775E-04	.8000E+00	.0000E+00	.0000E+00	.4170E+01	.0000E+00	-.9271E+02	
.1058E-03	.8000E+00	.0000E+00	.0000E+00	.3704E+01	.0000E+00	-.9271E+02	
.1148E-03	.8000E+00	.0000E+00	.0000E+00	.3473E+01	.0000E+00	-.8940E+03	
.1328E-03	.8000E+00	.0000E+00	.0000E+00	.3034E+01	.0000E+00	-.8940E+03	
.1508E-03	.8000E+00	.0000E+00	.0000E+00	.2635E+01	.0000E+00	-.8940E+03	
.1688E-03	.8000E+00	.0000E+00	.0000E+00	.2275E+01	.0000E+00	-.8940E+03	Zone 2
.1868E-03	.8000E+00	.0000E+00	.0000E+00	.1953E+01	.0000E+00	-.8940E+03	
.2048E-03	.8000E+00	.0000E+00	.0000E+00	.1671E+01	.0000E+00	-.8940E+03	
.2228E-03	.8000E+00	.0000E+00	.0000E+00	.1428E+01	.0000E+00	-.8940E+03	

.2318E-03	.8000E+00	.0000E+00	.0000E+00	.1319E+01	.0000E+00	-.4017E+03
.2498E-03	.8000E+00	.0000E+00	.0000E+00	.1116E+01	.0000E+00	-.4017E+03
.2678E-03	.8000E+00	.0000E+00	.0000E+00	.9297E+00	.0000E+00	-.4017E+03
.2858E-03	.8000E+00	.0000E+00	.0000E+00	.7611E+00	.0000E+00	-.4017E+03
.3038E-03	.8000E+00	.0000E+00	.0000E+00	.6100E+00	.0000E+00	-.4017E+03
.3218E-03	.8000E+00	.0000E+00	.0000E+00	.4764E+00	.0000E+00	-.4017E+03
.3398E-03	.8000E+00	.0000E+00	.0000E+00	.3604E+00	.0000E+00	-.4017E+03
.3578E-03	.8000E+00	.0000E+00	.0000E+00	.2618E+00	.0000E+00	-.4017E+03
.3758E-03	.8000E+00	.0000E+00	.0000E+00	.1808E+00	.0000E+00	-.4017E+03
.3938E-03	.8000E+00	.0000E+00	.0000E+00	.1173E+00	.0000E+00	-.4017E+03
.4118E-03	.8000E+00	.0000E+00	.0000E+00	.7133E-01	.0000E+00	-.4017E+03
.4298E-03	.8000E+00	.0000E+00	.0000E+00	.4286E-01	.0000E+00	-.4017E+03
.4500E-03	.8000E+00	.0000E+00	.0000E+00	.3191E-01	.0000E+00	-.4017E+03

Zone 3

APPENDIX H: GLUCOSE CONSUMPTION CALCULATION

A glucose utilisation graph was obtained by plotting the amount of glucose used daily over a period of time. The amount of glucose consumed by the biofilm was calculated as an accumulative function (i.e. the amount of glucose consumed daily was added to that which was previously consumed). This graph was better described by a 3rd order polynomial function in the format,

$$C_s = a_1 t^3 + a_2 t^2 + a_3 t + a_4 \tag{1}$$

The differential format of equation 1 is equivalent to the substrate (glucose) utilisation described by equation 2.

$$\frac{dC_s}{dt} = 3a_1 t^2 + 2a_2 t + a_3 = r_B = \frac{r_m C_s}{K_m + C_s} \tag{2}$$

Therefore the inverse of each part in equation 2 yields a function that describes the relationship between the inverse first order derivative and the inverse glucose utilisation equation as shown in equation 3,

$$\left(\frac{dC_s}{dt}\right)^{-1} = \frac{1}{3a_1 t^2 + 2a_2 t + a_3} = \left(\frac{K_m}{r_m}\right)\frac{1}{C_s} + \frac{1}{r_m} \tag{3}$$

By plotting $\left(\dfrac{1}{3a_1 t^2 + 2a_2 t + a_3} \right)$ against $\dfrac{1}{C_s}$ at different time intervals, K_m, was obtained by

dividing the slope $\left(\dfrac{K_m}{r_m} \right)$ by the intercept $\left(\dfrac{1}{r_m} \right)$

APPENDIX I: ARTICLES SUBMITTED FOR PUBLICATION AND CONFERENCE ATTENDANCE

Journal Articles:

Ntwampe, SKO and Sheldon, MS. 2005. Quantifying growth kinetics of *Phanerochaete chrysosporium* immobilised on a vertically oriented capillary polysulphone membrane: biofilm development and substrate consumption. *Biochemical Engineering Journal* [first submitted 22 February 2005; revised 18 May 2005, resubmitted 4th November 2005]

Oral presentations:

Ntwampe, SKO and Sheldon, MS. 2005. Quantifying growth kinetics of *Phanerochaete chrysosporium* immobilised on a vertically oriented capillary polysulphone membrane. 6th WISA-MTD Symposium and Workshop [George, South Africa, 13-15 March 2005].

Poster snapshot presentations:

Ntwampe, SKO. and Sheldon, MS. The effect of spore concentration on growth kinetics of *Phanerochaete chrysosporium* immobilised on a vertically orientated polysulphone capillary membrane bioreactor. SAIChE R & D 2005 [UCT, 3 June 2005].

f – Biofilm

g - Glucose

L – Lumen

m – Matrix

r – Radial direction

s – Substrate

s0 – Initial substrate concentration

x, y, z – directional coordinates

O_2 - oxygen

z- Axial direction

LIST OF ABBREVIATIONS

DMAB – 3-dimethylamino benzoic acid

LiP – Lignin Peroxidase

MBTH – 3-methyl-2-benzothiazolinone hydrazone

MCMBR – Multi capillary membrane bioreactor

MnP – Manganese Peroxidase

P. chrysosporium – Phanerochaete chrysosporium

SFCMBR – Single fibre capillary membrane bioreactor

WRF – White rot fungus

u_0 - Inlet lumen centre line velocity   m/s

v - Molar velocity   mol/s

$\bar{v}$ - Molar average velocity   mol/s

V_r - Dimensionless radial velocity $(u_r L / u_0 R_L)$ -

V_z - Dimensionless axial velocity (u_z / u_0) -

X - Biomass density   g/m³

$\bar{X}$ - Dimensionless axial coordinate (z'/L)   -

X_m - Maximum cell density   g/m³

$Y_{X/S}$ - Growth yield coefficient (glucose consumed/g biofilm)   -

z' - Axial coordinate   m

GREEK LETTERS

$\bar{\mu}$ - Specific growth rate   hr⁻¹

$\bar{\mu}_m$ - Maximum specific growth rate   hr⁻¹

μ - Viscosity   Pa.s

ρ - Density   kg/m³

δ – Biofilm thickness   μm

θ – 3 dimensional coordinate   -

ε – Membrane porosity   -

ξ - Molar fraction   -

∇ - Triangular coordinates   -

π – pie   -

β – Mass transfer coefficient   m/hr

Subscripts

0 - Initial

1 – Inlet

2 – Outlet

3 – Shell side

LIST OF SYMBOLS